Metabolic Regulation in Diabetic Kidney Disease

by

Judy J. Baek

A dissertation submitted in partial fulfillment
of the requirements for the degree of
Doctor of Philosophy
(Molecular and Integrative Physiology)
in the University of Michigan
2021

Doctoral Committee:

Professor Subramaniam Pennathur, Chair
Professor Charles Burant
Professor Ken Inoki
Professor David Lombard
Professor Joel M. Weinberg

Judy J. Baek

judybaek@umich.edu

ORCID iD: 0000-0002-7662-2362

Dedication

This thesis is dedicated to my husband, Kunal Bailoor. Thank you for your encouragement and support while you were on your own arduous journey through medical school and residency. You inspire me.

Acknowledgements

I want to first and foremost thank my mentor Professor Pennathur. Thank you for your mentorship on all aspects of my training, from discussions about metabolomics to career advice for a physician scientist hopeful. Thank you for believing in my potential as scientist. I want to thank the members of the Pennathur lab for their help, advice and discussions concerning science and my work. I want to thank Dr. Stefanie Wernisch, who took me under her wing and taught me the basics of LC-MS theory and instrumentation. I want to thank Dr. Chenchen He, who helped me tremendously with method development and gave me valuable scientific input. I also want to thank you for your encouragement and kind words during graduate school. I want to thank members of the metabolomics core for their help. I want to thank Dr. Charles Evans for always taking time out of his busy schedule to help me troubleshoot numerous LC-MS related issues. I want to thank Professor David Lombard for his mentorship and always being open to giving me advice and resources. I want to thank his lab members Dr. Billy Giblin, Dr. Surinder Kumar, and Dr. Mary Skinner for their help. I really could not have made my foray into studying Sirtuin 5 without your guidance. Finally, I want to thank all of my previous scientific mentors; you all helped make it possible.

Table of Contents

Dedication ii

Acknowledgements iii

List of Tables viii

List of Figures ix

List of Abbreviations xi

Abstract xiii

Chapter 1: Introduction 1

1.1 Diabetic Kidney Disease – Clinical Manifestations and Its History 1

1.2 Brief Overview of The Endothelial, Podocyte And Tubular Changes In DKD 3

1.3 Cell-To-Cell Communications in DKD and Proximal Tubular Role in Kidney Homeostasis 5

1.4 SGLT2 Inhibitors Underscore the Role of Proximal Tubules In DKD Pathogenesis 7

1.5 Renal Energy Metabolism in DKD 10

1.6 Glucose Metabolism in DKD 11

1.7 Fatty Acid Oxidation in Proximal Tubules DKD 13

1.8 Role of Post-Translational Modification in Metabolism 16

1.9 Role of SIRT5 and PTMs in Regulating Glucose Metabolism 19

1.10 Role of SIRT5 and PTMs in Regulating Fatty Acid Oxidation 20

1.11 Malonylation and Succinylation Roles in Regulating Metabolism 21

1.12 Role of Sirtuin 5 in Obesity and Diabetes 23

1.13 Role of SIRT5 in Kidney Disease 24

1.14 Commentary on LC-MS Metabolomics as a Method in Studying Metabolism 25

1.15 Thesis Aims 27

Chapter 2: Decreased Malonylation in Non-Mitochondrial Pathways in the db/db Kidney Cortex 30

2.1 Abstract 30

2.2 Introduction 31

2.3 Results 33

2.3.1 Malonylation is Decreased in db/db Kidney Cortex Potentially Due to Upregulation in SIRT5 Levels 33

2.3.2 Malonylation ss Decreased Specifically in Proximal Tubules in the db/db Kidney 34

2.3.3 SIRT5 Increases Glucose Flux into Glycolysis and Decreases Flux into the TCA Cycle in HK-2 Cells 35

2.3.4 Sirt5 Expression is Elevated in the Tubulointerstitium off Diabetic Pima Indian Patients 36

2.4 Discussion 37

2.5 Materials And Methods 40

Chapter 3: Role of SIRT5 in Mouse Models of DKD 57

3.1 Abstract 57

3.2 Introduction 58

3.3 Result 59

3.3.1 HFD-STZ Mice Kidney Cortex Demonstrate Reduced Malonylation 59

3.3.2 HFD-STZ Of SIRT5 WT and OE Mice Demonstrate No Significant Differences in Systemic Metabolism 60

3.3.3 Diabetic SIRT5 OE Mice Display Reduced Urinary Levels of DKD Biomarkers 61

3.3.4 Diabetic SIRT5 WT and OE HFD-STZ Mice Display No Significant Difference in Kidney Fibrosis 62

3.4 Discussion 63

3.5 Materials and Methods 65

Chapter 4: Urinary 2-Hydroxyglutarate Enantiomers Are Markedly Elevated in A Murine Model of Type 2 Diabetic Kidney Disease 77

4.1 Abstract 77

4.2 Introduction 78

4.3 Results 79

4.3.1 Urine, Plasma Concentration and Percent Fractional Excretion of D and L-2HG 79

4.3.2 Elevated TCA Cycle Metabolites Drive Increased D and L-2HG Fractional Excretion 81

4.3.3 Hyperglycemia Increases D And L-2HG Production in Human Proximal Tubular HK-2 Cells 82

4.4 Discussion 83

4.5 Materials and Methods 85

Chapter 5: C6-Glucose Metabolic Flux Analysis Reveals Reduced Mitochondrial Metabolism in T1D Subjects 94

5.1 Abstract 94

5.2 Introduction 94

5.3 Results 95

5.3.1 Study Design and Patient Data 95

5.3.2 Euglycemic Clamp Study Demonstrates Minimal Incorporation of Glucose into Urinary Metabolites 97

5.4 Discussion 98

5.5 Materials and Methods 100

Chapter 6 106

6.1 Discussion 106

References 114

List of Tables

Table 1-1 Relative advantages and disadvantages of alternative metabolomics analytical methods to LC-MS. 26

Table 4-1 Concentration of TCA cycle metabolites from db/+ vs. db/db kidney cortex.. 91

Table 4-2 TCA cycle metabolites in db/db and db/+ plasma. 91

Table 4-3 TCA cycle metabolites in db/db and db/+ urine. 91

Table 4-4 TCA cycle metabolites in HK-2 cells under 5 mM glucose (low glucose), 25 mM glucose (high glucose), and 5 mM glucose and 20 mM mannitol (osmotic control). 93

Table 5-1 Clinical characteristics of study participants. 102

List of Figures

Figure 2-1 Malonylation is decreased in the db/db kidney cortex 49

Figure 2-2 Compartment specific reduction in protein malonylation levels. 50

Figure 2-3 SIRT5 protein level is elevated in db/db kidney cortex 51

Figure 2-4 Immunofluorescence (IF) of Kmal residues in db/db and db/+ cortex 52

Figure 2-5 Immunoaffinity enriched proteomics for malonylation 53

Figure 2-6 Proteins in glycolysis/gluconeogenesis with significantly reduced malonylation levels in the db/db cortex 54

Figure 2-7 Proteins in peroxisomal fatty acid oxidation pathway with significantly reduced malonylation levels in the db/db cortex 54

Figure 2-8 Overexpression of SIRT5 in HK-2 cells. 55

Figure 2-9 Knockdown of SIRT5 in HK-2 cells. 55

Figure 2-10 SIRT5 transcript levels from kidney biopsies of living donor (LD; control) volunteers and diabetic Pima Indian patients (Pima). 56

Figure 3-1 Malonylation and succinylation levels in control and HFD-STZ diabetic mouse kidney cortex. 69

Figure 3-2 HFD-STZ SIRT5 mouse study design. 70

Figure 3-3 Hyperglycemia in control and HFD-STZ SIRT5 WT and OE mice between 34-38 weeks of age. 71

Figure 3-4 Fasting plasma lipid panel from SIRT5 WT and OE control and HFD-STZ mice 72

Figure 3-5 Urinary markers of DKD from 24-hr urine cages. 73

Figure 3-6 Glomerular histology in SIRT5 WT and OE HFD-STZ mice. 74

Figure 3-7 Fibrosis in SIRT5 WT and OE control and HFD-STZ mice. 74

Figure 3-8 Expression of fibrosis genes in SIRT5 WT and OE control and HFD-STZ mice..... 75

Figure 3-9 Examples of cortex metabolites that are significantly elevated between control and HFD-STZ mice..... 76

Figure 4-1 Concentration of L and D-2HG (±SD) in plasma and urine and calculated percent fractional excretion of each metabolite from Control (db/+) and Diabetic (db/db) and mice..... 90

Figure 4-2 Kidney cortex levels of TCA cycle metabolites drive D and L-2HG production. 92

Figure 4-3 HK-2 production of D and L-2HG in high glucose media. 93

Figure 5-1 Schematic of euglycemic-hyperglycemic study..... 103

Figure 5-2 Glucose flux study information..... 103

Figure 5-3 Labeled urinary TCA cycle metabolites from hyperglycemic clamp study.. 104

Figure 5-4 Labeled urinary glycolytic metabolites from hyperglycemic clamp study. .. 104

Figure 5-5 Labeled urinary TCA cycle metabolites from euglycemic clamp study..... 105

List of Abbreviations

2-hydroxyglutarate (2-HG)
Acute Kidney Injury (AKI)
Acyl-Coenzyme A Oxidase 1 (ACOX1)
Advanced Glycation End Products (AGEs)
BMP And Activin Membrane Bound Inhibitor (BAMBI)
Brown Adipose Tissue (BAT)
Carbamoyl Phosphate Synthase 1 (CPS1)
Carnitine O-acetyltransferase (CRAT)
Chronic Renal Insufficiency Cohort (CRIC)
Carnitine Palmitoyltransferase 1a (CPT-1a)
Chronic Kidney Disease (CKD)
Diabetic Kidney Disease (DKD)
Diacylglycerols (DAGs)
Diet-Induced Obesity (DIO)
End-stage renal disease (ESRD)
Enoyl-CoA Hydratase (ECHA)
Enoyl-CoA Hydratase And 3-Hydroxyacyl CoA Dehydrogenase (EHHADH)
Estimated Glomerular Filtration Rate (eGFR)
Extracellular Acidification Rate (ECAR)
Fatty Acid Oxidation (FAO)
Fatty Acid Synthase (FASN)
Formic Acid (FA)
Glomerular Filtration Rate (GFR)
Glyceraldehyde 3-Phosphate Dehydrogenase (GAPDH)
High-fat Diet (HFD)
Hydrophilic Interaction Chromatography (HILIC)
Immunofluorescence (IF)
Insulin Growth Factor 1 (IGF-1)
Intraperitoneal Glucose Tolerance Test (ipGTT)
Intraperitoneal Insulin Tolerance Test (ipITT)
Iothalamate Glomerular Filtration Rate (iGFR)
Isocitrate Dehydrogenase 1 (IDH1)
Kidney Injury Molecule 1 (KIM-1)
Knockout (KO)
Lipopolysaccharide (LPS)
Matrix-Assisted Laser Desorption/Ionization (MALDI)
Time Of Flight (TOF)
Malonyl-CoA Decarboxylase (MCD)

Mammalian Target of Rapamycin (mTOR)
Mass spectrometry imaging (MSI)
Malony-lysine (Kmal)
Neutrophil Gelatinase-Associated Lipocalin (NGAL)
Nicotinamide mononucleotide (NMN)
Nitric Oxide (NO)
Overexpressor (OE)
Oxidative Phosphorylation (OXPHOS)
Phosphoenolpyruvate Carboxykinase (PEPCK)
Post-Translational Modification (PTM)
Pyruvate Dehydrogenase (PDH)
Pyruvate Kinase M2 (PKM2)
Quadruple Time-of-Flight (QTOF)
Sirtuin (SIRT)
Sodium Chloride (NaCl)
Sodium Glucose Transporter 2 (SGLT2)
Sterol Regulatory Element-Binding Proteins (SREBP)
Streptozotocin (STZ)
Time-of-Flight (TOF)
Transverse Aortic Constriction (TAC)
Tricarboxylic acid (TCA)
Trichostatin A (TSA)
Triosephosphate Isomerase 1 (TPI1)
Type 1 Diabetes (T1D)
Type 2 Diabetes (T2D)
Uncoupling Protein 1 (UCP1)
Vascular Endothelial Growth Factor A (VEGF-A)
Very Long-Chain Acyl-Coa Dehydrogenase (VLCAD)
Wildtype (WT)

Abstract

Diabetic kidney disease (DKD) is the leading cause of end-stage renal disease in the US and developed countries. Metabolomics studies have demonstrated that significant renal metabolic reprogramming occurs in DKD and potentially contributes to disease pathogenesis and progression. In this thesis, I explored the regulatory mechanisms of nutrient metabolism in DKD and how this altered metabolism may serve as a biomarker of disease severity and progression. We found that malonylation, a non-enzymatically acylated post-translation modification (PTM), is reduced in the kidney cortex of the type 2 diabetic T2D *db/db* mice and that this process is regulated by Sirtuin 5 (SIRT5), which removes negatively charged lysine modifications such as malonylation. Proteomic analysis of *db/db* and *db/+* kidney cortex found that targets with significant reduction in malonylation are enriched in non-mitochondrial metabolic pathways such as glycolysis/gluconeogenesis and peroxisomal fatty acid oxidation (FAO). We generated diabetic SIRT5 knockout (KO) and overexpression (OE) mouse models to understand the role of SIRT5 in DKD with high-fat diet and streptozotocin (HFD-STZ) treatment. We found that increased SIRT5 levels are protective against DKD; SIRT5 OE mice were relatively protected against DKD. These studies highlight an important adaptive role for SIRT5 in DKD. However, we also observed a large effect of mouse genetic background strains on the development of diabetes and kidney disease, especially for SIRT5 KO mice, confounding our observations. We then investigated potential biomarkers of DKD.

We found that higher levels of L and D 2-hydroxyglutarate (2-HG) are found in the urine of *db/db* mice and that this increase likely driven by increased kidney tricarboxylic acid (TCA) cycle levels and hypoxia and acidosis that occurs in DKD. Elevations in 2-HG may lead to altered epigenetic programming, in particular by inhibiting α-ketoglutarate-dependent dioxygenases and may contribute to DKD. We also conducted a study to assess whether increased glucose flux, which has been demonstrated to occur in the *db/db* kidney cortex, also occurs in diabetic DKD patients. We conducted euglycemic and hyperglycemic clamp studies with $^{13}C_6$ - glucose in healthy subjects, patients with type 1 diabetes (T1D) and no microvascular complications and patients with T1D and DKD. We analyzed urine collected during the clamp studies for relative glucose incorporation and found decreased incorporation of glucose into urinary metabolites, especially TCA cycle metabolites, in the T1D subjects. Our findings suggest that glucose incorporation into TCA cycle is blunted in T1D and potentially reflects reduced mitochondrial activity in the diabetic kidney. However, as urine metabolites are a culmination of systemic and renal metabolism, further investigation is necessary to understand exactly how glucose metabolism is altered between the three groups.

Chapter 1

Introduction[1]

1.1 Diabetic Kidney Disease – Clinical Manifestations and Its History

DKD is the leading cause of end-stage renal disease (ESRD) in the developed countries in the world[1]. In the US, amongst Medicare beneficiaries between 2015-2018, diabetes was the primary cause of ~38.7% of all ESRD cases[2]. In addition, diabetes status is associated with higher mortality, even after adjustments for chronic kidney disease (CKD) stage, age, race and sex[2], suggesting that patients with DKD have an increased disease and mortality burden compared to patients with CKD of alternate disease etiologies.

In the 1990s, DKD progression was identified to be primarily driven by glomerular pathology, supported by the discovery that advanced glycation end products (AGEs), a marker of hyperglycemic damage, localized to the glomeruli and affected primarily the mesangial cells[3]. Indeed, mesangial expansion due to extracellular matrix deposition and mesangial cell hypertrophy have been identified in some early histological studies to correlate best with glomerular filtration rate (GFR), proteinuria and hypertension[4,5]. Therefore, DKD has been classically characterized as a disease of nephropathy, in which

[1] Portions of this chapter have been published in:
Baek, J., He, C., Afshinnia, F., Michailidis, G., & Pennathur, S. Lipidomic approaches to dissect dysregulated lipid metabolism in kidney disease. *Nat Rev Nephrol.* In Press.

albuminuria, which represents glomerular filtration barrier effacement, precedes loss of GFR and drives disease progression.

However, it is now established that there is significant heterogeneity in the histopathology amongst DKD patients[6–8]. In addition, the clinical course of DKD varies widely amongst DKD patients. In the National Health and Nutrition Examination Survey cohort, the prevalence of albuminuria decreased from 20.8% to 15.9% and the prevalence of reduced eGFR (below 60 mL/min/1.73 m^2) from 9.2% to 14.1% and prevalence of reduced eGFR (below 30 mL/min/1.73 m^2) from 1.0% to 2.7% when comparing populations between 1988-1994 and 2009-2014[9]. A study of T1D and T2D patients from the Joslin clinic found that among patients with normo-albuminuria, GFR decline of at least 3 ml/min/yr occurred in 9% in T1D and 20% in T2D patients[10]. The Southwestern American Indians of the Gila River Indian Community, a genetically homogenous group whose population develops T2D diabetes at one of the highest rate in the world (~38% of the population)[11], exhibit dramatic hyperfiltration with onset of insulin-resistance and gradual increase in iothalamate GFR (iGFR) with GFR reduction upon development of macroalbumniuria[12]. This dramatic increase in GFR has not been observed in Caucasian patients with DKD, who exhibit only modest increases[13]. Glomerular hyperfiltration in early DKD is thought to contribute to albuminuria due to intraglomerular hypertension[14]. The Southwestern American Indian Community has higher rates of DKD progression to ESRD compared to many other populations, and although the reasons are multifold, this dramatic hyperfiltration is thought to contribute to the severity of disease in the Gila River Indian Community[13].

In summary, DKD encompasses a large range of disease phenotypes with disparate cell-type susceptibilities to injury.

1.2 Brief Overview of The Endothelial, Podocyte And Tubular Changes In DKD

All cell types in the kidney, including the mesangial cells, podocytes, endothelial cells, and tubules all contribute to the disease pathogenesis. In DKD, endothelial cells are characterized by abnormal angiogenesis; histological studies have demonstrated that these new vessels populate the periphery of the glomerulus[15]. The angiogenesis is driven by increased vascular endothelial growth factor-A (VEGF-A) expression by podocytes[16] and glomerular hypertension. Of note, specific isoforms of VEGF are associated with disease progression or disease protection: VEGF-A_{165}b is protective whereas VEGF-A_{165}a is pathogenic[17]. Dysregulation of nitric oxide (NO) levels is thought to lead to increased vessel permeability that contributes to breakdown of glomerular filtration barrier, in addition to loss of VEGF-A regulation by NO. The importance of endothelial nitric oxide synthase in DKD has been well-demonstrated in *db/db* BKS eNOS$^{-/-}$[18] and STZ-eNOS$^{-/-}$[19] mouse models. Lipid deposition occurs in various cells in the kidney in DKD, and endothelial lipid accumulation in both large and small vessels contributes to atherosclerosis, cardiovascular disease and microvascular complications[20–22].

Podocytes are terminally differentiated epithelial cells whose interdigitating foot-processes around fenestrated endothelial cells and the glomerular basement membranes form the glomerular filtration barrier[23]. In DKD, podocyte detachment, apoptosis, and foot-process effacement contribute to albuminuria and glomerulosclerosis. Increased mammalian target of rapamycin (mTOR) activity is observed in the glomeruli of DKD patients and diabetic mice, and reduction in mTORC1 activity in podocytes in *db/db* and

T1D STZ mice ameliorates podocyte foot-process effacement, improper nephrin localization, and proteinuria[24,25]. Increased Notch signaling in glomerular compartment from DKD patient biopsies and mouse models of DKD contributes to podocyte apoptosis and glomerulosclerosis, and podocyte-specific reduction in notch signaling with Rbpj KO results in DKD amelioration[26]. Wnt/β-catenin signaling, which is not expressed after differentiation, is upregulated in human and mouse DKD podocytes, although both the reduction and stabilization of Wnt/β-catenin signaling results in increased podocyte susceptibility to DKD; a tight regulation of this pathway is important to podocyte structure and function[27]. Of note, some researchers have proposed that podocyte destruction drives all glomerulopathies, as it is a differentiated cell population that cannot easily be regenerated. This “podocyte-centric” model is supported by increased urinary podocyte mRNA in patients with established glomerular disease[28,29]. While podocyte loss is an inevitable event in glomerular damage of any etiology and serves as an important biomarker of glomerular disease, further work is needed to ascertain podocyte role in DKD progression.

Tubular structure and function vary along the nephron. Proximal tubules are responsible for the reabsorption of most of nutrients and water from the filtrate. Perhaps in reflection of their importance, proximal tubules comprise >60% of the entire kidney by cell number and volume[30]. Interstitial fibrosis is considered a relatively “late” histological finding and is considered the final common pathway of ESRD development regardless of the CKD etiology. Atubular glomeruli, which are glomeruli not attached to proximal tubules due to tubular death and fibrosis, are estimated to compromise 8-12% of glomeruli in diabetic kidney according to studies of human biopsies[31–33]. Some researchers use the

example of atubular glomeruli occurring in patients with low proteinuria to claim that proteinuria and glomerular histology are not necessarily best predictors of disease and instead the degree of tubulointerstitial fibrosis and the number of atubular glomeruli best predict disease progression in DKD.

Changes in tubular structure also occur early in DKD. Specifically, proximal tubular hypertrophy is thought to occur in DKD due to the expression of growth factors such as insulin growth factor 1 (IGF1)[34,35] and the action of mTORC1[36]. Abnormal glucose metabolism due to increased generation of hypertrophy-inducing metabolites such as polyamines[37,38] and glycosphingolipids[39] is also hypothesized to contribute to DKD pathogenesis. Proximal tubular hypertrophy is thought, in part, to drive increased sodium glucose transporter 2 (SGLT2) synthesis and therefore the tubular hyper-reabsorption of sodium chloride (NaCl) and glucose in diabetes. This in turn increases glomerular hyperfiltration due to the reduced delivery of NaCl to the macula densa, in a model first proposed by Vallon and his colleagues[40,41]. The hypertrophy likely also leads to increased oxygen consumption and upregulation of hypoxic signaling. Proximal tubular hypertrophy has been linked to increased disease progression in clinical studies with DKD patient biopsies, and in the “tubulocentric” model, is thought to be a foundational event for DKD pathogenesis[42].

1.3 Cell-To-Cell Communications in DKD and Proximal Tubular Role in Kidney Homeostasis

Alterations in cell-to-cell communication occur in DKD. For example, in the glomerulus, the aforementioned NO signaling between endothelial cells and podocytes is important in regulating VEGF signaling. Immune system infiltration and activation of

complement receptors on kidney disease have also been identified to contribute to DKD[43]. Another instance of the importance of cell-to-cell communication in DKD was demonstrated by Lai *et. al.,* via comparison of disease severity in diabetic mice with podocyte or endothelial cell-specific KO of TGFβ negative regulator. TGFβ is a crucial mediator of DKD, and its activity could be inhibited by BMP And Activin Membrane Bound Inhibitor (BAMBI), which is an endogenous pseudoreceptor inhibitor for TGFβ signaling. A recent study of endothelial cell-specific and podocyte-specific BAMBI KO mice found that endothelial cell-specific BAMBI KO cells demonstrated worse disease, including increased podocyte loss in comparison to the podocyte-specific BAMBI KOs, suggesting glomerular endothelial function influences podocytes in DKD[44].

In addition to regulating GFR, proximal tubular health has been demonstrated to affect glomerular function and structure in DKD. In the STZ mouse model of proximal-tubular-specific KO of Sirtuin 1 (SIRT1), Itoh and colleagues found that the proximal tubular-specific reduction in SIRT1 levels resulted in podocyte effacement and albuminuria[45]. They hypothesized that the downregulation of nicotinamide mononucleotide (NMN) delivery to podocytes led to increased claudin-1 expression, leading to podocyte effacement. In support of this paracrine role of proximal tubules, decreased photo-activable NMN analog (N-methylanthraniloyl (Mant)-NMN) delivery from the tubules to the podocytes *in vivo* were observed after injection into the mice. In the absence of SIRT1, this delivery did not occur. This hypothesis has been further supported by finding that Nicotinamide Phosphoribosyltransferase OE in proximal tubules reduced albuminuria and podocyte effacement in STZ DKD[46]. Further work remains to elucidate the role of proximal tubules in maintaining glomerular integrity in DKD, but the

aforementioned studies suggest a regulatory role of proximal tubules on podocytes and potentially other renal cells. Of particular interest is the role of the delivered NMN in podocytes; in addition to signaling, does proximal tubule-derived NMN, which is thought to be the limiting factor in NAD^+ *de novo* biosynthesis, also supplement podocyte metabolism? Podocytes may have limited capacity for nutrient synthesis in comparison to proximal tubules; for example, proximal tubules have significantly higher number of mitochondria per volume of cell[47]. Further investigation of whether proximal tubules supplement podocytes with metabolic intermediates, and if this process is altered in DKD may be of interest in understanding the role of proximal tubules in glomerular health.

Of note, glomerular filtration barrier damage and the resulting albuminuria have been demonstrated, in its own right, to lead to tubular damage, as exemplified by murine models of albumin-overload induced tubular injury[48–50]. Non-esterified fatty-acid conjugated albumin can be taken up by proximal tubules from the apical surface by the action of fatty-acid transporter 2[51] and cluster of differentiation 36[52] and further exacerbate lipid-associated damaged in DKD. There is also *in vitro* evidence that urinary extracellular vesicles of podocyte origin can induce fibrosis in proximal tubular epithelial cell sodium PTEC cultures[53,54].

1.4 SGLT2 Inhibitors Underscore the Role of Proximal Tubules In DKD Pathogenesis

Due to the multifold dysfunction of the different cell-types in the kidney, it is challenging to identify therapeutic targets that can systematically treat DKD. Sodium glucose transporter inhibitors (SGLT2i) have emerged as a new therapy that has demonstrated superiority over the traditional glycemic control and ACE/ARB therapy for

both DKD progression and cardiovascular mortality. SGLT2s are expressed mainly in the apical membranes early proximal tubular segment in the kidney[55]. SGLT2s were identified as a potential therapeutic target for diabetes as patients with familial renal glucosuria with mutations in the SLC5A2 gene generally do not exhibit serious clinical consequences from the increased glycosuria[56].

The EMPA-REG[57], CANVAS[58], DECLARE-TIMI 58[59], and CREDENCE[60] clinical trials found hazard ratios of between 0.61-0.86 for primary kidney disease outcomes, demonstrating reduction in progression in patients with SGLT2i treatment. Some caveats in interpretation included slight, but significant reduction in glycated hemoglobin levels, bodyweight, and systolic blood pressure with SGLT2i therapy. The reduction in blood pressure likely contributes to improved cardiovascular disease and mortality outcomes in these trials, and is attributed in part to the reduction of the aforementioned NaCl hyper-reabsorption that occurs in hyperglycemia[42]. In support of this hypothesis, studies of diabetic mouse models such as the Akita[61] and *db/db* mice[62] found significant reductions in kidney size after treatment with empagliflozin. SGLT2is likely mediate this process by downregulating mTORC1 activity. In a recent study, Kogot-Levin *et.al.,* found that dapagliflozin reduces mTORC1 activation, and the efficacy of the SGLT2i is eliminated in proximal tubular-specific Tsc1 KO mice[63]. This reduction in activity is thought to be mediated in part by increase in circulating ketone levels; SGLT2is upregulate ketosis, and in a murine model of non-proteinuric tubular DKD ($ApoE^{-/-}$ high-fat diet mice); elevated ketone-body levels or exogenous supplementation of ketones ameliorates disease by suppressing mTORC1 activity[64].

Of note, SGLT2i affect nearly all cell-types to confer cardiorenal protection. SGLT2i upregulation of ketone body production has been identified to reduce NRLP inflammasome activity in human macrophages[65]. Ketone bodies are hypothesized to be more readily metabolized in comparison to glucose and fatty acids, and therefore improve energetics under stress[66]. Canagliflozin, in particular, has been of interest as an inhibitor of oxidative phosphorylation (OXPHOS) complex I, which results in an increase in AMP and ADP levels to activate AMPK[67], and partly drives lipid catabolism and improvements in plasma lipid profiles in murine models[68]. SGLT2is are thought to bind to glucose transporters other than SGLT2is such as GLUT1 and GLUT2 and this promiscuity can confer direct tissue protection in non-proximal tubular cells[69]. Aberrant SLGT2 expression in mesangial cells[70] and podocytes[71] under various disease states (metabolic and non-metabolic) has also been observed, and SGLT2is may act directly on these non-proximal tubular channels. Recently, dapagliflozin has been demonstrated to reduce CKD of non-diabetic etiology related mortality and renal progression (fall in measured GFR) in DAPA-CKD amongst patients with eGFR 20-75 in the DIAMOND trial[72]. Empagliflozin has been demonstrated to reduce cardiovascular event-related hospitalization and death in heart-failure with reduced ejection fraction (EMPEROR Reduced)[73] and heart-failure with preserved ejection fraction patients regardless of diabetes status[74]. For SGLT2is with moderate specificity for SGLT2 instead of SGLT1s such as canagliflozin, their SGLT1 inhibition in the small intestine has been attributed to reduction in post-prandial glucose levels and sustained glucagon-like peptide-1 release and therefore improve blood glucose levels and weight loss in diabetics[75]. Currently, sotagliflozin, a dual SGLT1 and

SGLT2 inhibitor that is currently under investigation for blood glucose control in type 1 diabetics and cardiovascular disease[76].

The new clinical findings also support a therapeutic potential of SGLT2is in non-diabetic related conditions; whether proximal tubules are a major target in these contexts remains to be elucidated.

1.5 Renal Energy Metabolism in DKD

The kidney is an energy intensive organ. The substrate and energy generating pathways are cell-type-specific in the kidney, and also depend on nutritional challenges or availabilities. In the glomeruli, podocytes harbor a strong preference for anaerobic glycolysis, and rely little on mitochondrial OXPHOS for energy generation, although they are capable of FAO[47,77]. Of note, podocytes, unlike endothelial cells and proximal tubules, are insulin dependent for intracellular glucose transport[78]. A recent study demonstrated that lack of mitochondrial regulators specifically in podocytes (PGC1α, DRP1 and TFAM) did not result in abnormal podocyte development, structure or glomerular disease[47]. It is likely that podocytes are more dependent on mitochondrial function in DKD; for instance, reduction in podocyte expression of PGC1α is found in DKD patient biopsies and DKD mouse models. However, restoration of podocyte levels of PGC1α by two-fold overexpression in STZ mice did not prevent albuminuria[77].

Significant heterogeneity of substrate preferences also exists amongst the different kidney tubules, depending on their location along the nephron and the kidney[79]. Proximal tubules, which have a large mitochondrial content, prefer to use free fatty-acids, along with glutamine as their main source of energy and display a severely limited capacity to use glucose as fuel under normal nutritional condition[79–82]. This inflexibility is

thought to occur due to the low activities of glycolytic enzymes in proximal tubules, and proximal tubular role in gluconeogenesis[83].

1.6 Glucose Metabolism in DKD

However, under disease conditions such as acute-kidney injury (AKI) and DKDl proximal tubular metabolism of glucose is thought to occur[79]. Whether this increase in metabolic fuel preference is adaptive or maladaptive is unclear. In addition, how glucose is metabolized in proximal tubules *in vivo* in DKD is also relatively unknown. The Brownlee hypothesis states that in cells independent of insulin for glucose uptake, high extracellular levels of glucose are directly reflected intracellularly. This elevation of intracellular glucose ultimately results in increased mitochondrial overload and oxidative stress. This oxidative stress leads to PARP-mediated downregulation of glycolysis, by the action of GAPDH, and leads to glucose shunting into secondary glycolysis pathways, including the polyol, pentose-phosphate, hexosamine, AGE pathway, diacylglycerol/PKC pathways, some of which produce toxic metabolites that eventually activate fibrosis, inflammatory, and oxidative stress pathways[84]. Of note, many of the studies referenced in his hypothesis were conducted on endothelial and mesangial cells *in vitro* and is therefore difficult to generalize this model to all the cell types in DKD.

In vivo metabolic flux-analysis with $^{13}C_6$-glucose demonstrated increased glucose flux in the cortex of diabetic mice, at first (12 weeks of age) with upregulation of glucose flux through glycolysis, TCA cycle and into the pentose-phosphate pathway but later (24 weeks of age) preferentially metabolizing glucose through the central carbon metabolic pathway and reducing glucose shunting into the pentose-phosphate pathway[85]. Interestingly, this increased glucose utilization occurred concomitantly with increased

palmitate flux, potentially due to reduction in mitochondrial ATP generation capacities; we hypothesized that increased substrate utilization occurs in lieu of efficient ATP production in DKD to maintain sufficient levels of ATP for kidney function. Increased urinary lactate production is a well-established finding in DKD in both murine models and DKD patients[86–89]. Therefore, increased glucose metabolism in DKD may occur in part due to metabolic reprogramming in the context of mitochondrial damage[85,90].

On the other hand, how glucose is processed in the kidney, not necessarily how much, may explain differences in patient susceptibilities to DKD development and progression. Study of the Medalist cohort found that long-term T1D who did not develop DKD had higher expression of glycolytic proteins, including pyruvate kinase M2 (PKM2)[91]. Plasma metabolomics from DKD resistant and progressor populations demonstrated lower levels of glycolytic and TCA cycle intermediates in the resistant population. Overexpression of PKM2 or activation of the protein with TEPP-46 in podocyte cell culture and STZ mice reduced glucose flux into the secondary pathways and reduced accumulation of central carbon metabolic intermediates. Qi *et. al.* proposed that being able to properly dispose of glucose through the entirety of glycolysis and the TCA cycle is protective against hyperglycemic damage.

Increased glucose utilization, specifically aerobic glycolysis, is associated with cellular growth and proliferation, as this allows generation of lipids, amino acids, nucleotides, NADPH, etc. from glucose in addition to ATP production[92]. In the context of DKD, aerobic glycolysis may contribute to the aforementioned renal hypertrophy that occurs early in disease. Researchers have suggested that high glucose levels also lead to cellular de-differentiation of tubules, and SGLT2i treatment can reduce expression of

markers associated with endothelial-mesenchymal transition in mouse models of DKD[93]. A study of proximal tubules after an ischemia reperfusion injury demonstrated that injured tubules initially upregulate glycolysis but tubules that successfully recover from the insult can generate energy from FAO and reduces expression of glycolytic protein, whereas the atrophic tubules maintain high levels of glycolysis and do not change their fuel preferences[94]. Increased glycolysis is associated with fibroblast proliferation in the context of kidney fibrosis[95]. In summary, increased and sustained glucose utilization is associated with aberrant cellular growth and/or dedifferentiation in the kidney.

In conclusion, hyperglycemia poses unique challenge for proximal tubules as they are insulin-independent with regards to glucose transport and possess little innate capacity to metabolize glucose. Increased glucose utilization in DKD is associated with cellular dedifferentiation, fibrosis, and mitochondrial damage, and although the exact mechanisms of how glucotoxicity occurs in the tubules have yet to be elucidated, reduction in glucose load (e.g. SGLT2is) and/or “proper” glucose processing is important in maintaining proximal tubules health in DKD.

1.7 Fatty Acid Oxidation in Proximal Tubules DKD

While glucotoxicity contributes to tubular apoptosis, cellular de-differentiation, fibrosis and eventual reduction in GFR, reduced and inefficient FAO has been long thought to be the major mechanism of tubular injury and fibrosis in not only DKD but CKD in general. A landmark study demonstrated that FAO transcripts and its regulatory genes are down-regulated in the tubulointerstitium of CKD patients of various etiologies including diabetes, and several mouse models of tubulointerstitial fibrosis[96]. PGC1α upregulation by drugs or transgenic overexpression is associated with disease

amelioration in murine models DKD[97], and the improvement in disease is thought in part to be upregulation in FAO by these regulators, amongst many other mechanisms. A recent study of renal tubular-specific conditional carnitine palmitoyltransferase 1A (CPT1a) over-expression demonstrated reduced fibrosis and disease in unilateral ureteral obstruction, folic-acid induced nephropathy, and adenine-induced nephropathy[98]. CPT1a overexpression improved mitochondrial morphology and improved FAO, supporting the hypothesis that FAO downregulation is a key driver of kidney fibrosis. Further studies, however, need to be conducted to evaluate whether upregulation of CPT1a and other enzymes in the FAO pathway can ameliorate tubular fibrosis in DKD.

Incomplete FAO leads to acylcarnitines accumulation[99] in tissues that become eventually reflected in the plasma. Studies of diabetic patients have found higher levels of plasma/serum acylcarnitines in DKD patients compared to diabetic patients without kidney disease[100–102], and can predict DKD progression when compared between progressors and non-progressors in prospective cohort studies[100,101,103,104]. Apart from measuring the absolute levels of acylcarnitines, another marker of mitochondrial inefficiency is the relative abundance of various acylcarnitines by chain length, including short, medium, and long chain acylcarnitines. Relatively low levels of long-chain acylcarnitine and high levels of medium and short-chain acylcarnitine and CKD status were found to be associated with DKD progression (defined as a decrease in iGFR by at least 40%) in the Southwestern American Indian cohort at baseline before onset of iGFR reduction[105]. Lower levels of long-chain acylcarnitines were associated with decreased expression of FAO genes in the glomerular compartment and genes regulating FAO in

the tubulointerstitial compartment[106], suggesting inefficient β-oxidation of longer chain fatty acids with DKD progression.

Acylcarnitine export into plasma and elimination in urine may be an adaptive method of dealing with mitochondrial overload, preventing fatty acid mediated cellular damage, and freeing CoA from acyl-CoAs to participate in other energy generating capacities especially in early CKD. Studies of carnitine-acetyltransferase (CrAT) demonstrate the important role of acylcarnitine, especially of acetylcarnitine, efflux out of the mitochondria. Muscle-specific deletion of CrAT, which serves to remove short-chain acetyl-CoAs out of the mitochondria by conjugation to carnitines, leads to decreased glucose tolerance and increased insulin resistance, attributed due to the increased inhibition of pyruvate dehydrogenase (PDH) by accumulating acetyl-CoA[107]. A recent study of proximal tubular cell-specific CrAT deficient mice demonstrated that CrAT function is indispensable to the normal function of proximal tubules. CrAT deficient mice develop tubulointerstitial fibrosis and secondary glomerulosclerosis, which is worsened by a high-fat diet challenge. CrAT deficient kidneys accumulated long-chain acylcarnitines and decreased mitochondrial oxygen-consumption rate. Interestingly, these CrAT deficient mice secreted less short chain and medium chain acylcarnitines in the urine, supporting the notion that efflux of short and medium chain efflux into plasma and urine aid in mitochondrial homeostasis with FAO[108].

Decreased FAO, in addition to causing insufficient ATP production, is also thought to contribute to increased kidney lipid accumulation in CKD. Increased neutral lipid accumulation in the kidney occurs after many types of hypoxic, ATP-depleting, and inflammatory insults[109–111]. Histological studies of patients with DKD have also found lipid

deposits in the glomeruli and tubules[112]. It is thought that accumulations of bioactive diacylglycerol (DAGs), ceramides, and mitochondrial overloading with fatty-acids leads to cellular toxicity[113]. Upregulation in sterol-regulatory binding element (SREBP) transcripts, which induce increased expression of lipogenic enzymes such as fatty-acid synthase and acetyl-CoA carboxylase, is thought to be a maladaptive response in several models of CKD. This increase in SREBP transcripts leads to increased triacylglycerol synthesis, but also cholesterol and intracellular fatty-acid synthesis, which likely confer the harmful effects of increased lipid accumulation in CKD[114–116].

1.8 Role of Post-Translational Modification in Metabolism

PTMs such as malonyl-lysine, succinyl-lysine and glutaryl-lysine are thought to occur non- enzymatically on lysine residues of proteins by their respective reactive CoA metabolites. Acetyl-lysine residues, which are catalytically conjugated to histones by acetyltransferases, are thought to be mainly also non-enzymatically acylated by acetyl-CoA on non-histone (e.g. mitochondrial) proteins[117]. The relatively basic pH and high concentration of succinyl-CoA and acetyl-CoA in the inner mitochondrial matrix are thought to promote the deprotonation of the ε-amino group and subsequent reaction with the CoA metabolites[118]. The biological basis of why certain enzymes and lysine sites are preferentially associated with a particular acyl-lysine modification requires further research. Many metabolic enzymes are subject to several different modifications; it appears that pathways associated with the production or degradation of the acylation substrates are subject to feedback regulation by its own metabolic intermediates/productions. For example, the top metabolic pathways enriched for

succinylation sites are in branched chain amino acid degradation pathways, the TCA cycle, and propionate metabolism in the SIRT5 KO mice liver[119].

Why specific proteins and sites are subject to malonylation, succinylation or glutarylation is unclear. Profiling of CoA metabolites from different mouse tissues demonstrated significantly higher levels of succinyl-CoA and acetyl-CoA compared to other CoA metabolites in many tissues, including the heart and the kidneys[120]. There is likely asymmetrical distribution of the CoA metabolites amongst the different cellular compartments. Succinyl-CoA is generated primarily in the mitochondria. Malonyl-CoA is primarily generated by the action of ACC in the cytoplasm, but a recent study demonstrated that mitochondrial malonyl-CoA can be produced from malonate by the action of Acyl-CoA synthetase family member 3[121]. In our own and other published studies, succinylation is enriched in mitochondrial proteins[119,122] and malonylation is enriched in mitochondrial and cytoplasmic proteins[119]. Comparison of the acetylated, malonylated and succinylated proteins from mouse liver mitochondria demonstrated that ~47% of malonylated mitochondrial proteins were not also regulated by acetylation or succinylation. In contrast, 80% of succinylated lysine sites are also regulated by acetylation, suggesting that succinylation and malonylation regulate more distinct processes compared to succinylation and acetylation[123].

PTMs are thought to regulate the activity of the modified protein in several different ways. As the modification of lysine alters the charge of the amino acid side-chain from positive to neutral (acetyl-lysine) or negatively charged (malonyl-lysine, succinyl-lysine), modification of lysines crucial to the enzymatic activity can alter its rate of catalysis. Site specific mutations of such lysines to glutamine (acetylation mimetic) or aspartic acid

(malonylation or succinylation mimetic) have been demonstrated to either reduce or increase activity in metabolic proteins. Activity of the enzyme can also be altered due to the effect of lysine modification on subunit assembly: succinylation of K311 of PKM2 reduces PKM2 tetramer formation and therefore decreases its enzymatic activity, and increases dimerization and nuclear translocation[124]. For metabolic proteins with multiple functions, modification of specific lysines can reduce the activity of a specific function. For instance, malonylation of K213 in lipopolysaccharide (LPS)-activated macrophages reduces glyceraldehyde 3-phosphate dehydrogenase (GAPDH) RNA binding function and therefore increases its metabolic activity[125]. Lysine modifications can also affect the stability of proteins. Modification of K56 and K151 of uncoupling protein 1 (UCP1) in brown fat reduces the protein activity as well as its half-life[126]. Of note, which lysines are modified are often context dependent, and therefore it is difficult to extend the effect of increased or decreased PTMs across different biological systems.

While acylation is thought to be largely unregulated, deacylation is known to be catalyzed by sirtuins. Acetylation is largely removed by SIRT3. SIRT5 is a weak deacetylase[127], and instead prefers negatively charged lysine modifications such as malonylation[127,128], succinylation[127,128] and glutarylation[129]. SIRT3, 4 and 5 are considered "mitochondrial" sirtuins[127], although SIRT5 additionally localizes to the cytosol[122], the nucleus[122] and peroxisomes[130]. Sirtuins utilize NAD^+ as cofactor, and therefore their activity is thought to reflect the intracellular concentration of NAD^+[131]. SIRT5 expression is upregulated by PGC1α and downregulated by AMPK in cultured mouse hepatocytes[132]. Induction in SIRT5 has been observed in hepatocytes of fasted rat[132] and hepatocytes of

high-fat diet (HFD) fed mice[133], but overall, regulators of SIRT5 levels and activity is relatively unknown.

1.9 Role of SIRT5 and PTMs in Regulating Glucose Metabolism

Regulation of glycolysis by SIRT5 is thought to be mediated mainly by malonylation, rather than other modifications, and its removal by SIRT5 activity[134]. Proteomics analysis of malonylated proteins have consistently identified glycolysis/gluconeogenesis to be one of the most significantly enriched for malonylated proteins[135]. Primary hepatocytes from SIRT5 KO mice demonstrated significantly decreased glucose oxidation and lactate production[123]. SIRT5 overexpression in HEK293 cells increases extracellular acidification rate (ECAR) and glucose oxidation in the context of high glucose (25 mM), although incubation in 5 mM of glucose normalized its glucose utilization rates comparable to control HEK293 levels[136]. Malonylation in general has been demonstrate to reduce protein activity, and therefore, SIRT5 KO results in increased malonylation levels and decreased glucose utilization. The increased glucose flux through glycolysis, however, is thought to be mainly converted to lactate instead of entering the TCA cycle as PDH as decreased succinylation of PDH reduces its activity[122]. From these findings, SIRT5 likely promotes aerobic glycolysis in many biological contexts.

SIRT5 also activates the pentose-phosphate pathway by increasing the activity of enzymes in the pathway; deglutarylation of glucose-6-phosphate dehydrogenase[137], desuccinylation of isocitrate dehydrogenase I (IDH1) which increases NADPH production[137], and increased shunting of glucose from glycolysis to the pentose-phosphate pathway by demalonylating triose-phosphate I (TPI1) and reducing its activity[138]. The result of SIRT5 activation of pentose-phosphate pathway is increased

reducing equivalents of reduced glutathione and ribose-5-phosphate for nucleotide synthesis.

In summary, SIRT5 increases glucose utilization, and malonylation has been identified in many studies to be the PTM enriched in glycolysis and gluconeogenesis.

1.10 Role of SIRT5 and PTMs in Regulating Fatty Acid Oxidation

FAO occurs in the mitochondria, and its enzymes are modified by acetylation, succinylation and malonylation. β-oxidation metabolic proteins are frequently identified in functional enrichment analysis in biological contexts that induce hypermalonylation or hyerpersuccinylation such malonyl-CoA decaryboxylase deficiency (MCD)[139], succinyl-CoA ligase deficiency[140], and SIRT5 KO tissues (heart and liver)[119,120]. Hypermalonylation or succinylation of these enzymes has been associated with reduction in their activity. MCD KO fibroblasts demonstrate reduced oxygen consumption with octanylcarnitine/malate incubation[139]. Succinylation of K351 in Enoyl COA hydratase (ECHA) leads to reduction in activity[120] and succinylation of very long-chain specific acyl-CoA dehydrogenase (VLCAD) at K507[141], in particular, leads to decreased binding of the enzyme to cardiolipins. Hearts of SIRT5 KO mice demonstrate accumulation in long-chain acyl-CoA, consistent with reduction in FAO activity. In mice fed with a diet high in coconut oil (C_{12} triglycerides), SIRT5 KO mice develop periportal hepatic steatosis due to reduction in mitochondrial FAO[142].

A recent study demonstrated that SIRT5 KO mice are resistant to AKI, and Chiba *et. al.,* proposed that increased peroxisomal FAO in SIRT5 KO mice is responsible for maintenance of FAO in the context of mitochondrial distress in proximal tubules[143]. The increase in peroxisomal FAO is attributed to the increased level of peroxisomal FAO

enzyme levels such as Acyl-CoA Oxidase 1 (ACOX1), and not specifically due to increased PTMs in the peroxisomes due to SIRT5 KO. This increase in peroxisome FAO machinery in proximal tubules was proposed to serve as compensation for decreased mitochondrial FAO from SIRT5 KO. However, SIRT5 has been demonstrated to inhibit ACOX1 via desuccinylation in hepatocytes, resulting in reduced H_2O_2 production and its fatty acid desaturation activity[130]. As ACOX1 serves as the first and rate limiting step in peroxisomal β-oxidation, SIRT5 likely reduces peroxisomal β-oxidation via desuccinylation.

In summary, SIRT5 increases mitochondrial FAO and may reduce peroxisomal activity. In certain biological contexts, compensatory peroxisomal FAO may increase in SIRT5 KO or hyperacylation conditions.

1.11 Malonylation and Succinylation Roles in Regulating Metabolism

Whether PTMs can actually mediate significant metabolic changes especially *in vivo* is heavily debated. The abundance of non-enzymatically acylated PTMs in the proteome is low. Stringent quantitative proteomics studies of acetylation sites have found low stoichiometry (<1%) in most acetylated sites and proteins with higher acetylation rates (>1%) are generally found on nuclear proteins, such as histones and acetyltransferases[144–146]. Studies of malonylation and succinylation stoichiometries are relatively limited, but stable isotope labeling by amino acids in cell culture studies have found similar stoichiometric levels for both modifications as acetylation (<1% for most sites)[122,139], but higher levels have been found in certain proteins. Absolute peptide quantification using synthetically generated peptide standards are less commonly performed, but likely generate the most accurate quantification of the modified and

unmodified peptide for a specific protein. Using this approach, Bruning *et. al.,* determined that 4.5% of mTORC1 was malonylated in fatty acid synthase (FASN) knock-down endothelial cells[147]. Researchers have proposed that it is the cumulative modification of proteins within a pathway, gain-of-function, and disruptions in protein degradation and/or protein aggregation from these lysine modifications that are responsible for the PTM mechanism of action despite the overall low stochiometry[148].

Consistent with the idea that these low-level PTMs are stochastically generated modifications that have very little biological consequence, whole-body SIRT5 KO and OE mice are phenotypically similar to their wildtype (WT) counterparts despite changes in their acylation levels[133,149]. SIRT5 KO mice demonstrate mild age-related cardiomyopathy and reduced ejection fraction[120]. Whole-body SIRT5 KO challenged with HFD demonstrated no significant differences with regards to body weight, fat and lean body mass, and energy expenditure. Slight improvements in systemic glucose metabolism were observed with intraperitoneal insulin tolerance test (ipITT) and intraperitoneal glucose tolerance test (ipGTT) for the DIO SIRT5 KO mice[149]. On the other hand, SIRT5 global OE mice demonstrated no differences in any of the metabolic parameters, including ipGTT. Study of SIRT3, SIRT5, and MCD cardiomyocyte specific KO mice, which all contribute to increased PTM levels, found minimal effect on metabolism in all three models; these models demonstrate only slightly decreased ATP production[150].

However, tissue-specific knock-out of SIRT5 or various disease states induced in SIRT5 KO mice demonstrate significant phenotypic differences compared to their WT counterparts. For example, pressure-induced cardiac hypertrophy with transverse aortic constriction (TAC) leads in SIRT5 KO mice results in significant cardiac myopathy,

reductions in cardiac output, and increased mortality in comparison to their WT mice[151], although this result has been proposed to be dependent on the mechanism of TAC induction[152]. Brown adipose tissue (BAT) specific KO of SIRT5 leads to reduction in BAT energetic capacity, attributed due to increased UCP1 malonylation, and results in alterations to systemic metabolism such as reduced glucose tolerance from ipGTT[126]. However, it is unclear whether these phenotypes are due to SIRT5 regulation of metabolic proteins.

1.12 Role of Sirtuin 5 in Obesity and Diabetes

Obesity and/or diabetes often results in elevated levels of post-translational modifications, thought to be as a result of increased levels of metabolic substrates for acylation. In diabetes, increased malonyl-CoA levels are found in the muscle and is partly responsible for reduction in FAO activity as malonyl-CoA itself negatively regulates CPT-1a activity. The increased level of PTMs derived from metabolic intermediates has been termed “carbon stress[135].” Whether carbon stress results in significant contributions to disease pathogenesis requires further investigation. Increased malonylation occurs in *db/db* and *ob/ob* mice livers[153], although HFD feeding in another study resulted in decreased malonylation[133], thought to be due to increased fatty acid oxidation and reduced malonyl-CoA production. In the *db/db* mice[154], diet-induced obesity (DIO) model, and POMC deficient hyperphagic mice[155], increased malonylation occurs in chondrocytes. SIRT5 KO mice, which also display increased malonylation and succinylation in chondrocytes, exhibited increased joint dysfunction and early osteoarthritic phenotype, correlating PTM accumulation with tissue dysfunction[155]. Conversely, liver-specific SIRT5 OE in the *ob/ob* background found decreased hepatic

steatosis and reduced hepatic triglyceride content[156], consistent with decreased PTM levels with improved tissue function.

1.13 Role of SIRT5 in Kidney Disease

Unlike SIRT1[157] or SIRT6[158], absence of SIRT5 does not appreciably affect kidney development and function in mice. SIRT5 KO mice demonstrate increased plasma ammonia levels due to decreased carbamoyl phosphate synthase 1 (CPS1) during prolonged fasting, but the reduction in CPS1 activity and its effect on the kidney is unknown.[149] Reduction in SIRT5 levels results in resistance to AKI in mice, attributed due to basal compensatory increase in peroxisomal FAO in the SIRT5 KO mouse proximal tubules[143], although reduction in SIRT5 levels in cultured human epithelial cell line results in mitochondrial fragmentation and disruptions in fission and fusion machinery[159].

The role of SIRT5 in DKD is unknown. In this thesis, we explored the role of SIRT5 in DKD. We initially hypothesized that increased SIRT5 expression that occurs in the diabetic kidney cortex is detrimental to proximal tubules. We hypothesized that upregulation of glucose utilization, particularly upregulated aerobic glycolysis, will lead to generation of unwanted metabolic glucose-derived byproducts and lead to cellular reprogramming that destabilizes proximal tubules. In our HFD-STZ model, we found that SIRT5 OE mice are relatively protected from DKD, although the mechanism for its protection is unclear and metabolic differences between SIRT5 WT and OE mice were not observed. We suspect that the pleiotropic mechanism of action of SIRT5 leads to alterations in many cellular functions that confer protection in early DKD. Some of these mechanisms are discussed in chapters 2 and 3. However, whether SIRT5 plays a

significant role in DKD pathogenesis or is ultimately a maladaptive force in proximal tubular health in DKD requires further research.

1.14 Commentary on LC-MS Metabolomics as a Method in Studying Metabolism

Metabolomics can be conducted using a variety of techniques. Liquid chromatography-mass spectrometry is however the most used analytical method in metabolomics. LC-MS requires comparatively little processing for samples and provide high reproducibility when combined with quality-control strategies. The high sensitivity of LC-MS requires minimal amounts of sample, making it ideal for clinical studies of patient samples. The relative advantages and disadvantages of other analytical techniques have been briefly outlined in table 2.

Method	Advantages	Disadvantages
Nuclear magnetic resonance	Uniquely suited to be able to identify the chemical locations of isotopically labeled nuclei in isotopic labeling studies (fluxomics)	Low sensitivity
Matrix-assisted laser desorption ionization-time of flight mass spectrometry	Localize measured metabolites to sub-tissue structures; it has been used to provide glomerular and tubulointerstitial metabolite information in the kidney	Can be poorly reproducible; results variable depending on prepared matrix
Direction-infusion (shotgun) lipidomics	Average more mass scans to achieve better signal-to-noise ratio and accomplish more sophisticated structural analysis of lipids	Lack of chromatographic separation means loss of retention time information and matrix effects, which occurs in complex biological samples
Gas-chromatography tandem mass spectrometry (GC-MS)	High-reproducibility	Extensive sample preparation and derivatization, which is time-

		consuming and potentially results in irreproducibility.
Ion-mobility spectrometry (IMS)	Orthogonal separation method to GC and LC, can be used to separate lipid isomers Can be added to other separation workflows as an additional separation method	Depending on the IMS method and design, low sensitivity due to the ion-mobility compartment
Liquid-chromatography tandem mass spectrometry (LC-MS)	Relatively minimal sample preparation, high sensitivity	Reproducibility can depend on chromatography methods

Table 1-1 Relative advantages and disadvantages of alternative metabolomics analytical methods to LC-MS.

Table created with references: [160–168]

All of our studies have been conducted with LC-MS. Although LC-MS technology has made immense technological advancements in terms of its application to biological studies, several large issues remain and need to be addressed for reproducible and meaningful data acquisition and analysis. A large issue we had to address in our studies was LC separation of polar metabolites with sufficient peak resolution and shape that allowed for metabolite quantification. Polar metabolite separation was accomplished with hydrophilic interaction chromatography (HILIC), which in our past experience is a relatively irreproducible method. New developments in zwitterionic columns and phosphate additives that improve peak shape[169,170] were crucial in our metabolomics experiments.

Another issue in metabolomics is the lack of internal standards for every compound and that extraction processes such as sample drying can lead to conversion of compounds such as NADPH and reduced glutathione to $NADP^+$ and oxidized glutathione disulfide[171]. Careful optimization of samples processing methods for each metabolite of

interest and comparing ratios of metabolites, such as malonyl-CoA/CoA ratio or $NADP^+$/NADPH levels, may better reflect relative levels of such metabolites in samples.

1.15 Thesis Aims

Aim 1: Characterize the targets and metabolic role of decreased malonylation and increased SIRT5 expression in proximal tubules in *db/db* mice.

For aim 1, I characterized the differences in the PTM malonylation in the cortex of *db/+* and *db/db* mice. I identified that malonylation is significantly reduced in the *db/db* cortex, specifically in proximal tubules and that this decrease is likely driven by increased SIRT5 expression and not due to reduction in substrate or cofactor levels. Fractionation studies of the mice kidney cortex also demonstrate that this decrease is exclusive to the cytosolic fraction of the cortex. Proteomics analysis of malonylated peptide with immunoaffinity enrichment demonstrated that proteins with significantly decreased malonylation in *db/db* cortex were enriched in glycolytic proteins and peroxisomal proteins, in particular peroxisomal FAO proteins. Overexpression of SIRT5 in HK-2 cells leads to increased aerobic glycolysis, as demonstrated by increased $^{13}C_6$-glucose-derived metabolite labeling of glycolytic intermediates, but decreased labeling of mitochondrial $^{13}C_6$-glucose-derived metabolites. Knock-down of SIRT5 in HK-2 cells results in the converse to the SIRT5 overexpression. The aforementioned findings and data are presented in chapter 2.

Aim 2: Assess the effect SIRT5 knockout or overexpression on DKD pathogenesis

For aim 2, I generated diabetic mice models of whole-body embryonic SIRT5 KO and OE mice with HFD-STZ. The OE mice were aged to 36 weeks of age and the SIRT5 OE mice exhibited decreased urinary ACR, kidney injury molecule (KIM1) to creatinine

ratio, and neutrophil gelatinase (NGAL) to creatinine ratio, suggesting that increase in SIRT5 levels ameliorate DKD. Tissue fibrosis was mild and not significantly different between the WT and OE mice, likely due to the mild kidney disease from the protective effect of the mouse genetic background. SIRT5 KO and WT mice did not develop robust and sustained hyperglycemia, with higher STZ doses leading to development of hepatic non-alcoholic fatty liver disease and progression into what is likely hepatic carcinoma. These findings and data are presented in chapter 3.

Aim 3: Elucidate if metabolic reprogramming in DKD leads to elevations in production of potentially harmful metabolic by-products.

For aim 3, I investigated whether metabolic reprogramming that occurs in DKD may lead to increased production of the metabolic by-products L and D 2-HG. I found significantly increased urinary excretion of both L and D 2-HG from *db/db* mice. Percent fractional excretion for both isomers were elevated, suggesting that increased urine 2-HG levels are due to increased kidney production or secretion of the metabolites and not due to increased systemic production or increased renal filtration. Further investigation demonstrated that 2-HG levels are elevated likely due to significantly increased levels TCA cycle metabolites, including the 2-HG precursor α-ketoglutarate, as demonstrated by tissue measurement of TCA cycle metabolites from *db/+* and *db/db* kidney cortex and HK-2 cells incubated with normal and high glucose media. These findings are data are presented in chapter 4.

Aim 4: Investigate whether differences in glucose utilization can serve as a potential biomarker of human DKD.

For aim 4, I assessed how glucose is metabolized by healthy human subjects, T1D patients with no microvascular complications, and T1D patients with established DKD. Urine samples from study subjects from three groups were collected while the subjects underwent euglycemic and hyperglycemic clamp studies with $^{13}C_6$-glucose. The study was conducted to answer how glucose metabolism differs between the three groups at blood glucose concentrations of 100 mg/dl (euglycemic) and 300 mg/dl (hyperglycemic) conditions. The urine samples were analyzed for ^{13}C labeling in glycolytic and TCA cycle metabolites. Urinary metabolites from the euglycemic clamp portion of the study demonstrated minimal labeling. Urinary metabolites from the hyperglycemic clamp portion demonstrated significantly elevated ^{13}C labeling in TCA cycle metabolites and lactate in the healthy control group in comparison to the T1D DKD and T1D no microvascular complication groups. Although no significant differences between T1D DKD and T1D no microvascular complication groups, the difference in incorporation between the control and T1D DKD groups were significant in more metabolites than with the healthy control and T1D no microvascular complication group. These findings are presented in chapter 5.

Chapter 2

Decreased Malonylation in Non-Mitochondrial Pathways in the *db/db* Kidney Cortex

2.1 Abstract

Early diabetic kidney disease (DKD) is marked by dramatic metabolic reprogramming due to nutrient excess, mitochondrial dysfunction, and increased renal energy requirements from hyperfiltration. We hypothesized that changes in metabolism in DKD may be regulated by Sirtuin 5 (SIRT5), a deacylase that removes post-translation modifications derived from acyl-coenzyme A and has been demonstrated to regulate numerous metabolic pathways. We found decreased malonylation in the proximal tubules of *db/db* mice, likely due to the increased SIRT5 expression. Proteomics analysis of malonylated peptides found that proteins with significantly decreased malonylated lysines in the *db/db* cortex were enriched in non-mitochondrial metabolic pathways: glycolysis and peroxisomal fatty acid oxidation (FAO). Overexpression of SIRT5 in cultured human proximal tubules demonstrated increased aerobic glycolysis with increasing SIRT5 levels, and conversely with decreased SIRT5 expression, suggesting that SIRT5 may lead to metabolic reprogramming in tubules in DKD.

2.2 Introduction

DKD is the most prevalent etiology of ESRD accounting for ~40% of all ESRD cases in the United States[172]. Until recently, the mainstay of treatment has been renin-angiotensin aldosterone (RAAS) inhibitors; sodium-glucose co-transporter 2 (SGLT2) inhibitors have demonstrated to be protective against disease progression, superior to only glycemic and blood pressure control[59,60,173,174]. Although the mechanism of SGLT2 inhibitors is multifold, the reduction in glucose load into proximal tubules underscores the fact that preserving metabolic homeostasis of proximal tubules may be an important mechanism in treatment of DKD.

Proximal tubules undergo significant metabolic reprogramming in DKD. Under normal physiologic conditions, proximal tubules prefer fatty acids and glutamine and demonstrate low capacity for glucose utilization[175]. In DKD, proximal tubules upregulate glucose utilization, potentially to supplement energy production in the context of mitochondrial dysfunction that occurs in DKD. DKD is associated with increased urinary lactate production[86–89], and metabolomics studies of patient urine samples demonstrate reduction in TCA cycle metabolites in patients with DKD and decreased level of these mitochondrial metabolites to predict DKD progression. Our previous *in vivo* metabolic flux study demonstrated that glucose utilization is increased in the cortex (~80% proximal tubules by volume[176]) in the B6.BKS(D)-Lepr db/J mice, a pathophysiologically relevant model of T2D DKD[85]. This increase in glucose occurred concurrently with increased pyruvate and palmitate catabolism and reduced mitochondrial ATP production capacity, supporting the idea that increased nutrient metabolism of many different substrates, not only glucose, occurs in the DKD cortex to accommodate mitochondrial dysfunction.

In a normal physiological setting, glycolysis and FAO are coordinated through the negative regulation of each respective metabolic enzymes by metabolic intermediates and products derived from the contralateral pathway. One mechanism by which glycolysis negatively regulates mitochondrial β-oxidation is malonyl-CoA mediated reduction in carnitine palmitoyl transferase 1 (CPT1) activity[177]. Another potential way by which malonyl-CoA modulates metabolic activity is by serving as substrate for PTMs that can alter protein activity. Malonylation is reversible covalent lysine modification by malonyl-CoA that can be removed by SIRT5. Malonylation has been found in many contexts to regulate glycolysis and gluconeogenesis[123,135,153,154,156]. SIRT5 KO cultured hepatocytes exhibited increased malonylation of glycolytic enzymes, which results in decreased glucose flux attributed to reduction in enzymatic activity of the modified enzymes[123]. Therefore, we hypothesized that malonylation contributes to altered glucose flux in DKD

Lysine can be modified by energetic intermediates other than malonyl-CoA such as acetyl-CoA, succinyl-CoA and glutaryl-CoA. Excessive accumulation of these modifications that ultimately perturb protein function, a phenomenon described as “carbon-stress,” may occur in diabetes and obesity at faster rates due to the nutrient overload that leads to increased generation of acylating metabolites and contribute to metabolic dysfunction[178]. Indeed, studies of *db/db* mice and other various murine models of obesity found increased malonylation of proteins in various tissues[153–155]. In contrast to these previous findings, we found decreased levels of malonylation in the *db/db* kidney cortex with increase in SIRT5 levels, suggesting a potential regulatory role of SIRT5 in DKD.

In this work, we present the targets of decreased malonylation in the *db/db* cortex and demonstrate that SIRT5 may be a regulator of extra-mitochondrial ATP production in DKD.

2.3 Results

2.3.1 Malonylation is Decreased in *db/db* Kidney Cortex Potentially Due to Upregulation in SIRT5 Levels

To determine whether PTM levels are altered in the *db/db* kidney cortex, we assessed the levels of various PTMs and found that malonylation levels, in particular, were significantly decreased in the diabetic kidney cortex (**Fig. 2-1 A, C**). In contrast, succinylation levels were not significantly different between the *db/+* and *db/db* kidney cortex (Fig. 2-1B, C), even though SIRT5 catalyzes removal of both malonyl and succinyl moieties. Cellular fractionation of the kidney cortex revealed that while levels of malonylated proteins were visually decreased in both mitochondrial and cytoplasmic compartments from the *db/db* mice (**Fig. 2-2**), the decrease in malonylation is only statistically significantly in the cytoplasmic compartment of *db/db* mice when the Western blot signal intenstities were normalized. In order to understand why malonylation levels are decreased in the *db/db* cortex, we assessed for the levels of SIRT5 by Western blot, and quantitatively measured by LC-MS kidney cortex levels of malonyl-CoA, which serves as the acylating substrate for malonylation, and the NAD+/NADH ratio, as NAD+ serves as the cofactor for SIRT5 catalytic activity. Malonyl-CoA levels (**Fig. 2-3C**) and NAD+/NADH (**Fig. 2-3D**) ratio were unchanged in the diabetic kidney cortex, whereas SIRT5 protein levels were significantly upregulated in the *db/db* cortex (**Fig. 2-3A, B**),

suggesting that SIRT5 activity, and not alterations in substrate or cofactor levels drive the decrease in malonylation.

2.3.2 Malonylation ss Decreased Specifically in Proximal Tubules in the *db/db* Kidney

Proximal tubules compromise of the majority of cells in the cortex, but also in the entire kidney by mass (~60% by mass)[30]. To confer that the changes in malonylation were primarily driven by proximal tubules, we conducted immunofluorescence (IF) analysis of malonylation residues in the *db/+* and *db/db* kidney cortex. Proximal tubules were identified with fluorescein labeled Lotus Tetragonolobus Lectin (LTL) which binds to the brush borders of proximal tubules. Malonylation-associated fluorescence was decreased in the *db/db* kidney proximal tubules (**Fig. 2-4A, B**), consistent with the Western blot data in Fig. 1. Quantification of malonylation-associated fluorescence in non-proximal tubules (without brush borders) demonstrated no significant differences in malonylation levels between the control and diabetic kidneys (**Fig. 2-4A, C**).

Immunoaffinity enriched proteomics for malonylated peptides identifies metabolic pathways with significantly decreased malonylated enzymes in the db/db kidney cortex

To identify differentially malonylated proteins in the *db/+* and *db/db* kidney cortex, we enriched for malonylated peptides with pan-antimalonyllysine antibodies and conducted label-free proteomics analysis. For relative quantification, we used Skyline MS1 filtering with normalization to a spiked heavy-labeled malonylated peptide standard, as previously published[123,179]. In total, we found 1719 malonylated peptides, of which 199 peptides exhibited significantly higher levels of malonylation in the *db/db* cortex, whereas 259 peptides exhibited significantly lower levels of malonylation levels in the *db/db* cortex

(**Fig. 2-5A**). Using DAVID functional enrichment analysis with KEGG pathway as the search database, pathways significantly enriched for peptides with significant downregulation of malonylation included “peroxisomes”, “ribosomes”, “pyruvate metabolism”, “glycolysis/gluconeogenesis” and “glutathione metabolism” (**Fig. 2-5B**). Glycolytic targets in our assay with significantly decreased malonylation included aldolase A and B (**Fig. 2-6A**), and assessment of aldolase activity from *db/db* and *db/+* cortex demonstrated higher relative activity in the diabetic conditions (**Fig. 2-6B**), consistent with previous findings. Peroxisomal targets were the most significantly enriched according to the functional enrichment analysis, and a manual examination of the individual members demonstrated many of the proteins with decreased malonylation were involved in peroxisomal FAO (**Fig. 2-7**).

2.3.3 SIRT5 Increases Glucose Flux into Glycolysis and Decreases Flux into the TCA Cycle in HK-2 Cells

Increased SIRT5 expression has been associated with increased glucose flux in multiple contexts. In order to assess the role of SIRT5 in glucose metabolism in proximal tubules, we either overexpressed SIRT5 with lentiviral vector or knocked down SIRT5 with siRNA in human proximal tubules (HK-2). We then supplemented the cell culture media with 5 mM of $^{13}C_6$- glucose and allowed cells to metabolize the labeled glucose for 30 min, 2 hrs and 4 hrs. Glycolytic and TCA cycle metabolites were then analyzed on a quadrupole time-of-flight mass spectrometer and relative abundances for isotopologues due to $^{13}C_6$- glucose catabolism. We found that overexpression of SIRT5 in HK-2 leads to increased labeling of glycolytic metabolites such as pyruvate (M+3; **Fig. 2-8A**) but decreased labeling of TCA cycle intermediates such as fumarate and citrate/isocitrate

(M+2; **Fig. 2-8B, C**). In contrast, SIRT5 knock down led to decreased labeling of glycolytic intermediates such as fructose-6-phosphate (M+6; **Fig. 2-9A**), but increased labeling of TCA cycle intermediates such as α-ketoglutarate and citrate/isocitrate (M+2; **Fig. 2-9B, C**), suggesting increased glucose derived intermediate entry into the TCA cycle. We interpret these findings to mean that SIRT5 increases glucose metabolism into lactate and reduces pyruvate entry into mitochondria; indeed, previous studies have demonstrated that SIRT5 decreases activity of pyruvate dehydrogenase through desuccinylation[122]. Decreased SIRT5 levels lead to increased glucose metabolism through the mitochondria despite overall decreased levels of glucose flux into glycolysis. Of note, we did not find significant differences in lactate labeling in either condition, likely due to extracellular release of lactate and the near 100% rapid labeling of lactate (M+3) with the labeled glucose in both SIRT5 overexpression and knock down.

2.3.4 Sirt5 Expression is Elevated in the Tubulointerstitium off Diabetic Pima Indian Patients

In order to assess whether elevated SIRT5 levels are also observed in human DKD, we compared SIRT5 transcript levels derived from kidney biopsies of healthy control living donors (LD) and Southwestern American Indian T2D patients with DKD (**Fig. 2-10**). SIRT5 transcript levels derived from the glomerular compartment of the kidney were unchanged between the two groups, whereas SIRT5 transcript levels from the tubulointerstitial compartment were elevated, suggesting tubulointerstitial specific increase in SIRT5 in T2DKD patients.

2.4 Discussion

In summary, we found decreased malonylation in proximal tubules of *db/db* mice that is likely mediated by increased SIRT5 protein levels. Proteomic analysis of malonylated peptides from *db/db* and *db/+* cortex demonstrated that proteins with significantly decreased malonylation were enriched in glycolysis/gluconeogenesis and peroxisomes, consistent with the fractionation data that demonstrates a reduction in malonylation levels specifically in the *db/db* cortex cytosol. Overexpression of SIRT5 in HK-2 cells levels was associated with increased glucose utilization but reduced glucose-derived pyruvate shunting into TCA cycle metabolites. Reduction of SIRT5 levels in HK-2 cells was associated with the converse, suggesting that SIRT5 contributes to aerobic glycolysis in HK-2 cells.

Our findings support the hypothesis that the decreased malonylation observed in the *db/db* cortex results in increased glucose flux observed from our *in vivo* flux studies. Absence of SIRT5 and increased malonylation has been demonstrated to result in decreased glycolytic rate in cultured hepatocytes[123] and chondrocytes[154] from SIRT5 KO mice. Glucose utilization is upregulated in HEK293 cells with SIRT5 overexpression, only under high glucose (25 mM) conditions and not normoglycemic conditions (5 mM), suggesting that SIRT5 may only regulate glucose utilization in hyperglycemic conditions[136].

The role of SIRT5 in diabetes and obesity is not well understood. Increased malonylation occurs in *db/db* and *ob/ob* mice livers[153], although HFD feeding in another study resulted in decreased malonylation[133], thought to be due to decreased malonyl-CoA production due to increased lipid consumption. In the *db/db* mice[154], diet induced obesity

(DIO) model, and POMC deficient hyperphagic mice[155], increased malonylation occurs in chondrocytes. SIRT5 KO mice, which also display increased malonylation and succinylation in chondrocytes, exhibited increased joint dysfunction and early osteoarthritic phenotype, correlating PTM accumulation with tissue dysfunction[155]. Conversely, liver-specific SIRT5 OE in the *ob/ob* background found decreased hepatic steatosis and reduced hepatic triglyceride content[156], consistent with decreased PTM levels with improved tissue function. SIRT5 mice treated with STZ to generate T1D demonstrate no appreciable impact on diabetic retinopathy, but SIRT5 and SIRT3 double knock-out diabetic mice demonstrated inner retinal dysfunction[180]. Therefore, data suggests that hyperacylation and/or absence of SIRT5 levels contribute to tissue dysfunction, particularly in the context of metabolic diseases.

The increased level of SIRT5 we observed in the in the *db/db* cortex may therefore be an adaptive mechanism to reduce excess PTMs in DKD. Reduction in the malonylation of glycolytic enzymes, thereby increasing glucose flux through the entirety of glycolysis, may prevent glucose shunting into secondary pathways such as the polyol pathway and methylglyoxal pathway that generate toxic metabolic byproducts. This mechanism of upregulating glycolysis may be particularly important in proximal tubules, which have little innate glycolytic capacity[79–82], and thus benefit from any compensatory mechanisms to allow for proper glucose metabolism in DKD. SIRT5 also increases aerobic glycolysis, which generates energy without burdening the mitochondria. Mitochondria from the *db/db* mice cortex at 24 weeks of age demonstrate significantly elevated TCA cycle, suggesting that mitochondrial overload in early DKD[85,181].

However, the increased SIRT5 levels in the kidney cortex may instead be detrimental. As SGLT2 inhibitors have demonstrated, decreasing glucose uptake by proximal tubules leads to disease amelioration. SIRT5 encourages glucose metabolism. Furthermore, aerobic glycolysis is associated with cellular hypertrophy and proliferation, fibroblast activation[94,95] and epithelial-mesenchymal-transition[93], which are all processes that contribute to DKD pathogenesis and progression. A recent study demonstrated that SIRT5 KO mice are protected from different forms of AKI, attributed to the compensatory increase in peroxisomal FAO activity due to the dampened baseline mitochondrial β-oxidation from the SIRT5 deficiency[143]. The elevated peroxisomal FAO is thought to abrogate the loss in mitochondrial β-oxidation and dysfunction that occurs in AKI. From our proteomics analysis, peroxisomal proteins, in particular the peroxisomal fatty acid machinery, were prominently affected by decreased malonylation in the *db/db* cortex. Although the effect of decreased malonylation of the specific lysine of the peroxisomal proteins identified in our study is currently unknown, SIRT5 mediated desuccinylation of ACOX1 has been associated with decrease in its activity in hepatocytes[130]. In addition, acetylation of Enoyl-CoA Hydratase And 3-Hydroxyacyl CoA Dehydrogenase (EHHADH), has been associated with increase in its activity[182], and therefore decreased levels of another PTM may result in reduced activity, although the charge state of the two modifications are different.

In our study, we found that only malonylation, not succinylation, levels were decreased in the *db/db* cortex despite increased SIRT5 expression. In addition, the decrease in malonylation was compartment specific, occurring only in the cytoplasmic compartment at significant levels. A potential reason for this discrepancy is that

succinate[85,181] levels are significantly elevated in the *db/db* cortex and the rate of acylation offsets SIRT5 activity on mitochondrial succinylation. Another potential mechanism for the observed compartment specificity is that increased lactate production due to increased glucose flux and hypoxia in DKD may lead to increased NAD^+/NADH ratio, activating SIRT5 activity specifically in the cytosol.

Further research is necessary to understand the role of SIRT5 in proximal tubular physiology in DKD. A limitation in our study is that tubular metabolism is difficult to recapitulate in immortalized cell culture or isolated tubular culture systems. HK-2s readily metabolize glucose, and therefore it is difficult to ascertain whether our observations of SIRT5 expression and its role in glucose flux will translate to *in vivo* models. Future studies with SIRT5 mouse models of DKD will elucidate the role of SIRT5 in regulating metabolism in DKD.

We found increased SIRT5 transcript levels in the tubulointerstitium of the Southwestern American Indian T2 DKD cohort in comparison to the non-diabetic living donors, consistent with the rodent studies. Further assessment of whether SIRT5 levels are similarly elevated in other DKD cohorts and whether the level of SIRT5 expression can predict disease progression will aid in elucidating the importance of SIRT5 in DKD.

2.5 Materials And Methods

Materials: $^{13}C_6$ glucose was purchased from Cambridge Isotope Labs Inc. Human kidney 2 (HK2) cells were purchased from American Type Culture Collection (ATCC® CRL-2190™). LC–MS-grade water, acetonitrile (ACN), chloroform and methanol were obtained from Fisher Scientific. Malonyl-CoA and $^{13}C_3$-malonyl-CoA standards were

purchased from Sigma Aldrich. All other chemicals used in the study were purchased from Sigma Aldrich unless otherwise indicated.

Cell culture: Cells were cultured in DMEM/F12 (11320033, Gibco; Thermofisher) supplemented with 1% pen/strep (Invitrogen), and 10% FBS (FBS; Corning®) in humidified atmosphere of 5% CO_2 and 95% air at 37 °C.

Animals: Male BKS *db/db* mice (BKS.Cg-m +/+ Lepr db/J) and littermate controls (*db/+*) were purchased from Jackson Labs at 12 wks of age. Mice were housed in a climate-controlled, light-regulated facility with a 12:12 hour light-dark cycle with water and chow ad libitum. At 24 weeks of age mice were harvested. Prior to sacrifice, mice were fasted for 4 hrs. Kidney was perfused with ice-cold PBS through the left ventricle and the kidney was dissected for the cortex region on ice. All samples were snap frozen and stored at -80 °C until analysis. The study was conducted according to the guidelines of the University of Michigan Committee on Use and Care of Animals.

Western blot: Cells and tissues were lysed in lysis buffer (2% SDS (w/v), 10% glycerol, 60 mM Tris-HCl pH 6.8) with 1 µM trichostatin A (TSA; Cayman), 20 mM nicotinamide, and 1X HALT™ protease inhibitor cocktail (Thermofisher). Samples were sonicated briefly on ice and centrifuged for 10 min at 17,000 x g. The supernatant was collected and protein concentration was determined with DC protein assay (Bio-Rad). The lysates were separated by SDS-PAGE and transferred to PVDF membranes. Signals were then visualized with Pierce ECL reagent (Thermofisher). Antibodies against Pan anti-malonyllysine (PTM-901) and Pan anti-succinyllysine (PTM-401) were purchased from PTM biolabs. Antibodies against SIRT5 (8782) and β-Actin were purchased from (8H10D10) Cell Signaling Technologies.

Kidney malonyl-lysine Immunofluorescence: Kidney sections were fixed in 4% paraformaldehyde (Electron Microscopy Sciences) overnight at room temperature. Sections were paraffin-embedded and cut into 3 µm sections for analysis. Slides were de-paraffinized and incubated at 95 ºC in antigen-unmasking solution (H-3300, Vector laboratories) for 2 hrs. Sections were blocked and permeablized with 10% donkey serum and 0.5% tween-20, respectively. Sections were incubated with pan anti-malonyllysine (PTM-901, PTM-biolabs) and Lotus Tetragonolobus Lectin (LTL) tagged with Fluorescein (FL-1321-2, Vector laboratories) overnight at 4 ºC. Sections were then incubated with anti-rabbit IgG Alexa Fluor 647 (A-31573, Thermofisher). Resulting sections were visualized with Leica SP5 Confocal TCS Microscope. Semi-quantitation of IF malonylation signals was analyzed with Leica Application Suite Lite 2.6.3.

Aldolase B activity assay: Activity assay was performed according to the manufacturer's directions with freshly perfused and dissected kidney cortex from *db/db* and *db/+* mice (ab196994; Abcam).

Kidney cortex fractionation: Freshly dissected cortex were stored in PBS on ice and homogenized with Teflon homogenizer in isolating medium (230 mM mannitol, 70 mM sucrose, 5 mM EGTA pH 8.0, 10 mM K-HEPES pH 7.4, 20 mM NAM, 1 µM TSA, Protease inhibitor cocktail, 1 mM DTT). The homogenate was centrifuged at 1000 x g for 5 min at 4 ºC. The supernatant was centrifuged at 10,000 x g for 10 min and the resulting supernatant was collected as the cytosolic fraction. The pellet was resuspended in isolating medium and layered on 4 mL of 25% Percoll solution (GE healthcare; 90:10 Percoll: 2.5 M sucrose solution diluted 1:4 with 0.25 M Sucrose solution). The resuspension was centrifuged at 80,000 x g for 20 min at 4 ºC. The resulting lower layer

was collected as the mitochondrial fraction. The mitochondrial fraction was diluted with 30 mL with the isolating medium and centrifuged at 10,000 x g for 10 min. The resulting pellet was resuspended in 1X Laemmali buffer and sonicated before Western blot analysis. The cytosolic fraction was diluted 1:2 with 2X Laemmali buffer and sonicated before Western blot analysis. The samples were probed for malonyl-lysine residues as previously described.

Malonyl-CoA quantification: Malonyl-CoA was quantified by LC-MS as previously described[183]. Briefly, tissue was sonicated in 10% trichloroacetic acid with $^{13}C_3$-malonyl-CoA. After sitting on ice, samples were centrifuged at 4500 x g for 5 min at 4 °C and supernatant was extracted with 2:1 chloroform:methanol (*v/v*) The aqueous phase was dried under nitrogen and reconstituted in 10 mM ammonium acetate in water. For LC/ESI/MS/MS analysis, an Agilent 6410 triple quadruple MS system equipped with an Agilent 1200 LC system and ESI source was operated in positive ion mode. Malonyl-CoA (854.2 → 428.2 *m/z*) and $^{13}C_3$-malonyl-CoA (857.2 → 428.2 *m/z*) were detected in MRM mode and relative peak areas were obtained and normalized to tissue weight.

NAD^+ and NADH quantification: Kidney cortex tissues were pulverized and sonicated in 80:20 acetonitirile: water (pH 9.0 with ammonium hydroxide) containing $^{13}C_6$-nicotinamide for internal standard. The homogenate was incubated on ice for 5 min and centrifuged for 10 min at 17,000 x g at 4 °C. LC-MS analysis was performed on an Agilent system consisting of a 1290 UPLC module coupled with a 6490 QqQ mass spectrometer (Agilent Technologies, CA, USA). Metabolites were separated on SeQuant® ZIC-cHILIC (3µm, 100 x 2.1 mm; Merck) with the following gradient: 0 – 2.5 min at 95% B, 2.5 – 8.5 min at 25% B, 8.5 – 8.6 min at 95% B, 8.6 – 12.6 min at 95% B. Solvent A was 50 mM ammonium

acetate pH 8.0 in water and solvent B was 100% acetonitrile. Column temperature was set at 30 °C and flow rate was 0.3 mL/min. $^{13}C_6$-nicotinamide (129.1 → 85.1 *m/z)*, NAD^+ (664.1 →136 *m/z*), and NADH (666.1 → 136 *m/z*) were monitored in MRM mode. Data was collected in positive mode.

Malonylation proteomics peptide preparation: Kidney cortex was homogenized in 5% SDS, 50 mM TEAB pH 7.55 supplemented with 1 uM TSA and 20 mM nicotinamide using a dounce homogenizer. Samples were sonicated for 20 s three times with 1 min rest on ice between cycles. Homogenates were spun at 17,500 x g for 20 min and the supernatant was heated to 95 °C for 5 min to remove any residual protein activity. Protein concentration was measured with the DC protein assay kit. 25 mg of proteins was treated with 5 mM DTT and incubated at 37 °C for 30 min with shaking. Samples were cooled and treated with 15 mM iodoacetamide at room temperature for 30 min with shaking in the dark. The alkylation reaction was quenched with 15 mM additional DTT. Protein was crashed from the solution by adding 12% phosphoric acid to 10% final volume of the sample. 7 volumes of 90% methanol: 10% TEAB solution was added to the samples. Samples were centrifuged at 1,000 x g for 2 mins and the pellet was resuspended in 50 mM TEAB with 0.1% deoxycholate. Trypsin was added at 1:50 trypsin to peptide ratio (wt/wt) and samples were digested at 37 °C with shaking for 24 hrs. Peptides were precipitated by adding formic acid (FA) to resulting final concentration of 0.5% (v/v) and centrifuging the samples at 3,400 x g for 10 min. The supernatant was lyophilized for 24 hrs. The lyophilized peptides were resuspended in 0.1% FA in water and any precipitates were removed with centrifugation. The supernatant was neutralized to pH 7.0 with

ammonium hydroxide and the peptide concentration was quantified with the Thermofischer peptide quantification kit.

Affinity enrichment of lysine malonylated peptides: 9.5 mg of peptides were affinity enriched for malonylated peptides by incubation with anti-malonyllysine antibody conjugated to Dynabeads in IAP buffer (50 mM MOPS–NaOH, pH 7.2, 10 mM Na_2HPO_4 50 mM NaCl) with 0.1% NP-40 at 4 °C for 24 hrs. Pre-selection, 250 ρg of heavy-labeled Malonyl-lysine (Kmal) peptide standards were added to each sample. The Kmal heavy-labeled peptide standard was synthesized by the University of Michigan peptide core. The synthesized sequence was as follows: H2N-TV*DGPSG(K/Malonyl)LWR-OH (V*: Valine $_{13}C^5$, $_{15}N$). Beads were washed twice with IAP + 0.1% buffer, twice with IAP and once with water. Samples were eluted with 0.1% TFA in water three times. Samples were desalted using desalting spin column as per manufacturer's directions. Peptides were dried in a speed-vac for 1 hr and samples were stored at -80 °C until analysis.

Proteomics analysis: Peptides were dissolved in 25 µL 0.1% FA and 10 µL of the sample was injected for analysis. Peptides were separated on reverse phase Thermo Scientific Acclaim PepMap 100: 75 µm x 2 cm (C18, 3 µm bead, 100 Å pore size) trap column and Thermo Scientific Acclaim PepMap C18, 2 µm particle size, RSLC 75 µm x 25 cm column. Data was acquired with Orbitrap QExactive coupled to Thermo Scientific Easy nLC-1000 UHPLC. Samples were run using a 90 min gradient from 5% "B" to 35% "B". Buffer "A" was 0.1% FA in water and buffer "B" was 0.1% FA in acetonitrile. All data were acquired in positive mode with a lock mass of 445.12002 using data dependent acquisition with a 15 sec dynamic exclusion. MS1 data were acquired in profile mode at a resolution of 70,000 with a maximum time of 75 msec and a range of 350 to 1500 m/z. MS2 spectra

were acquired in profile mode at a resolution of 15,000 and maximum integration time of 75 msec. The isolation window was 1.6 *m/z* and the collision energy was 20.

Proteomics data analysis: RAW files for each sample were grouped and analyzed by MaxQuant (version 1.6.14.0). MS2 spectra were searched against the UniProt complete mus musculus database concatenated with reverse decoy database (downloaded on August 20, 2020; http://www.uniprot.org) using the Andromeda search engine. Search parameters included up to three missed tryptic cleavages (Trypsin/P); 20 ppm match tolerance for the orbitrap; and variable modifications for n-terminal acetylation, lysine acetylation, lysine malonylation, methionine oxidation and fixed modification for cystine alkylation. A false discovery rate cutoff of 1% was used at the protein, peptide and modification site for identification. MS1 quantitation was accomplished with Skyline v. 20.1.0.155. A spectral library of malonylated peptides was built with MaxQuant results. Digestion was set as Trypsin (KR/P) with 3 maxed missed cleavages. Peptides were filtered by minimum length of 8 and max length of 25. Peak areas were normalized to peak area of the spiked malonylated standard. Peptides with more than 2 missing data points in each group were excluded from the analysis. Missing values were imputed with half-minimum of the lowest value in the group if all of the values in one group were lower than the lowest value in the other group. Otherwise, missing values were imputed with the k-NN method. Resulting values were normalized and student's t-test with FDR correction was conducted to identify peptides that were significantly altered between the two groups. Data processing was conducted with Metaboanalyst 5.0.

Lentivirus SIRT5 overexpression: 2 x 10^5 HK-2 cells were plated on 100 mm plates and allowed to attach overnight. Cells were treated with lentivirus with 8 µg/mL of polybrene

at MOI of 10 in DMEM/F12 with 10% FBS and no antibiotics. After 72 hrs since induction, 5 x 10^5 cells were plated on 6-well plates into each well and allowed to attach over-night. Cells were serum fasted in DMEM/F12, 0.05% FBS and 1% pen/strep for 24 hrs prior to labeling experiments.

SIRT5 siRNA knock-down: 4 x 10^5 HK-2 cells were plated on 6-well plates and allowed to attach overnight. Cells were treated with 100 ρmol of negative control or SIRT5 siRNA (AM4611, 19661; Thermofisher) with lipofectamine® 3000 (Thermofisher) as manufacturer's instructions for 8 hrs. Media was changed to DMEM/F12, 10% FBS and 1% pen/strep for 16 hrs. Cells were then serum fasted in DMEM/F12, 0.05% FBS and 1% pen/strep for 24 hrs prior to labeling experiments.

Glucose flux studies: DMEM media containing glutamine and 5 mM $^{13}C_6$- glucose were added to serum fasted cells for 30 min, 2 hrs, and 4 hrs. After the designated time course, media was removed and cells were washed once with ice-cold 150 mM ammonium acetate in LC-MS grade water. Cells were then harvested with 200 µL of ice-cold methanol and frozen at -80 °C until sample preparation. For extraction, 200 µL of cold water was added to the cells and cells were scraped. The resulting homogenate was sonicated on ice for 10 sec. 400 µL of chloroform were added to the homogenated. Samples were centrifuged at 17,000 x g for 10 min and the resulting top layer was collected and taken to dryness under nitrogen.

Metabolomics analysis of flux studies: Samples were reconstituted in 30 µL of 2:1 ACN: water, filtered and 5 µL were injected for analysis. Samples were separated as previously described. Metabolites were analyzed on the Agilent 6456 quadrupole time-of-flight (Q-TOF) mass spectrometer coupled to Agilent 1290 LC. Data was collected in negative

mode, with gas temp at 225 °C, drying gas at 10 L/min, nebulizer at 40 psi, sheath gas temp 300 °C, and sheath gas flow at 12 L/min. Fragmentor was set at 125 V, skimmer at 65 V, and VCap at 3000 V. Authentic standards of all measured metabolites were run separately and spiked into pooled samples for verification of metabolite identity and retention time.

Data analysis and statistical analysis: Quality control samples were made by pooling all the samples in the queue and run intermittently to control for machine drift and sample stability. For targeted quantitative analysis, peak areas were extracted with Agilent Mass Hunter Workstation Software Quantitiative Analysis for QQQ version B.07.01. Peak areas were normalized to internal standard before quantification. For flux samples, data was processed through Agilent Profinder. Statistics were performed with GraphPad Prism 7. Data was analyzed using student's t-test or One-way ANOVA with Tukey's post-hoc correction.

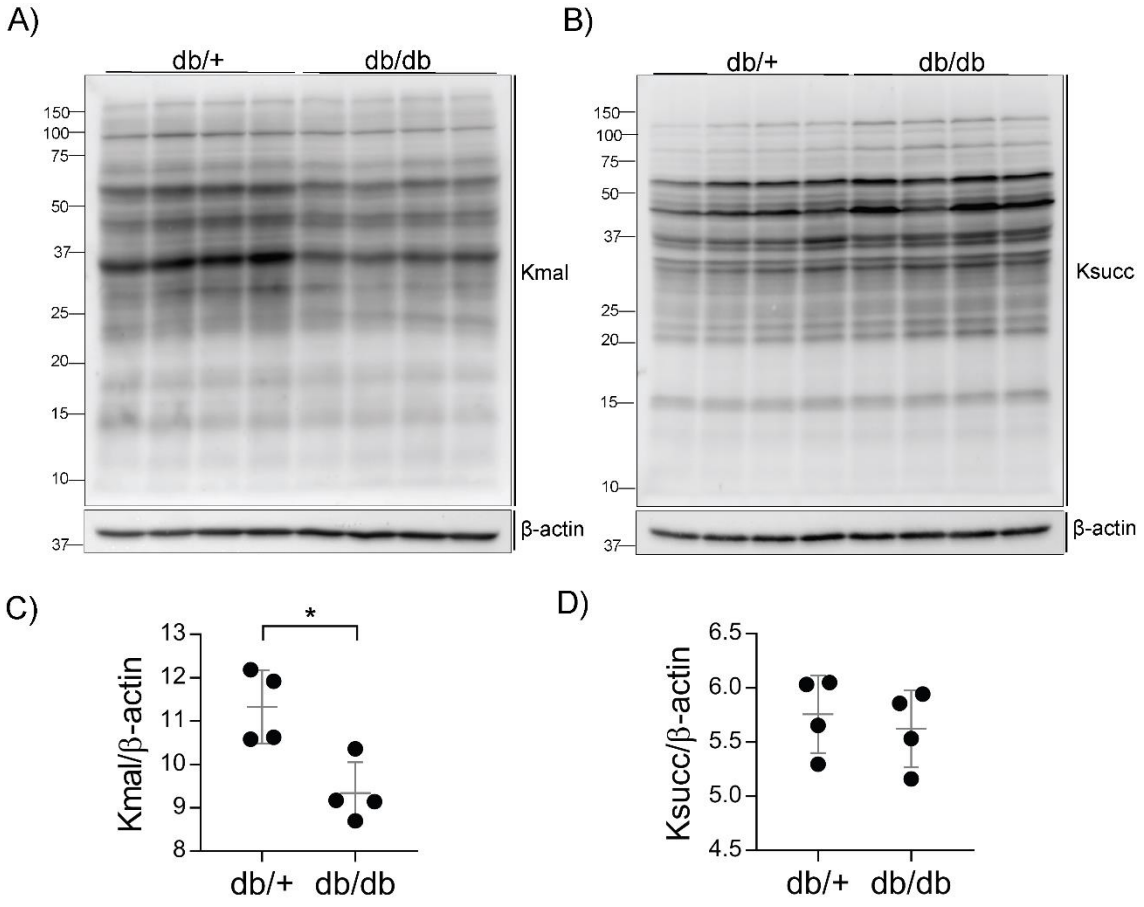

Figure 2-1 Malonylation is decreased in the *db/db* kidney cortex

A) Western blot of db/+ and db/db cortex lysate probed for Kmal residues. B) Western blot of *db/+* and *db/db* cortex lysate probed for Ksucc residues.C) Relative Western blot A) signal of Kmal normalized to normalized to β-actin. D) Relative Western blot B) signal of Ksucc normalized to normalized to β-actin. Student's t-test, *= $p \leq 0.05$.

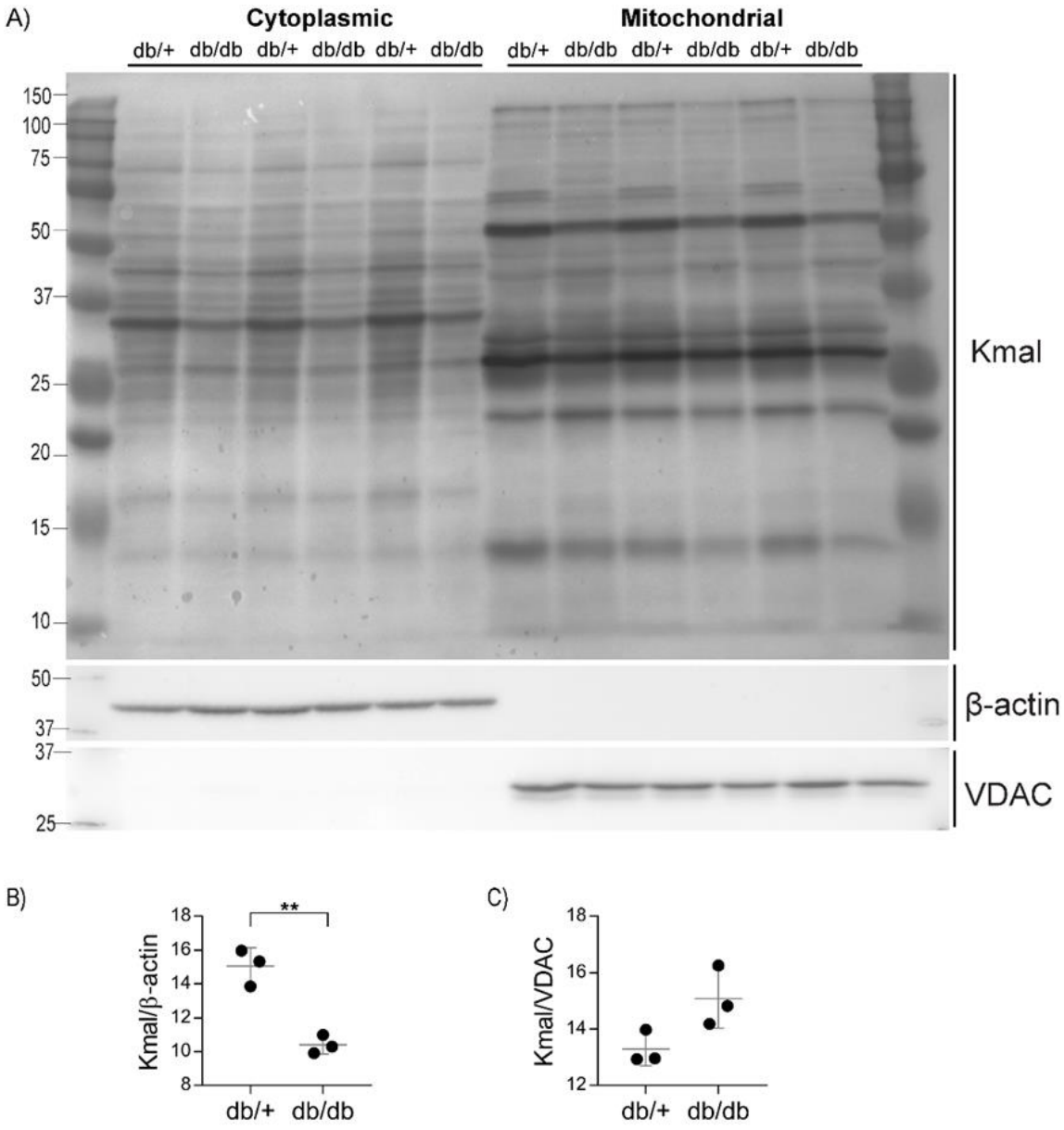

Figure 2-2 Compartment specific reduction in protein malonylation levels.

A) Western blot of proteins from the cytoplasmic and mitochondrial fractions *db/+* and *db/db* cortex probed for Kmal residues. B) Relative Western blot signal intensities normalized against β-actin for Kmal in the cytosolic fraction. C) Relative Western blot signal intensities normalized against VDAC for Kmal in the cytosolic fraction.

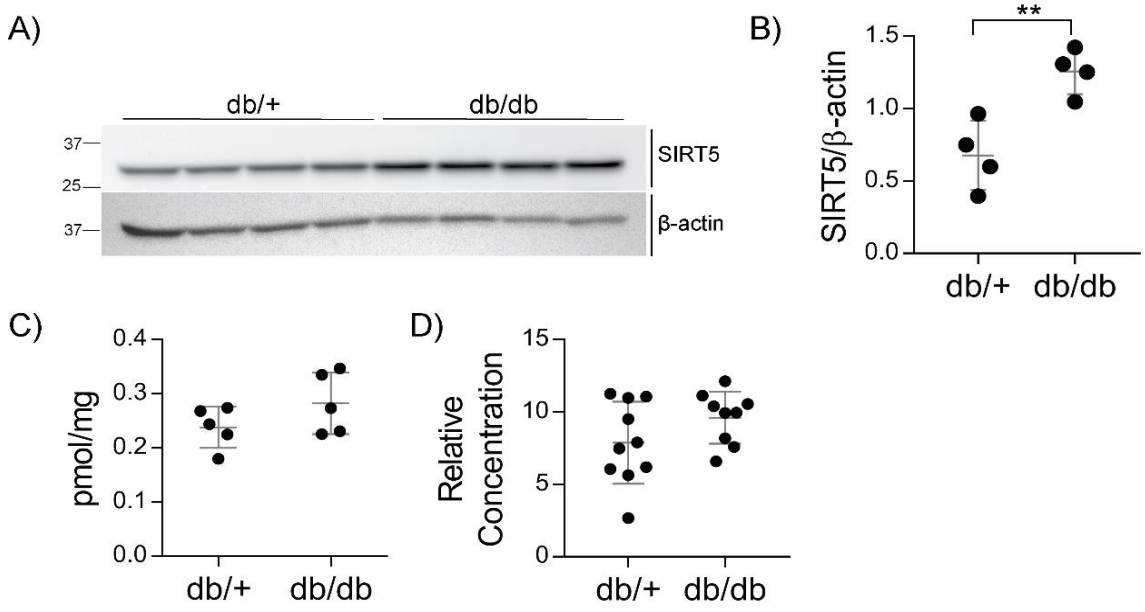

Figure 2-3 SIRT5 protein level is elevated in db/db kidney cortex

A) Western blot of *db/+* and *db/db* cortex lysate probed for SIRT5. B) Relative Western blot A) signal of SIRT5 normalized to β-actin. C) Malonyl-CoA concentration normalized to tissue weight from db/+ and db/db kidney cortex. D) NAD+/NADH concentration ratio from db/+ and db/db kidney cortex. Student's t-test, **= $p \leq 0.01$.

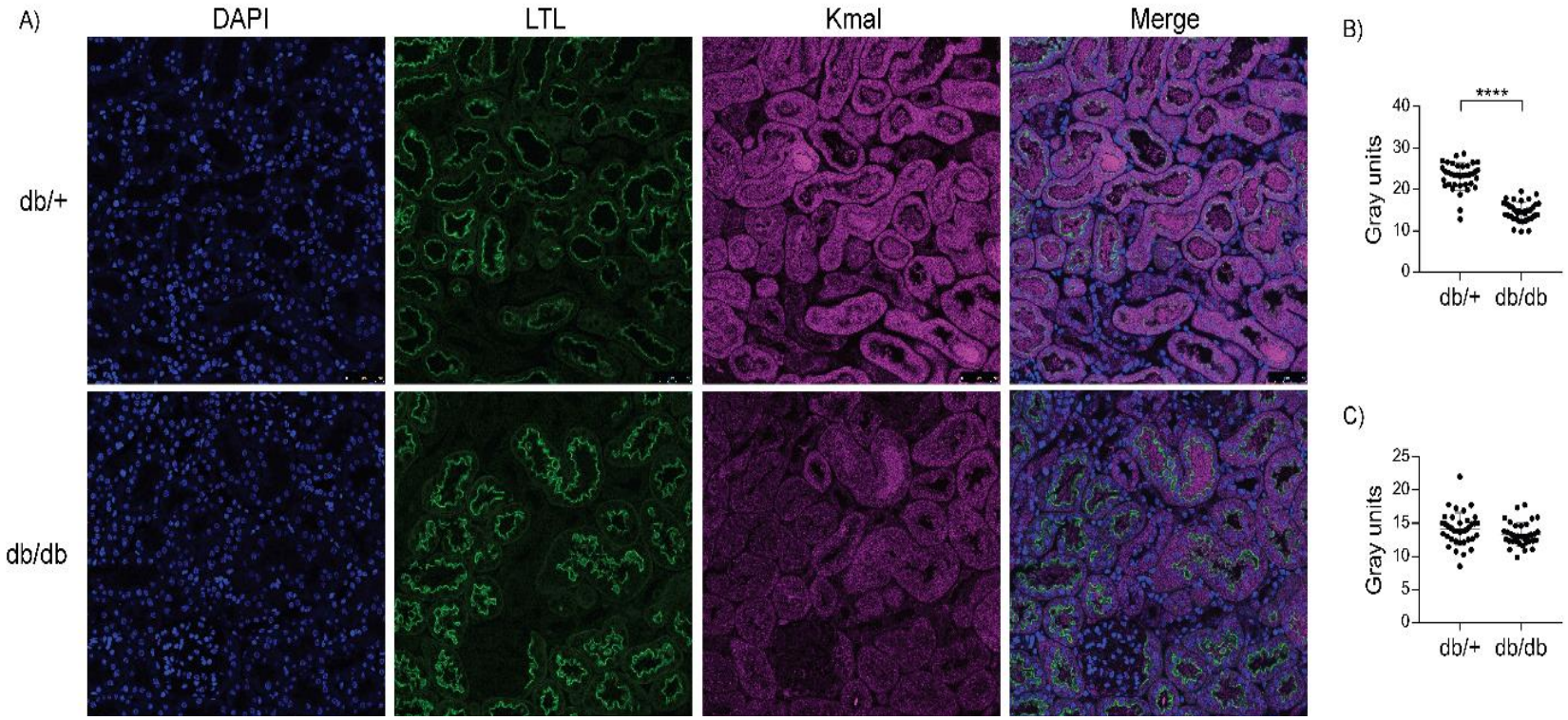

Figure 2-4 Immunofluorescence (IF) of Kmal residues in db/db and db/+ cortex

A) IF of db/db and db/+ cortex with DAPI for nuclear stain, lotus tetragonolobus lectin (LTL) for proximal tubular brush border stain, and Kmal for malonylated residues. B) Semi-quantitation of fluorescence associated with Kmal residues in proximal tubules. C) Semi-quantitation of fluorescence associated with Kmal residues in non-proximal tubules. n = 4, Student's t-test, ****= $p \leq 0.0001$.

A)

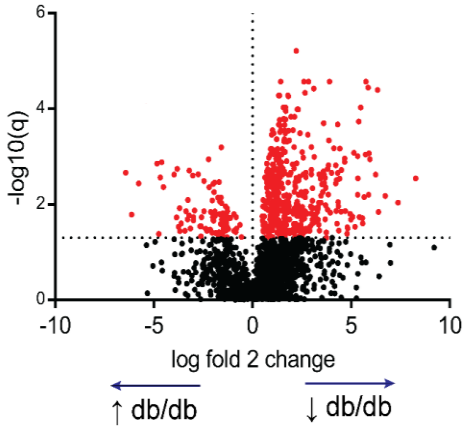

B)

Term	FDR (q-value)
mmu04146:Peroxisome	1.3E-06
mmu03010:Ribosome	6.8E-06
mmu00620:Pyruvate metabolism	1.5E-04
mmu00010:Glycolysis / Gluconeogenesis	1.1E-03
mmu00480:Glutathione metabolism	1.6E-03

Figure 2-5 Immunoaffinity enriched proteomics for malonylation

A) Volcano plot of malonylated peptides identified in the proteomics study. Peptides that were above the FDR cut-off of 0.05 are highlighted in red. B) List of top metabolic pathways with decreased malonylated proteins in db/db kidney cortex obtained with DAVID functional annotation

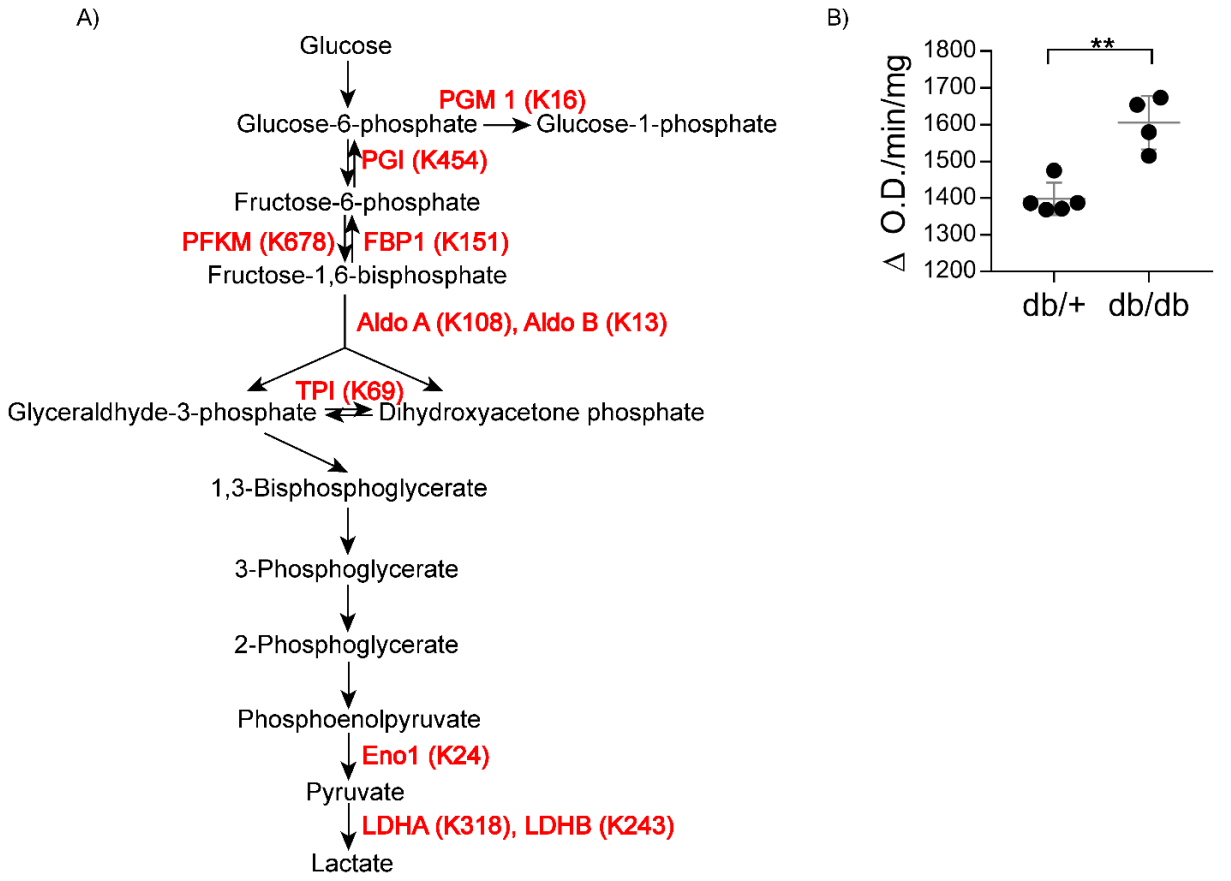

Figure 2-6 Proteins in glycolysis/gluconeogenesis with significantly reduced malonylation levels in the db/db cortex

A) Protein names and their malonylated lysines that are significantly decreased in db/db cortex are denoted on the pathway in red. B) Relative Aldolase A and B activity in the db/+ and db/db cortex. Student's t-test, ** = $p < 0.01$.

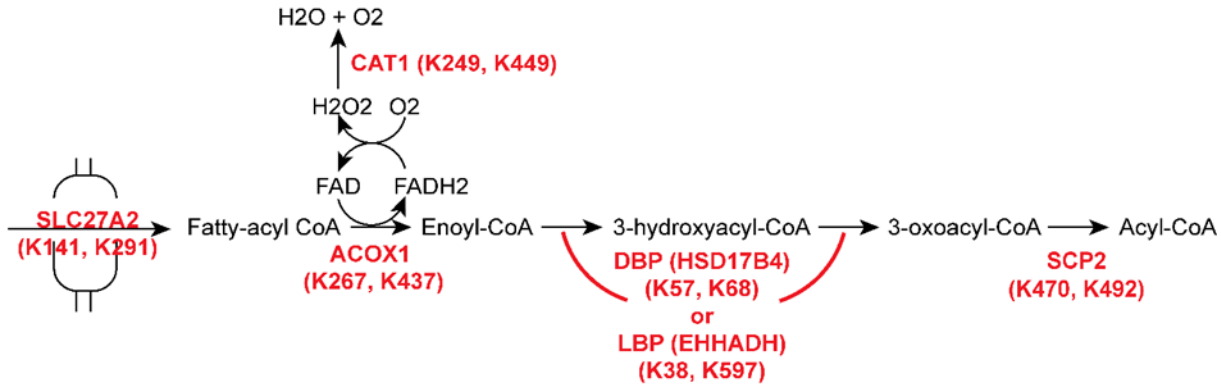

Figure 2-7 Proteins in peroxisomal fatty acid oxidation pathway with significantly reduced malonylation levels in the db/db cortex

Protein names and their malonylated lysines that are significantly decreased in the *db/db* cortex are denoted on the pathway in red.

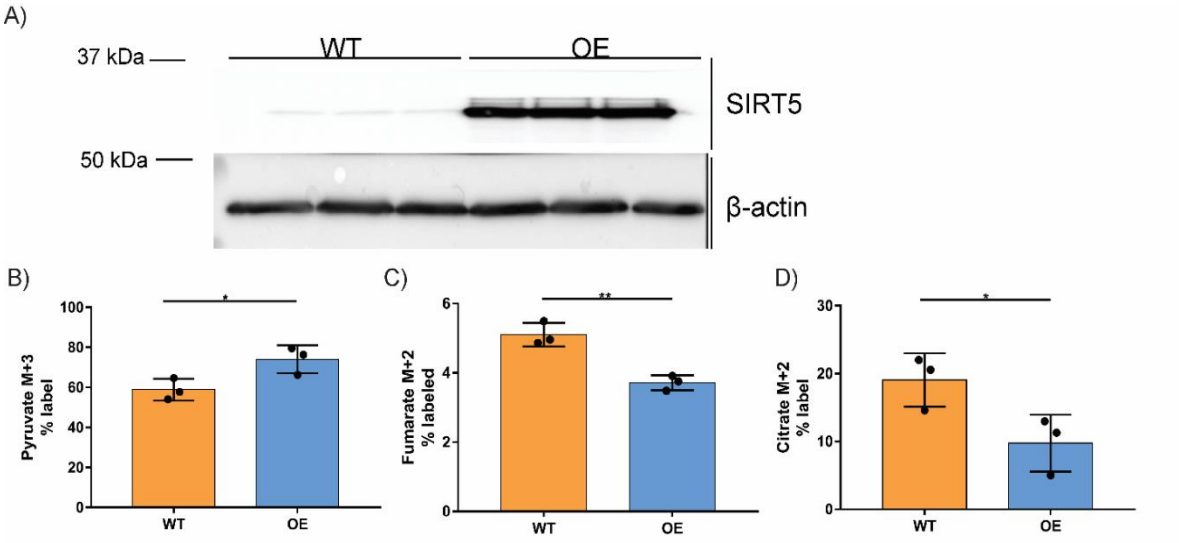

Figure 2-8 Overexpression of SIRT5 in HK-2 cells.

A) Western blot of SIRT5 in HK-2 cells for wildtype (WT) and overexpression (OE) conditions. B) M+3 pyruvate isotopologue levels represented by % total pyruvate level. C) M+2 fumarate % labeled. D) M+2 citrate % labeled.

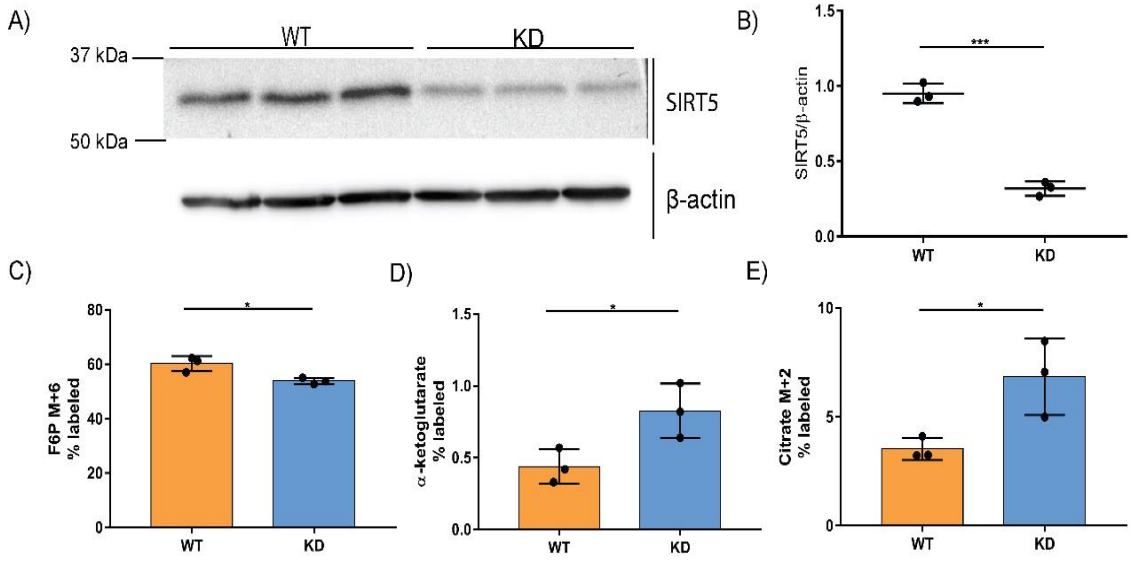

Figure 2-9 Knockdown of SIRT5 in HK-2 cells.

A) Western blot of SIRT5 in HK-2 cells for wildtype (WT) and knock down (KD) conditions. B) Relative band intensities of SIRT5 normalized to actin. C) M+6 fructose-6-phosphate (F6P) % labeled. D) M+2 fumarate % labeled. D) M+2 citrate % labeled.

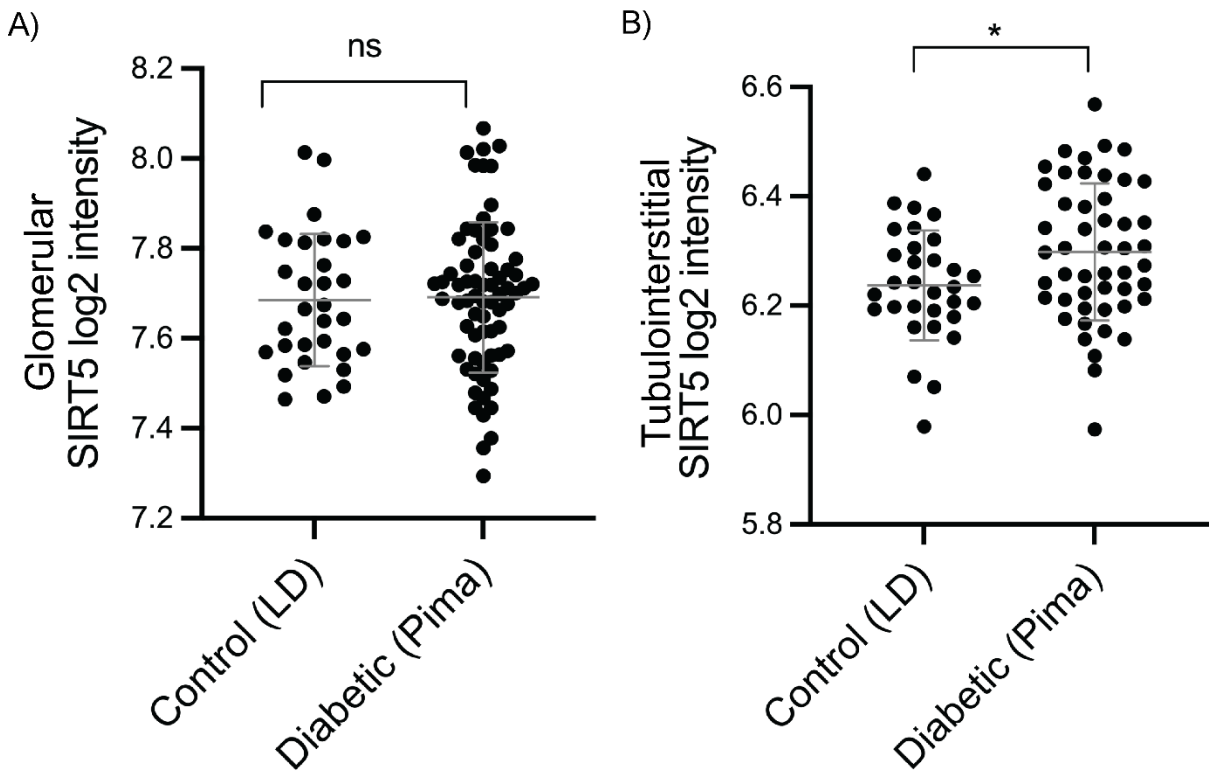

Figure 2-10 SIRT5 transcript levels from kidney biopsies of living donor (LD; control) volunteers and diabetic Pima Indian patients (Pima).

A) Glomerular SIRT5 transcript levels between LD and Pima kidney biopsies. B) Tubulointerstitial SIRT5 transcript levels between LD and Pima kidney biopsies. Student's t-test, ns = not significant, *= $p \leq 0.05$.

Chapter 3

Role of SIRT5 in Mouse Models of DKD

3.1 Abstract

Obesity and diabetes are associated with nutrient overload that ultimately leads to accumulation of metabolites that can react with and perturb protein function and activity. Sirtuin 5 (SIRT5) is a member of the NAD+ dependent histone deacetylase family which removes negatively charged lysine post-translational modification that results from reactive metabolites such as malonyl-CoA. SIRT5 has been implicated in metabolic reprogramming in various biological contexts and suggested to be a regulator of metabolic stress in obesity and diabetes. We hypothesized that SIRT5 regulates metabolism in diabetic kidney disease (DKD) and generated SIRT5 knockout (KO) and overexpressor (OE) diabetic mouse models to investigate the effect of SIRT5 expression on DKD pathogenesis. We found that SIRT5 overexpression is protective in DKD and results in decreased urinary excretion of albumin, kidney injury molecule-1, and neutrophil gelatinase-associated lipocalin. However, we also found a significant effect of the background strain of the mice on development of diabetes and kidney disease, making our results difficult to interpret.

3.2 Introduction

Nutrient excess in diabetes and obesity can lead to aberrant levels of metabolites that can perturb metabolic homeostasis. For example, in human diabetic and obese muscles, increased levels of malonyl-CoA levels is hypothesized to contribute to insulin resistance and decreased FAO[184]. It is now becoming recognized that such CoA metabolites may regulate metabolism by serving as modifiers of protein lysines, which can result in altered protein function and activity of various metabolic pathways. Studies have found increased protein malonylation, which is a reversible covalent modification of lysine by malonyl-CoA, in various tissues of diabetic and obese mice[153–156]. Contrary to these findings, we found that in the *db/db* kidney cortex, specifically in proximal tubules, malonylation levels are decreased. This process is likely mediated by SIRT5; a member of the histone deacetylase family that catalyzes the removal of negatively charged lysine PTMs such as malonylation, succinylation and glutarylation. We hypothesize that SIRT5 is a regulator of metabolism in DKD by modulating level of malonylation in proximal tubules.

The BKS-Lepr^{db}J (*db/db*) mice is a pathophysiologically relevant model of T2D and DKD, along with other microvascular complications. The spontaneous leptin receptor mutation causes hyperphagic obesity and hyperglycemia with hyperlipidemia and dyslipidemia[185]. In this study, we used an inducible model of DKD generated with prolonged HFD feeding with low-dose STZ to study the role of SIRT5 KO and OE on DKD. Previous studies of this model in rodents have demonstrated development of microvascular complications such as diabetic neuropathy and DKD with similar feeding and dosing schemes as presented in our study[186–189]. A study of HFD-STZ mice reported

hyperglycemia as well as hyperlipidemia, which is not observed in STZ-only models of T1D[190]. Most importantly, we found that the kidney cortex of HFD-STZ mice demonstrated reduction in malonylation, similar to what we observed in the *db/db* cortex. In summary, the HFD-STZ is an inducible model of DKD with hyperglycemia and hyperlipidemia that resembles the *db/db* mouse model.

In this study, our goal was to generate diabetic SIRT5 KO and OE mice that develop DKD. We assessed severity of disease with urinary markers of disease and evidence of tissue fibrosis and inflammation, and conducted steady-state metabolomics studies to understand the role of SIRT5 in metabolic regulation in DKD.

3.3 Result

3.3.1 HFD-STZ Mice Kidney Cortex Demonstrate Reduced Malonylation

In our previous study, we found reduced levels of malonylation in the cortex, specifically proximal tubules, of *db/db* mice, a pathophysiologically relevant mode of type 2 diabetes and DKD. To assess whether this reduction in post-translational modification occurs in other models of DKD, specifically models with hyperglycemia and hyperlipidemia, we probed for malonyl-lysine (Kmal) residues in a HFD-STZ model of DKD. At 36 weeks of age, the kidney cortex of HFD-STZ mice exhibited significantly decreased malonylation in comparison to control-chow fed and vehicle-treated mice (**Fig. 3-1A**). Moreover, the HFD-STZ mice did not demonstrate a significant difference in succinylation levels, consistent with our observations in the *db/db* mice (**Fig. 3-1B, C**). Of note, at 36 weeks of age, the HFD-STZ mice demonstrate significantly elevated urinary albumin to creatinine ratio (ACR; **Fig. 3-1 E**) and increased glomerular periodic acid-Schiff

(PAS) staining for mesangial expansion (**Fig. 3-1 F**), demonstrating that the decrease in malonylation occurs at a time-point in which markers of DKD are apparent.

3.3.2 HFD-STZ Of SIRT5 WT and OE Mice Demonstrate No Significant Differences in Systemic Metabolism

To investigate the role of SIRT5 in DKD, we performed HFD-STZ treatment in SIRT5 KO and SIRT5 OE and their respective WT. With our dosing scheme, SIRT5 WT and KO were unable to maintain hyperglycemia until 36 weeks of age, which we determined was the minimum amount of age the mice needed to reach in order to demonstrate increased urinary ACR. We suspect that the background strain of SIRT5 WT and KO mice contributed to the reduced susceptibility of STZ. SIRT5 OE mice were a mix of C57BL/6J and 129/Sv backgrounds and SIRT5 KO mice were of either C57BL/6J or 129/Sv backgrounds. The C57BL/6J SIRT5 KO mice did not develop hyperglycemia after STZ treatment, whereas the 129/Sv SIRT5 KO mice were unable to sustain hyperglycemia until 36 weeks of age. Therefore, I will only discuss the phenotypes of SIRT5 WT and OE mice in this chapter. We generated the HFD-STZ by feeding high fat (fat calories accounting for 60% of total calories) and high sucrose diet starting at 5 weeks of age (**Fig. 3-2A**). Mice were then injected with 50 mg/kg of STZ as per Diacomp protocol four times in total. Control mice were injected with vehicle only. Mice were then maintained on their respective diets until 34-36 weeks of age. Urine was collected at 24 weeks of age to monitor disease progress. SIRT5 WT and OE mice HFD-STZ exhibited significantly elevated body weight in comparison to their respective controls at 15 weeks of age, but their weight subsequently normalized to levels comparable to the control mice

post STZ injection. SIRT5 HFD-STZ WT and OE mice did not differ in body weight from each other.

HFD-STZ mice demonstrated significantly elevated fasting blood glucose levels and percent glycated hemoglobin level until harvest in comparison to the controls (**Fig. 3-3A, B**). Fasting plasma insulin levels were not elevated in the HFD-STZ mice in the context of hyperglycemia, demonstrating STZ-induced β-cell destruction (**Fig. 3-3C, D**). Between SIRT5 WT and OE HFD-STZ mice, no differences were observed for fasting blood glucose, percent glycated hemoglobin, plasma fasting insulin, and intraperitoneal insulin tolerance test.

HFD-STZ mice also exhibited increased elevated plasma total cholesterol and calculated plasma LDL concentration (Friedwald's equation), demonstrating hyperlipidemia (**Fig. 3-4**). No significant differences in HDL and triglyceride levels were observed between the diabetic and control mice. No significant differences were observed between the SIRT5 OE and WT HFD-STZ for any of the plasma lipid profiles.

3.3.3 Diabetic SIRT5 OE Mice Display Reduced Urinary Levels of DKD Biomarkers

Before harvest, urine was collected in 24-hr metabolic cages and assessed for urinary ACR ratio, and proximal tubular specific markers of disease: kidney injury molecule (KIM-1) and Neutrophil gelatinase-associated lipocalin (NGAL). HFD-STZ mice demonstrated increased ACR, KIM-1 and NGAL levels compared to control mice (**Fig. 3-5**). SIRT5 OE HFD-STZ mice exhibited significantly lower levels for all three urine disease markers in comparison to SIRT5 WT HFD-STZ, suggesting that increased SIRT5 expression is protective in DKD.

3.3.4 Diabetic SIRT5 WT and OE HFD-STZ Mice Display No Significant Difference in Kidney Fibrosis

Glomerular histological changes in DKD include mesangial expansion, podocyte effacement and loss. While these changes are frequently observed in mouse models of DKD, interstitial fibrosis and tubular loss observed in late-stage DKD in humans is often not found or only mildly occurs in mouse DKD. In the SIRT5 WT and OE mice, the HFD-STZ cohort demonstrated no significant changes in the glomerulus with PAS staining (mesangial expansion) and WT-1 staining (podocyte number; **Fig. 3-6**). Trichrome stain demonstrated little collagen deposition around the glomerulus. With respect to interstitial fibrosis, picrosirius red staining of the kidney demonstrated qualitatively elevated fibrosis in the HFD-STZ mice with respect to the control mice (**Fig. 3-7**). There was little difference with respect to picrosirius collagen staining between WT and OE SIRT5 HFD-STZ mice. Western blot of kidney cortex from HFD-STZ SIRT5 WT and OE mice demonstrated no significant difference with regards to fibronectin, smad2, and smooth muscle actin (SMA) protein expression (**Fig. 3-8**). There were no significant differences with regards to TGFβ and ColIV mRNA expression assessed with qPCR.

Metabolite levels between SIRT5 WT and OE HFD-STZ cortex are not significantly altered by SIRT5 levels

To understand if SIRT5 affects metabolism in DKD, we conducted targeted steady-state metabolomics analysis for glucose and fatty acid-derived metabolites from glycolysis, β-oxidation, pentose-phosphate, amino acids, and energy metabolites. **Figure 9A-D** are metabolites that were significantly elevated in the HFD-STZ mice, but none of the metabolites were significantly different between the HFD-STZ SIRT5 OE and WT

mice in the investigated pathways, suggesting no genotype specific differences in steady-state metabolite levels.

3.4 Discussion

We aimed to study the role of SIRT5 in DKD with HFD-STZ mouse models of diabetes. We were unable to generate SIRT5 KO mice with sustained hyperglycemia until 34-38 weeks of age, the time point in which diabetic mice develop elevated ACR, with our dosing scheme. However, SIRT5 WT and OE HFD-STZ developed sustained hyperglycemia and hyperlipidemia. SIRT5 OE HFD-STZ mice were relatively protected from DKD as indicated by urinary levels of ACR, KIM-1, and NGAL, suggesting that increased SIRT5 expression ameliorates DKD. However, SIRT5 WT and OE HFD-STZ mice did not demonstrate significant difference in glomerular podocyte number, mesangial expansion, tubulointerstitial fibrosis, and expression of fibrosis and inflammatory genes. In addition, no significant effect on metabolism by SIRT5 was observed.

The issues regarding sustaining hyperglycemia in SIRT5 WT/KO HFD-STZ mice and the mild DKD observed in the SIRT5 WT/OE HFD-STZ mice is likely due to the genetic background of the SIRT5 mice in our study. In the HFD-STZ, mice are fed HFD prior to STZ injections because HFD is hypothesized to cause β-cell dysfunction, and therefore more prone to death by STZ. On the contrary, HFD has also been demonstrated to cause islet hyperplasia and hypertrophy in C57BL/6J mice, and therefore may be less susceptible to STZ injury than mice not fed HFD[191,192]. In our study, we used SIRT5 WT/KO mice of C57BL6/J and 129Sv background, both with varying degrees of susceptibility to hyperglycemia. The BKS background of the *db/db* mice commonly used to study kidney disease is a mix of C57BL6/J (~84% alleles), which display resistance to

kidney disease development, and DBA/J (~16% alleles), which are susceptible to kidney disease[193]. The BKS *db/db* mice demonstrate β-cell atrophy in contrast to C57BL6/J mice. In addition, the *db/db* mouse represents early DKD; these mice do not develop renal failure or significant tubulointerstitial fibrosis. The *db/db* mice elevated fat mass at 3-4 weeks of age, frank hyperglycemia by 8 weeks of age and renal hypertrophy at 16 weeks of age[185]. In comparison, the HFD-STZ mice are subjected to hyperglycemia for ~20 weeks without obesity and likely model DKD of an earlier timepoint than that observed in *db/db* mice at 24 weeks of age. As a result, HFD-STZ mice demonstrate elevated urinary markers of disease but not histological signs of tissue dysfunction.

The role of SIRT5 in diabetes and obesity is relatively unknown. The global SIRT5 KO and OE mice demonstrate little difference in metabolic phenotype even after a HFD challenge. However, SIRT5 tissue or cell type-specific KO or OE mice demonstrate significant differences in metabolism. Hepatocyte-specific SIRT5 OE *ob/ob* mice display significantly lower levels of hepatic steatosis and lower levels of hepatic lipid levels[156]. Brown-adipocyte (BAT)-specific KO mice demonstrate significant reduction in BAT respiratory exchange ratio and cold intolerance[126], whereas SIRT5 global KO 129/Sv mice demonstrate cold intolerance due to reduced browning capacity of subcuntaneous inguinal white adipose tissue, but not due to the thermogenic function of BAT[194]. Why differences in metabolism occur in tissue-specific KO of SIRT5 is not well understood but may be due to compensatory whole-body adaptations to SIRT5 reduction. Therefore, it is potentially possible that proximal tubular-specific alterations in SIRT5 levels may uncover a more severe DKD phenotype.

While it is possible that SIRT5 may have mild metabolic effects in DKD, according to our metabolomics analysis, SIRT5 has numerous substrates that could be conferring the protective effect we observed in the SIRT5 HFD-STZ mice. SIRT5 has been demonstrated to increased superoxide dismutase 1 (SOD1) activity via desuccinylation[195,196], and SOD1 deficiency has been demonstrated to be detrimental to DKD in Akita mice[197]. Of note, SOD1 was identified as a protein that was significantly demalonylated in the *db/db* cortex from our screen (data not shown). In our previous study of *db/db* kidney cortex, we found decreased malonylation of peroxisomal targets including catalase, which have also been demonstrated to play an important role in reducing oxidative stress in DKD[198]. SIRT5 has also been demonstrated to deacetylate cytochrome C[199,200] and suppresses apoptosis in hepatocellular carcinoma cells[200]. SIRT5 overexpression may play a similar role and reduce proximal tubular death in our HFD-STZ model of DKD. In conclusion, SIRT5 likely modulates many different biological pathways to exert its protective effect on the HFD-STZ model of DKD.

3.5 Materials and Methods

Animals: SIRT5 WT and OE mice of mixed 129/Sv and C57Bl6/J background were bed and male litter mates were selected for experiments. At 5 wks of age, WT and OE mice were maintained on normal chow (5LOD; Lab Diets) or switched to high-fat diet (D12492; Research diets) *ad libitum*. Mice were injected with 50 mg/kg STZ in citrate buffer pH 4.0 four times or just citrate buffer for the control group, one injection per day after 4 hrs of fasting. Mice were aged until 34-38 weeks of age. Urine was collected for 24 hr metabolic cages and stored at -80 °C. Fasting blood glucose was assessed with handheld glucometers. Mice were harvested after 4 hrs of fasting. Kidneys were perfused with ice-

cold PBS containing heparin through the renal veins. Plasma was obtained by centrifuging blood in EDTA-coated tubes for 5 min at 2000 x g, snap frozen and stored at -80 °C. Kidney cortex was dissected on ice and snap frozen. For qPCR, kidney cortex was preserved in RNAlater Stabilization Solution (Thermofisher) as per manufacturer's instructions.

Western blot: Kidney cortex were pulverized in laemmali buffer with a dounce pestle homogenizer. The homogenate was sonicated for 30 s on ice. Samples were centrifuged at 17,000 x g for 10 min at 4 °C. The supernatant was collected and protein concentration was determined with DC protein assay (Bio-Rad). The lysates were separated by SDS-PAGE and transferred to PVDF membranes. Signals were then visualized with Pierce ECL reagent (Thermofisher). Antibodies against Pan anti-malonyllysine (PTM-901) and Pan anti-succinyllysine (PTM-401) were purchased from PTM biolabs. Antibodies against SIRT5 (8782) and β-Actin were purchased from (8H10D10) Cell Signaling Technologies (CST). Antibodies against fibronectin, Smad2 and smooth muscle actin were purchased from CST (77397).

Plasma lipid: Plasma cholesterol and triglycerides were measured by the Michigan Diabetes Research Center's Chemistry Laboratory clinical core.

ACR measurement: Urine creatinine was determined as previously published. Mouse urine albumin was measured with Albuwell M Elisa kit (Exowell; Ethos Biosciences).

KIM-1 measurement: Urinary KIM-1 was measured with Mouse TIM-1/KIM-1/HAVCR Quantikine ELISA Kit (R&D Systems).

NGAL measurement: Urinary NGAL was measured with Mouse Lipocalin-2/NGAL Quantikine ELISA Kit (R&D Systems).

Histology: Mouse kidneys were fixed in 4% paraformaldehyde (Electron Microscopy Sciences) at room temperature for 24 hrs. Samples were then preserved in 70% ethanol at 4 °C until further processing. Samples were paraffin embedded and sectioned into 3 um sections by the University of Michigan Research Histology and Immunohistochemistry Core.

PAS/WT-1 stain: Slides were probed for WT-1 and counterstained with PAS as previously described.

Trichrome stain: Samples were stained by the University of Michigan Research Histology and Immunohistochemistry Core.

Picrosirius red stain: Slides were deparaffinized and stained with Picro Sirius Red Stain Kit (ab150681; Abcam) as per manufacturer's instructions.

RNA extraction: Preserved kidney cortex was homogenized and processed as per manufacturer's protocol for the QIAGEN RNeasy® kit.

cDNA synthesis: 100 ng of RNA were used to generate cDNA using The SuperScript® III First-Strand Synthesis System (Thermofisher) following manufacturer's protocols.

qPCR: PowerUp™ SYBR™ Green Master Mix (Thermofisher) was used to perform qPCR with the synthesized cDNA. Primers for mouse TGFβ (NM_011577), ColIV (NM_007734), and PPia (NM_008907) were purchased from OriGene.

Metabolomics: Tissue samples were processed as previously reported. Samples were separated as previously described. Metabolites were analyzed on the Agilent 6456 Q-TOF mass spectrometer coupled to Agilent 1290 LC. Data was collected in negative mode, with gas temp at 225 °C, drying gas at 10 L/min, nebulizer at 40 psi, sheath gas temp 300 °C, and sheath gas flow at 12 L/min. Fragmentor voltage was set at 125 V,

skimmer at 65 V, and VCap at 3000 V. Authentic standards of all measured metabolites were run separately and spiked into pooled samples for verification of metabolite and retention time.

Data analysis and statistics: Resulting data was analyzed with Agilent MassHunter TOF quantitative analysis v. 10.1. Data was analyzed with student's t-test or Two-Way ANOVA with Tukey's post-hoc correction with Graph Pad Prism 7.0.

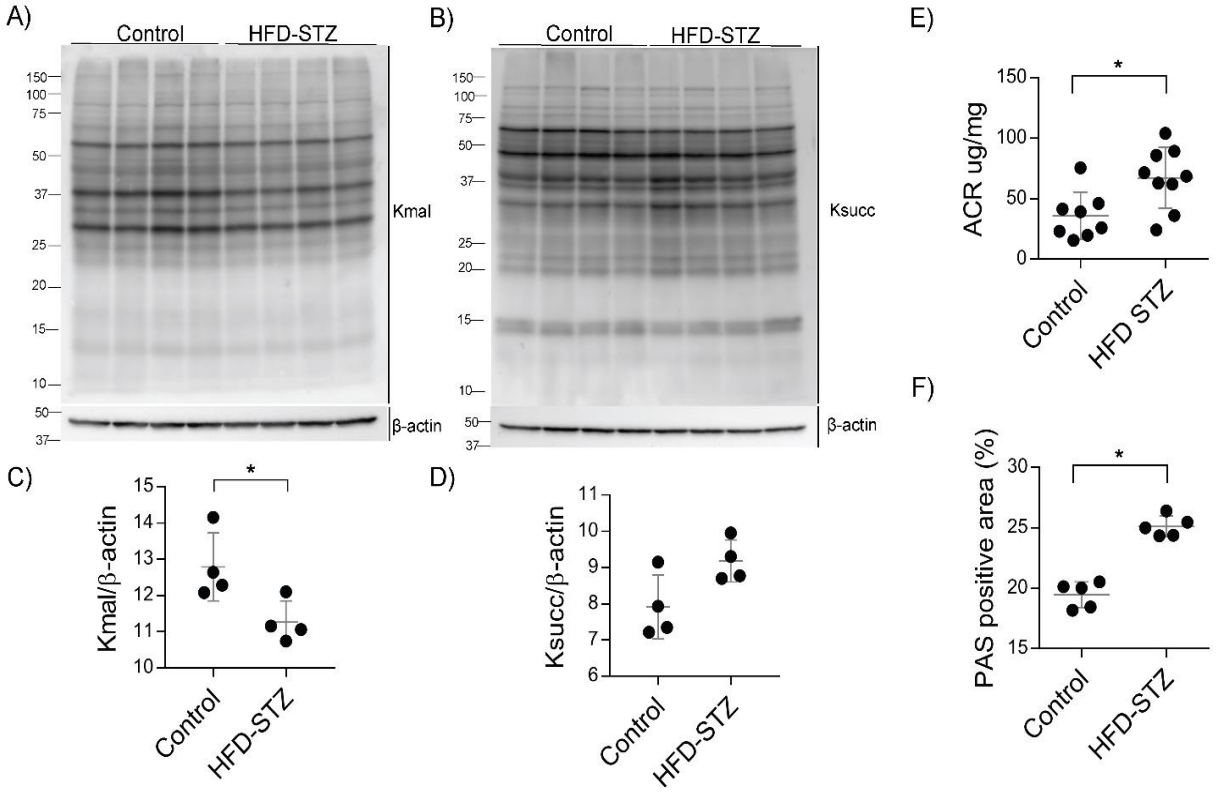

Figure 3-1 Malonylation and succinylation levels in control and HFD-STZ diabetic mouse kidney cortex.

A) Western blot analysis of Kmal residues in control and HFD-STZ kidney cortex. B) Western blot analysis of Ksucc residues in control and HFD-STZ kidney cortex. C) Relative Western blot A) signal of Kmal normalized to normalized to β-actin. D) Relative Western blot B) signal of Ksucc normalized to normalized to β-actin. Student's t-test, *= $p \leq 0.05$.

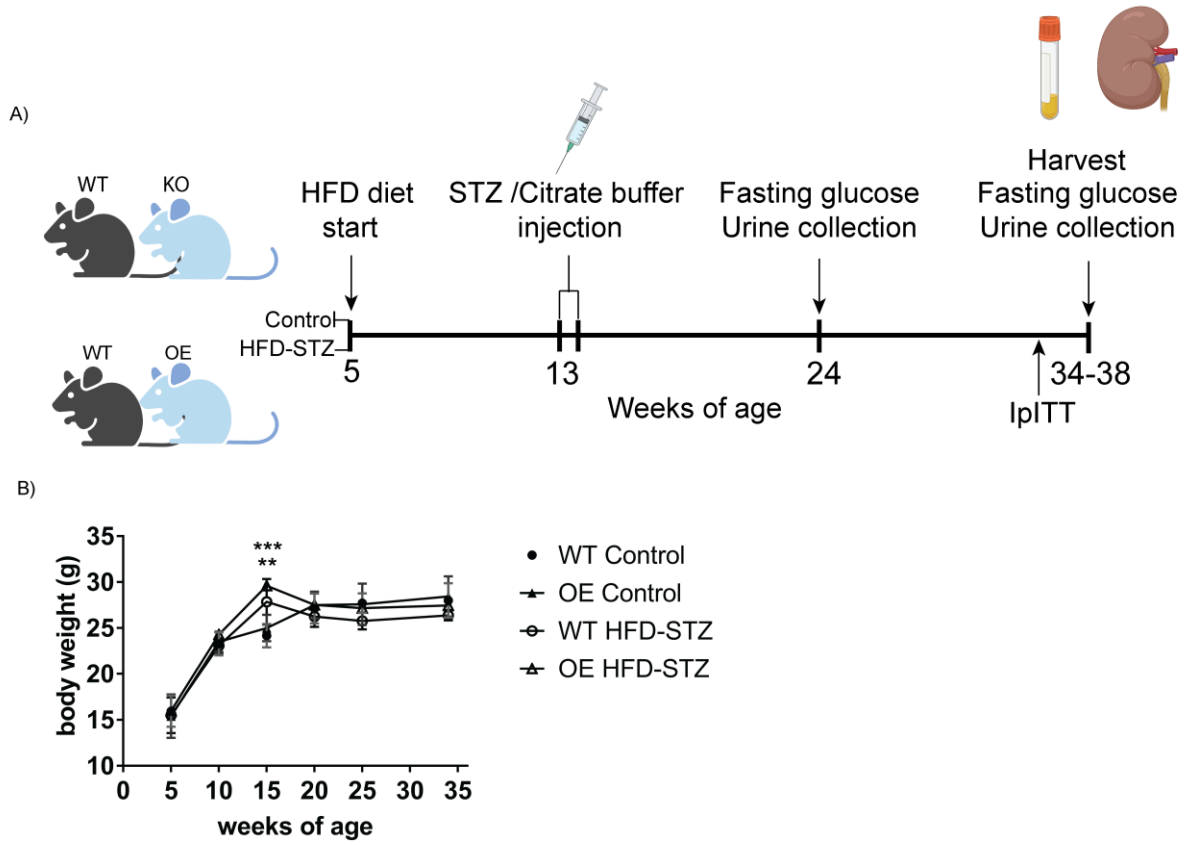

Figure 3-2 HFD-STZ SIRT5 mouse study design.

A) Timeline of HFD-STZ SIRT5 WT/KO and WT/OE study design. Mouse are divided into control and HFD-STZ group at 5 weeks of age, injected with STZ or vehicle (citrate buffer) between 13 and 14 weeks of age, tested for urinary ACR, KIM-1 and NGAL at 24 weeks of age, and harvested for kidney and plasma at 34-38 weeks of age. B) Body weight of SIRT5 WT and OE control and HFD-STZ mice. Two-way ANOVA with Tukey's post-hoc correction, **= $p \leq 0.01$, *** = $p \leq 0.001$.

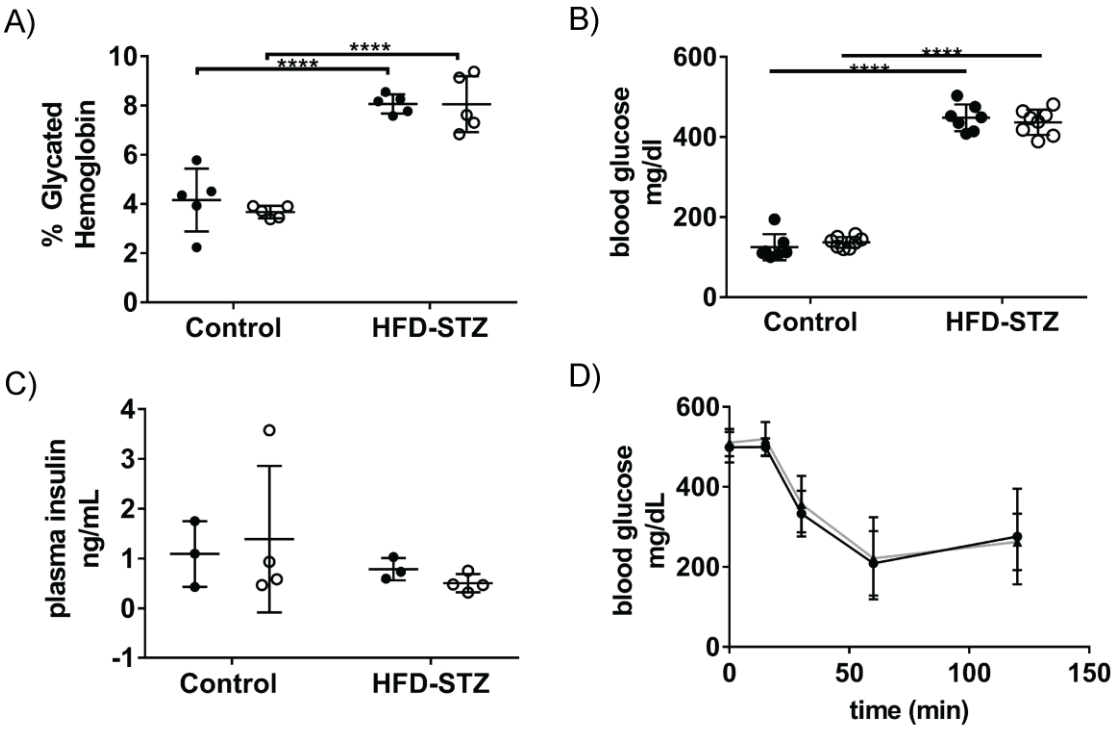

E)

Tukey's multiple comparisons test	Mean Diff.	95.00% CI of diff.	Significant?	Summary	Adjusted P Value
Control:WT vs. Control:OE	0.492	-1.11 to 2.094	No	ns	0.8158
Control:WT vs. HFD-STZ:WT	-3.904	-5.506 to -2.302	Yes	****	<0.0001
Control:WT vs. HFD-STZ:OE	-3.894	-5.496 to -2.292	Yes	****	<0.0001
Control:OE vs. HFD-STZ:WT	-4.396	-5.998 to -2.794	Yes	****	<0.0001
Control:OE vs. HFD-STZ:OE	-4.386	-5.988 to -2.784	Yes	****	<0.0001
HFD-STZ:WT vs. HFD-STZ:OE	0.01	-1.592 to 1.612	No	ns	>0.9999

F)

Tukey's multiple comparisons test	Mean Diff.	95.00% CI of diff.	Significant?	Summary	Adjusted P Value
Control:WT vs. Control:OE	-12.04	-52.59 to 28.52	No	ns	0.8472
Control:WT vs. HFD-STZ:WT	-323.3	-365.2 to -281.4	Yes	****	<0.0001
Control:WT vs. HFD-STZ:OE	-312	-352.6 to -271.5	Yes	****	<0.0001
Control:OE vs. HFD-STZ:WT	-311.3	-351.8 to -270.7	Yes	****	<0.0001
Control:OE vs. HFD-STZ:OE	-300	-339.2 to -260.8	Yes	****	<0.0001
HFD-STZ:WT vs. HFD-STZ:OE	11.25	-29.3 to 51.8	No	ns	0.8711

Figure 3-3 Hyperglycemia in control and HFD-STZ SIRT5 WT and OE mice between 34-38 weeks of age.

●: SIRT5 WT ○: SIRT5 OE A) Hemoglobin A1C from control and HFD-STZ mouse. B) Fasting blood glucose from control and HFD-STZ mouse. C) Fasting plasma insulin from control and HFD-STZ mouse. D) Blood glucose levels during IpITT from HFD-STZ SIRT5 WT and OE mouse. Two-way ANOVA with Tukey's post-hoc correction, **** = $p \leq 0.0001$. E) Table of statistics for Two-way ANOVA and multiple comparison test for figure A. F) Table of statistics for Two-way ANOVA and multiple comparison test for for figure B.

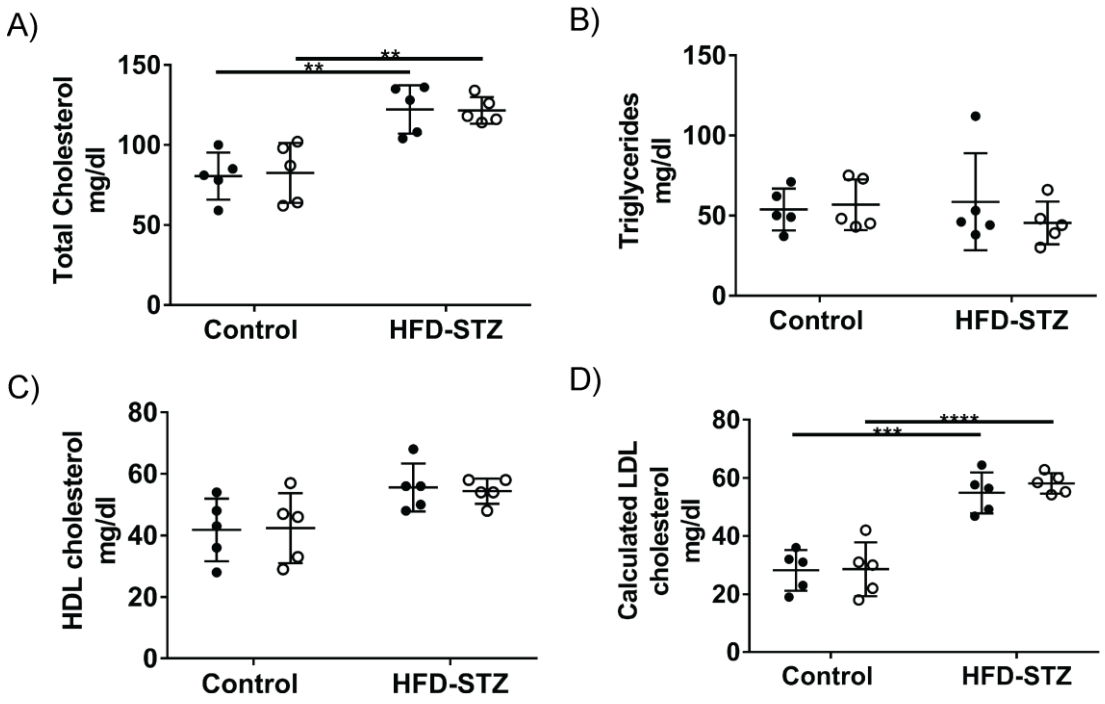

E)

Tukey's multiple comparisons test	Mean Diff.	95.00% CI of diff.	Significant?	Summary	Adjusted P Value
Control :WT vs. Control :OE	-2	-28.64 to 24.64	No	ns	0.9964
Control :WT vs. HFD-STZ:WT	-41.6	-68.24 to -14.96	Yes	**	0.0020
Control :WT vs. HFD-STZ:OE	-41	-67.64 to -14.36	Yes	**	0.0023
Control :OE vs. HFD-STZ:WT	-39.6	-66.24 to -12.96	Yes	**	0.0031
Control :OE vs. HFD-STZ:OE	-39	-65.64 to -12.36	Yes	**	0.0035
HFD-STZ:WT vs. HFD-STZ:OE	0.6	-26.04 to 27.24	No	ns	0.9999

F)

Tukey's multiple comparisons test	Mean Diff.	95.00% CI of diff.	Significant?	Summary	Adjusted P Value
Control :WT vs. Control :OE	-0.4	-13.08 to 12.28	No	ns	0.9997
Control :WT vs. HFD-STZ:WT	-26.68	-39.36 to -14	Yes	****	<0.0001
Control :WT vs. HFD-STZ:OE	-29.92	-42.6 to -17.24	Yes	****	<0.0001
Control :OE vs. HFD-STZ:WT	-26.28	-38.96 to -13.6	Yes	***	0.0001
Control :OE vs. HFD-STZ:OE	-29.52	-42.2 to -16.84	Yes	****	<0.0001
HFD-STZ:WT vs. HFD-STZ:OE	-3.24	-15.92 to 9.437	No	ns	0.8831

Figure 3-4 Fasting plasma lipid panel from SIRT5 WT and OE control and HFD-STZ mice.

●: SIRT5 WT ○: SIRT5. A) Total cholesterol. B) Triglycerides. C) HDL cholesterol. D) LDL cholesterol levels calculated with Friedwald's equation. Two-way ANOVA with Tukey's post-hoc correction, **= $p \leq 0.01$, *** = $p \leq 0.001$, **** = $p \leq 0.0001$. E) Table of statistics for Two-way ANOVA and multiple comparison test for figure A. F) Table of statistics for Two-way ANOVA and multiple comparison test for for figure D.

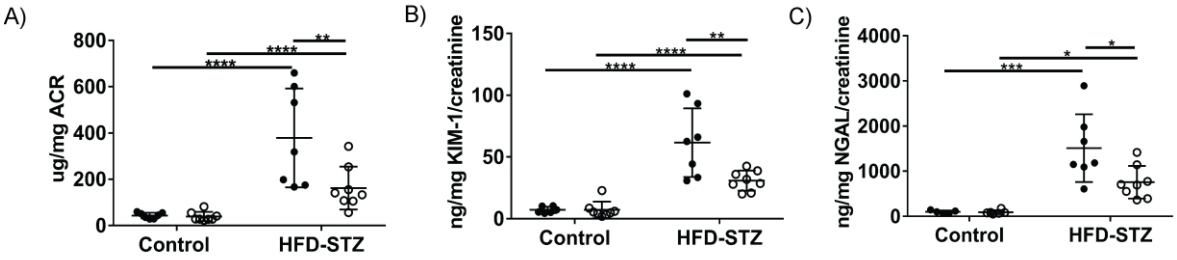

D)

Tukey's multiple comparisons test	Mean Diff.	95.00% CI of diff.	Significant?	Summary	Adjusted P Value
Control :WT vs. Control :OE	4.311	-157.5 to 166.1	No	ns	0.9999
Control :WT vs. HFD-STZ:WT	-335.4	-502.6 to -168.3	Yes	****	<0.0001
Control :WT vs. HFD-STZ:OE	-118.6	-280.5 to 43.22	No	ns	0.2100
Control :OE vs. HFD-STZ:WT	-339.7	-501.6 to -177.9	Yes	****	<0.0001
Control :OE vs. HFD-STZ:OE	-122.9	-279.3 to 33.42	No	ns	0.1621
HFD-STZ:WT vs. HFD-STZ:OE	216.8	54.98 to 378.7	Yes	**	0.0056

E)

Tukey's multiple comparisons test	Mean Diff.	95.00% CI of diff.	Significant?	Summary	Adjusted P Value
Control:WT vs. Control:OE	0.009093	-21.9 to 21.92	No	ns	>0.9999
Control:WT vs. HFD-STZ:WT	-54.52	-77.09 to -31.94	Yes	****	<0.0001
Control:WT vs. HFD-STZ:OE	-23.71	-45.62 to -1.794	Yes	*	0.0305
Control:OE vs. HFD-STZ:WT	-54.52	-75.52 to -33.52	Yes	****	<0.0001
Control:OE vs. HFD-STZ:OE	-23.72	-44 to -3.428	Yes	*	0.0176
HFD-STZ:WT vs. HFD-STZ:OE	30.81	9.809 to 51.81	Yes	**	0.0024

F)

Tukey's multiple comparisons test	Mean Diff.	95.00% CI of diff.	Significant?	Summary	Adjusted P Value
Control:WT vs. Control:OE	8.493	-736.2 to 753.2	No	ns	>0.9999
Control:WT vs. HFD-STZ:WT	-1411	-2131 to -690.5	Yes	***	0.0001
Control:WT vs. HFD-STZ:OE	-656.6	-1358 to 44.55	No	ns	0.0718
Control:OE vs. HFD-STZ:WT	-1419	-2103 to -734.9	Yes	****	<0.0001
Control:OE vs. HFD-STZ:OE	-665.1	-1329 to -0.8714	Yes	*	0.0496
HFD-STZ:WT vs. HFD-STZ:OE	754.1	117.6 to 1391	Yes	*	0.0163

Figure 3-5 Urinary markers of DKD from 24-hr urine cages.

●: SIRT5 WT ○: SIRT5. A) Urinary albumin to creatinine ratio (ACR) from control and HFD-STZ mice. B) Urinary KIM-1 to creatine ratio from control and HFD-STZ mice. C) Urinary NGAL to creatinine ratio from control and HFD-STZ mice. Two-way ANOVA with Tukey's post-hoc correction, * = $p \leq 0.05$, **= $p \leq 0.01$, *** = $p \leq 0.001$. D) Table of statistics for Two-way ANOVA and multiple comparison test for for figure A. E) Table of statistics for Two-way ANOVA and multiple comparison test for for figure B. F) Table of statistics for Two-way ANOVA and multiple comparison test for for figure C.

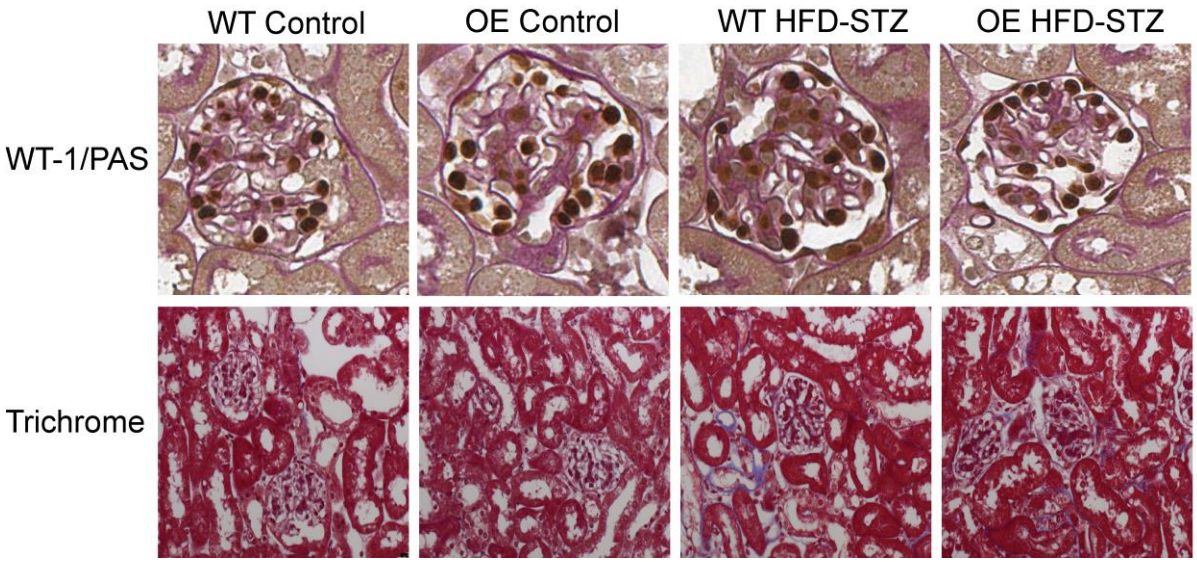

Figure 3-6 Glomerular histology in SIRT5 WT and OE HFD-STZ mice.

PAS and podocyte WT-1 stain in SIRT 5 WT and OE control and HFD-STZ kidney cortex. Trichome stain in SIRT5 WT and OE and controla nd HFD-STZ kidney cortex.

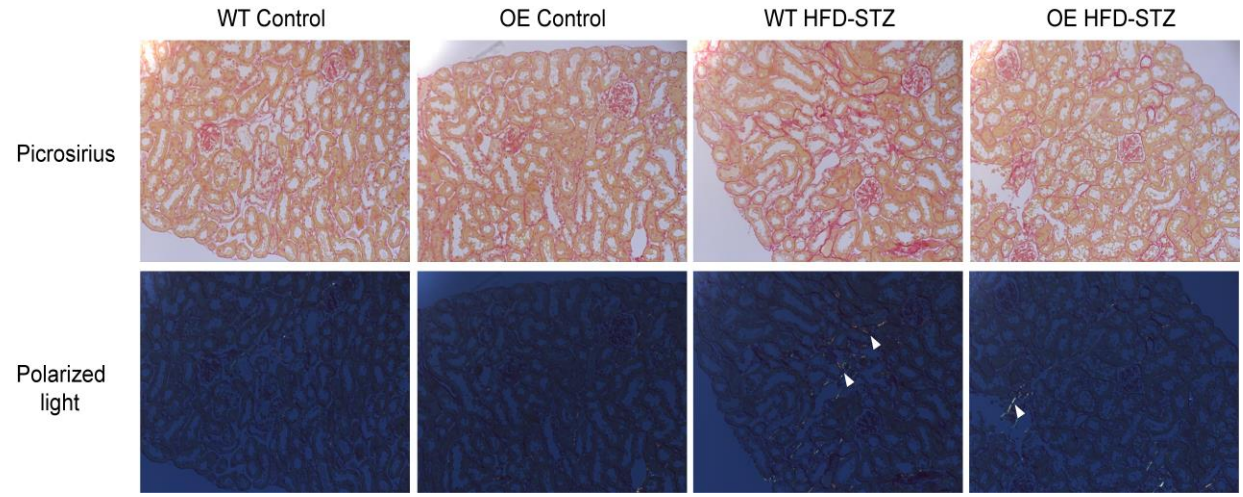

Figure 3-7 Fibrosis in SIRT5 WT and OE control and HFD-STZ mice.

Picrosirius stain of kidney cortex; red areas indicate collagen deposition. Polarized light view of the stain demonstrating different collagen fibers deposited in the tubulointerstitial region. White arrows denote examples of collagen fibers.

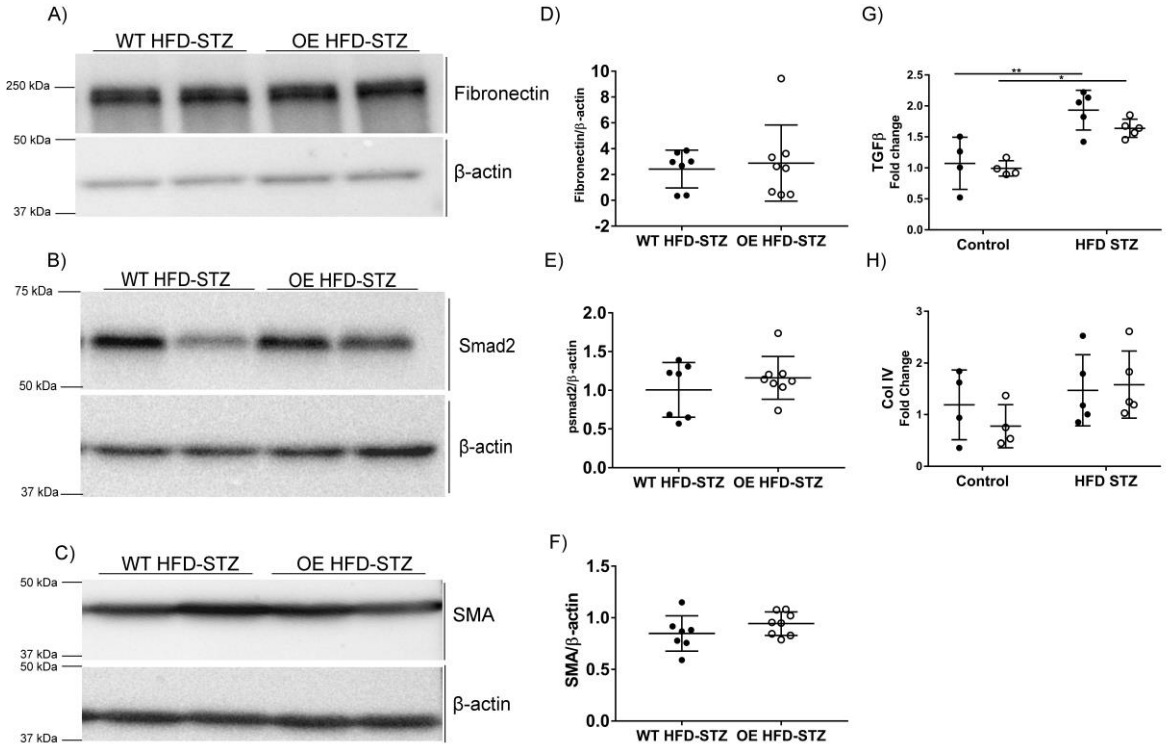

Figure 3-8 Expression of fibrosis genes in SIRT5 WT and OE control and HFD-STZ mice.

A) Western blot for fibronectin in SIRT5 WT and OE HFD-STZ kidney cortex. B) Western blot for Smad2. C) Western blot for smooth muscle actin (SMA). D) Relative Western blot A) signal of fibronectin normalized to normalized to β-actin. E) Relative Western blot B) signal of smad2 normalized to β-actin. F) Relative Western blot B) signal of SMA normalized to β-actin. G) Relative qPCR expression of TGFβ in SIRT5 WT and OE control and HFD-STZ kidney cortex (normalized to PPIA expression) H) Relative qPCR expression of ColIV in SIRT5 WT and OE control and HFD-STZ kidney cortex (normalized to PPIA expression).

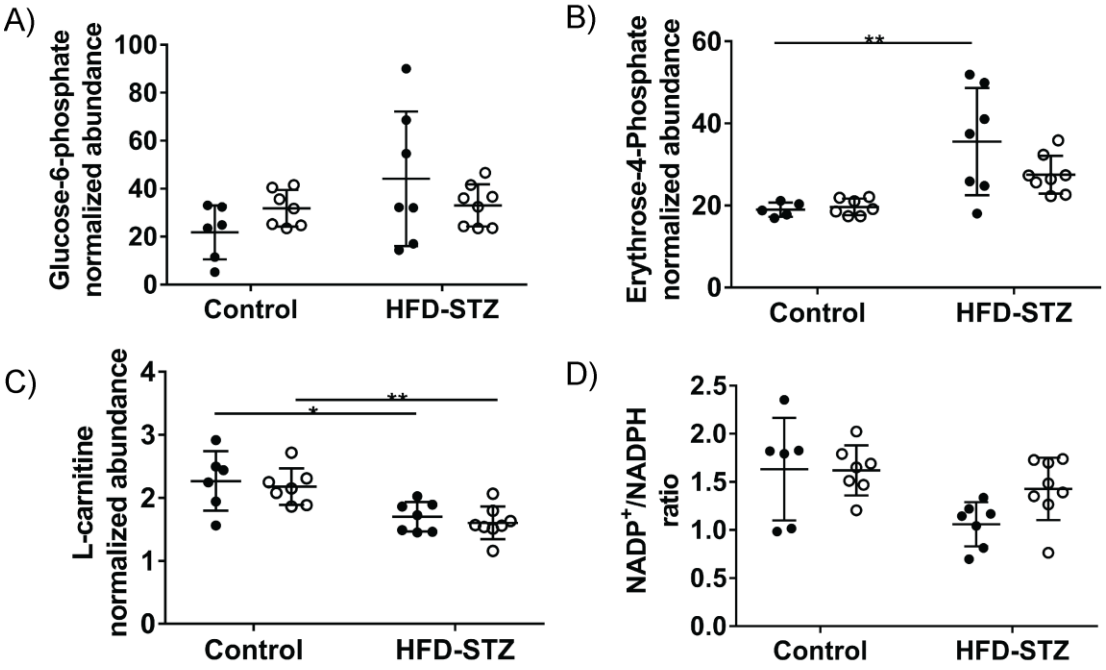

E)

Tukey's multiple comparisons test	Mean Diff.	95.00% CI of diff.	Significant?	Summary	Adjusted P Value
Control:WT vs. Control:OE	0.0117	-0.5197 to 0.5431	No	ns	>0.9999
Control:WT vs. HFD-STZ:WT	0.5719	0.0405 to 1.103	Yes	*	0.0316
Control:WT vs. HFD-STZ:OE	0.2045	-0.3113 to 0.7204	No	ns	0.6965
Control:OE vs. HFD-STZ:WT	0.5602	0.04964 to 1.071	Yes	*	0.0278
Control:OE vs. HFD-STZ:OE	0.1928	-0.3015 to 0.6872	No	ns	0.7070
HFD-STZ:WT vs. HFD-STZ:OE	-0.3673	-0.8617 to 0.127	No	ns	0.1983

F)

Tukey's multiple comparisons test	Mean Diff.	95.00% CI of diff.	Significant?	Summary	Adjusted P Value
Control:WT vs. Control:OE	-0.6625	-12.43 to 11.1	No	ns	0.9986
Control:WT vs. HFD-STZ:WT	-16.6	-28.37 to -4.837	Yes	**	0.0037
Control:WT vs. HFD-STZ:OE	-8.519	-19.97 to 2.937	No	ns	0.1968
Control:OE vs. HFD-STZ:WT	-15.94	-26.68 to -5.2	Yes	**	0.0023
Control:OE vs. HFD-STZ:OE	-7.856	-18.26 to 2.544	No	ns	0.1860
HFD-STZ:WT vs. HFD-STZ:OE	8.085	-2.315 to 18.49	No	ns	0.1671

D)

Tukey's multiple comparisons test	Mean Diff.	95.00% CI of diff.	Significant?	Summary	Adjusted P Value
Control:WT vs. Control:OE	0.08864	-0.3977 to 0.5749	No	ns	0.9576
Control:WT vs. HFD-STZ:WT	0.5657	0.07941 to 1.052	Yes	*	0.0184
Control:WT vs. HFD-STZ:OE	0.6631	0.1911 to 1.135	Yes	**	0.0038
Control:OE vs. HFD-STZ:WT	0.4771	0.009849 to 0.9443	Yes	*	0.0441
Control:OE vs. HFD-STZ:OE	0.5745	0.1221 to 1.027	Yes	**	0.0092
HFD-STZ:WT vs. HFD-STZ:OE	0.09741	-0.355 to 0.5498	No	ns	0.9329

Figure 3-9 Examples of cortex metabolites that are significantly elevated between control and HFD-STZ mice.

●: SIRT5 WT ○: SIRT5. Abundance normalized to tissue protein content. A) Glucose-6-phosphate. B) Erythrose-4-phosphate. C) L-carnitine. D) $NADP^+$/NADPH ratio. Two-way ANOVA with Tukey's post-hoc correction, * = $p \leq 0.05$, **= $p \leq 0.01$. E) Table of statistics for Two-way ANOVA and multiple comparison test for for figure B. F) Table of statistics for Two-way ANOVA and multiple comparison test for for figure C. G) Table of statistics for Two-way ANOVA and multiple comparison test for for figure D.

Chapter 4

Urinary 2-Hydroxyglutarate Enantiomers Are Markedly Elevated in A Murine Model of Type 2 Diabetic Kidney Disease[2]

4.1 Abstract

Metabolic reprogramming is a hallmark of diabetic kidney disease (DKD); nutrient overload leads to increased production of metabolic by-products that may become toxic at high levels. One metabolic byproduct may be 2-hydroxyglutarate (2-HG), a metabolite with many regulatory functions that exists in both enantiomeric forms physiologically. We quantitatively determined the levels of L and D-2HG enantiomers in the urine, plasma and kidney cortex of *db/db* mice, a pathophysiologically relevant murine model of type 2 diabetes and DKD. We found increased fractional excretion of both L and D-2HG enantiomers, suggesting increased tubular secretion and/or production of the two metabolites in DKD. Quantitation of tricarboxylic acid (TCA) cycle metabolites in *db/db* cortex suggests that TCA cycle overload and increase in 2-HG precursor substrate, α-ketoglutarate, drives the increased L and D-2HG production in DKD. In conclusion, we demonstrate increased 2-HG enantiomer production and urinary excretion in murine type 2 DKD, which may contribute to metabolic reprogramming and progression of DKD.

[2] This chapter has been published in:
Baek, J. & Pennathur, S. Urinary 2-Hydroxyglutarate Enantiomers Are Markedly Elevated in a Murine Model of Type 2 Diabetic Kidney Disease. Metabolites 11, 469 (2021).

4.2 Introduction

DKD is the most prevalent etiology of ESRD accounting for ~40% of all ESRD cases in the United States[2]. DKD is marked by dramatic metabolic reprogramming, in particular of proximal tubules, due to hypoxia from microvascular damage, increased energy demand due to the increased glucose load, mitochondrial dysfunction, and excess nutrient burden [201]. Under normal physiologic conditions, proximal tubules prefer fatty acids and glutamine as their main energy sources[62], but in diabetes, proximal tubules increase glucose utilization. As a result, tubules upregulate glucose flux into glycolysis [85] and increase lactate production and excretion in the urine [88,89]. In addition, increased glucose flux into the TCA cycle [85], *de novo* lipogenic pathways[106,202–205], and secondary glycolytic pathways [84] are thought to upregulate production of toxic metabolic by-products that in turn contribute to DKD pathogenesis in human and model system studies.

One potential toxic metabolic by-product may be 2-HG, which is derived from α-ketoglutarate by the promiscuous catalysis of various metabolic enzymes. 2-HG exists as two enantiomers, D-2HG and L-2HG. Of note, these enantiomers are normally produced and excreted in urine, but also converted back to α-ketoglutarate by the actions of mitochondrial enzymes D-2HG dehydrogenase (D-2HGDH) and L-2HG dehydrogenase (L-2HGDH)[206]. D-2HG is most well-known as an onco-metabolite that accumulates due to active site mutations in isocitrate dehydrogenase (IDH) 1 and IDH 2 that generate D-2HG[207,208]. D-2HG , however, can also be generated under physiological conditions by the action of phosphoglycerate dehydrogenase (PHGDH), although high production may only be achieved with PHGDH copy number amplification[209]. L-2HG is thought to be

mainly generated under hypoxic and acidic conditions by the promiscuous action of malate and lactate dehydrogenase (MDH and LDH ref: [210–212]).

Both enantiomers are structural analogues of α-ketoglutarate, and can therefore compete for proteins and enzymes that use α-ketoglutarate as cofactor or substrate, such as α-ketoglutarate-dependent dioxygenases[213]. Apart from its role in oncogenesis, studies have found physiological role of 2-HG in regulating T cell fate and function, in which accumulation of L-2HG precedes T cell differentiation and alters both T-cell metabolism and epigenetics[214,215]. A recent study found decreased production of L and D-2HG in a murine model of lipopolysaccharide-induced endotoxemia, driven by increases in D-2HGDH and L-2HGDH protein levels[216]. In conclusion, 2-HG is a metabolite with physiological regulatory roles and alterations in its levels can lead to significant changes in cellular function.

Elevations in L-2HG is particularly of interest because its production occurs in hypoxia and acidic conditions, and therefore can serve marker of metabolic reprogramming in DKD. We hypothesized that in DKD, due to increased lactate production and glucose-flux into the TCA cycle with potential consequential accumulation of α-ketoglutarate, will result in increased 2-HG production, in particular of L-2HG. We investigated the level of D and L-2HG in urine, plasma, and kidney cortex of B6.BKS(D)-Lepr db/J (*db/db*) mice, which is a pathophysiologically relevant model of type-2 diabetes DKD [217].

4.3 Results

4.3.1 Urine, Plasma Concentration and Percent Fractional Excretion of D and L-2HG

Derivatization of 2-HG with chiral agent (+)-O,O'-Diacetyl-L-tartaric anhydride (DATAN) allows for the separation of the enantiomers on reverse-phase column. Using this method, we quantitatively measured levels of D and L-2HG from diabetic *db/db* and control *db/+* littermates. We found increased levels of L-2HG in the *db/db* urine (**Fig. 4-1A**), while the plasma levels were not different between the groups (**Fig. 4-1C**). Of note, measured metabolites in the urine were normalized to urinary creatinine concentration, which is an accepted method of determination for urinary protein or metabolite levels in DKD. The major disadvantage of spot urine samples is that the hydration status and the resultant rate of production of urine makes urine concentration variable. In addition, disease-specific differences in concentrating function and osmotic diuresis in DKD can result in substantial variations in metabolite concentrations. In an attempt to adjust for this variation, urinary creatinine (UCr) concentration is most commonly used in a ratio to normalize analyte quantification for specimen concentration[218]. D-2HG levels were elevated in the *db/db* urine **(Fig. 4-1B**) although the levels did not reach significance ($p = 0.056$), while the plasma levels in the *db/db* urine were significantly decreased (**Fig. 4-1D**). Increased urinary excretion of metabolites can be due to increased filtration or increased production by the kidney. Hyperfiltration occurs in *db/db* mice and remains elevated compared to controls until at least 28 weeks of age[219], although the GFR eventually declines with age[89,219] . The reduction in plasma D-2HG levels in *db/db* mice, in particular, suggest that the increased GFR may lead to increased urinary excretion of D-2HG. We then calculated the fractional excretion of D (**Fig. 4-1F**) and L-2HG (**Fig. 4-1E**), which is calculated with the formula: $[\text{D or L-2HG}]_{\text{Urine}} \times [\text{Creatinine}]_{\text{Plasma}} / [\text{D or L-2HG}]_{\text{Plasma}} \times [\text{Creatinine}]_{\text{Urine}}$. Fractional excretion of both D and L-2HG were significantly

elevated in the *db/db* mice, suggesting that the increased urinary levels of both metabolites is independent of GFR and systematic production of the metabolite, and is likely due to increased tubular excretion, decreased tubular reabsorption or increased kidney production of D and L-2HG.

4.3.2 Elevated TCA Cycle Metabolites Drive Increased D and L-2HG Fractional Excretion

In order to assess for potential factors leading to increased D and L-2HG urinary levels, we quantified the levels of TCA cycle metabolites and D and L-2HG levels in the *db/db* and *db/+* mice kidney cortex. We found significant elevations in all TCA cycle metabolites **(Fig. 4-2A and Table 1**), including α-ketoglutarate, the substrate for D and L-2HG. In our previous work (Ref 4), α-ketoglutarate was not reliably detected, hence quantification was not feasible. Our new method increased sensitivity due to improvements in HILIC; improvements in sensitivity and peak shapes of organic acids has been observed with addition of phosphate[169] or phosphate containing additives[170] to the samples or mobile phases. Phosphates are thought to shield metal ion interaction with organic acids, improving peak shape and sensitivity. Kidney cortical levels of D and L-2HG were not significantly different between *db/db* and *db/+* (**Fig. 4-2A**), potentially due to the excretion of metabolites into the urine, maintaining normal intracellular levels of D and L-2HG. In order to determine increased levels of D and L-2HG levels are due to changes in D-2HGDH and L-2HGDH protein levels, we assessed the levels of the enzymes with Western blots (**Fig. 4-2B**) and found no difference between the two groups. We measured TCA cycle metabolites from the plasma and urine of *db/db* and *db/+* mice (**Table 2, 3**). There was no significant difference between the two groups in the metabolite

levels in either plasma or urine. Only α-ketoglutaric acid levels in urine samples met p-value < 0.05, but failed to meet significance with multiple testing correction. The urine and plasma data suggest that elevations in 2-HG are localized to the kidney.

4.3.3 Hyperglycemia Increases D And L-2HG Production in Human Proximal Tubular HK-2 Cells

As a proof-of-concept, we cultured human proximal tubular HK-2 cells in low glucose (5 mM), high glucose (25 mM) and low glucose (5 mM) with mannitol (20 mM) as osmotic control for 48 hours and assessed the levels of D and L-2HG production (**Fig 4-3A, B**). Studies have found HK-2 cell exposure to hyperglycemic conditions leads to metabolic reprogramming and leads to increased glucose metabolism and lactate production [220]. We found that in hyperglycemic conditions, cellular levels of D and L-2HG increased compared to low glucose and osmotic control conditions, suggesting that a diabetic milieu can lead to increased D and L-2HG production. LC/MS measurements of TCA cycle metabolites from HK-2 cells in low glucose, high glucose and low glucose with osmotic control are displayed in **Table 4**. Our analysis shows that all TCA cycle metabolites are elevated under the high glucose conditions above both the low glucose and osmotic control group. We did not detect 2-HG in the media consistently (below range of detection in several samples, Data not shown). This data is consistent with mouse kidney cortex data for TCA cycle intermediates. While 2-HG in media was not analogous to *in vivo* mouse data, it is likely due to the fact that transformed cell culture models are not fully representative of normal *in vivo* tissue. From our findings, we propose that increased glucose utilization in DKD can lead to increased levels of TCA cycle metabolites, including α-ketoglutarate, and drive 2-HG production.

4.4 Discussion

In summary, we found elevated levels of D and L-2HG enantiomers in *db/db* urine. Increased fractional excretion of D and L-2HG in *db/db* mice suggests that increased secretion or kidney production of D and L-2HG underline elevated levels of D and L-2HG in the DKD model. To our knowledge, this is the first investigation of 2-HG enantiomers in a murine model of DKD. A recent study by Hyeon *et. al.,* found that 2-HG was one of 16 urine metabolites in type-1 diabetic STZ mice whose levels were restored to baseline by treatment with the RAS inhibitor losartan [221]. This finding is consistent with our finding that overall levels of 2-HG are increased in the urine in *db/db* mice and suggest that it may serve as a biomarker for DKD. Cheng *et.al.,* [222] examined D and L-2HG urinary levels in diabetic and non-diabetic patients, but found no significant differences in the levels between the two groups for both enantiomers, potentially because of the relatively small sample size and because elevations of 2-HG may only occur in the context of DKD, and not necessarily in diabetes.

2-HG has been demonstrated in several circumstances to negatively regulate mitochondrial metabolism. In the context of IDH mutations, D-2HG has been found to inhibit ATP synthase activity[223] and impair α-ketoglutarate dehydrogenase in cardiac muscles and decrease mitochondrial membrane potential[224]. A study of L-2HGDH global knockout (KO) mice found the highest tissue accumulation of L-2HG in the kidney of the KO mice, compared to other metabolically active organs, liver and muscle. In the absence of L-2HGDH, the kidney displayed reduction in TCA cycle metabolites, proposed to occur due to inhibition of α-ketoglutarate dehydrogenase activity by L-2HG[225]. α-ketoglutarate

dehydrogenase generates NADH, serves as a redox sensor for the mitochondria, and regulates mitochondrial energy production[226].

In our studies, the downstream TCA intermediates distal to α-ketoglutaric acid are elevated in addition to 2 HG, suggesting not all α-ketoglutaric acid is converted to 2-HG. In addition, as the TCA cycle serves as a hub for central carbon metabolism, it has many sources of input into the cycle and therefore downstream metabolite levels could be changed even if substantial α-ketoglutaric acid is converted to 2-HG. While our data demonstrated significant elevations of TCA cycle metabolites in the *db/db* mice, multiple metabolomics studies of DKD patient urine have found disparate regulation of different TCA cycle metabolites. Studies have shown that acotinic acid and citrate/isocitrate urinary levels are downregulated in DKD patients, in comparison to diabetic patients[227–229], and potentially predict DKD progression[230], whereas urinary fumarate and malate levels are upregulated in DKD[227]. Since the *db/db* mouse is an early-model of DKD, clinical findings are likely to represent disease states more advanced than represented by the mouse model and it is likely that the TCA cycle becomes progressively more dysregulated with disease progression. We propose that 2-HG may play a role in mediating metabolic dysfunction in DKD.

Although tissue levels of D and L-2HG were not elevated, and instead reflected in the urine in the *db/db* mice, in the context of falling GFR and tubular damage, 2-HG levels may become elevated and become a uremic solute. The kidneys, in particular the tubules, maintain metabolic homeostasis by excreting excess metabolic intermediates into the urine, such as short-chain acylcarnitines[108]. 2-HG may be similarly excreted to reduce metabolic stress. A limitation of our study is that while the cortex is mainly composed of

proximal tubules by volume, it still represents a mixture of different cell types in the kidney and spatial localization of 2-HG remains unknown. Mass spectrometry imaging (MSI) with Desorption Electrospray Ionization Mass Spectrometry and matrix-assisted laser desorption/ionization (MALDI) time of flight (TOF) has been used in human and murine-models of DKD for compartment-specific expression of metabolites[231–233] and 2-HG detection with MALDI-TOF has been accomplished in brain tumors with IDH mutations[234]. However, no current MALDI-TOF data is available for 2-HG levels in DKD. To understand whether alterations in the TCA cycle and 2-HG are specific to proximal tubules in DKD, a future MSI imaging study may provide compartment specific spatial information.

Elevations in 2-HG may also lead to altered epigenetic programming, in particular by inhibiting α-ketoglutarate-dependent dioxygenases. Altered methylation patterns have been associated with DKD in the Chronic Renal Insufficiency Cohort (CRIC)[230], Pima Indians[235] and the Diabetes Control and Complications Trial/Epidemiology of Diabetes Interventions and Complications cohort[236]. Future studies of clinical samples from these cohorts may uncover the role of 2-HG in epigenetic regulation in DKD.

4.5 Materials and Methods

Materials: Male BKS *db/db* mice (BKS.Cg-m +/+ Lepr db/J) and littermate controls (*db/+*) were purchased from Jackson Labs at 12 wks of age. L-α-Hydroxyglutaric acid disodium salt (L-2HG), D-α-Hydroxyglutaric acid disodium salt (D-2HG), L-α-Hydroxyglutaric acid-$^{13}C_5$ disodium salt, α-ketoglutarate, α-ketoglutarate, cis-aconitate, citrate, fumarate, malate, succinate, glucose, mannitol, ammonium formate, formic acid, (+)-O,O′-Diacetyl-L-tartaric anhydride (DATAN) and dichloromethane were purchased from Sigma-Aldrich. $^{13}C_5$ α-ketoglutarate, $^{13}C_6$ citrate, $^{13}C_4$ fumarate, $^{13}C_4$ malate, $^{13}C_4$ succinate were

purchased from Cambridge Isotope Labs Inc. Human kidney 2 (HK2) cells were purchased from American Type Culture Collection (ATCC® CRL-2190™). LC–MS-grade water, acetonitrile, chloroform and methanol were obtained from Fisher Scientific. Antibodies for L-2HGDH and D-2HGDH were purchased from Proteintech Group Inc.

Animals: Mice were housed in a climate-controlled, light-regulated facility with a 12:12 hour light-dark cycle with water and chow ad libitum. At 24 weeks of age prior to sacrifice, blood and urine were collected. Plasma was obtained by centrifuging blood in ethylenediaminetetraacetic acid-coated tubes for 2 min at 5000 x g. Before sacrifice, mice were fasted for 4 hrs. Kidney was perfused with ice-cold PBS through the left ventricle and the kidney was dissected for the cortex region on ice. All samples were snap frozen and stored at -80°C until analysis. The study was conducted according to the guidelines of the University of Michigan Committee on Use and Care of Animals (project identification code: PRO00009416, date of approval: 2/14/2020)

Cell culture: Cells were grown in Dulbecco's Modified eagle Medium, low glucose (ThermoFisher Scientific, Invitrogen) supplemented with 10% heat-inactivated fetal bovine serum (FBS; Corning®) and 1% Penicillin/Streptomycin (Invitrogen), at 37 °C in 5% CO_2. Cells were cultured between 1-10 passages. Media was changed every 24 hrs. For experiments, 4 x 10^5 cells were plated in 6-well plates per well and grown to 80% confluence. Cells were serum deprived for 24 hrs and cultured with 5 mM glucose (low glucose), 25 mM glucose (high glucose), and 5 mM glucose with 20 mM mannitol (osmotic control) supplemented with 0.1% FBS and 1% pen/strep for 48 hrs. The experiment was performed in triplicate, with two extra wells for each condition for cell counting in order to

normalize metabolite concentrations. Cell counts were conducted with hemocytometers and 0.4% trypan-blue solution to assess for cell viability.

Creatinine analysis: Urine creatinine was measured as previously published [237]. Plasma creatinine was measured with the same method by precipitating protein by pipetting 10 µLof plasma into 90 µL of methanol, and injecting 5 µL for analysis.

2-HG (L- and D-Isomer) sample preparation and analysis: Samples were prepared using modified versions of previously reported [211]. Briefly, 0.5 mL of a chilled mixture of methanol, chloroform and water (7:2:1) containing 1 µM of the internal standard, $^{13}C_5$-L-2HG, was added to 15 µL of plasma or urine volume consisting of 200 ρmoles of creatinine. Tissue samples and HK-2 cells were homogenized and sonicated in methanol, and chloroform and water with 1 µM internal standard were added to a final ratio of 1:2:1 of methanol: chloroform: water. All samples were centrifuged at 17,000 x g, for 10 mins in 4 °C and the supernatant was transferred to a glass vial and dried under nitrogen. For tissue and cell culture samples, only the resulting upper layer was dried. Samples were then derivatized with DATAN in dichloromethane: acetic acid (4:1) solution at 75 °C for 1 hour. Samples were dried in a speed-vac at 45 °C for 1 hr. A standard curve of a mixture of D- and L-2-HG authentic samples, was created and derivatized in the same manner as the samples for quantification and retention time confirmation purposes. Samples were reconstituted in water and 5 µL were injected. LC-MS analysis was performed on an Agilent system consisting of a 1290 UPLC module coupled with a 6490 or 6495 triple quadrupole mass spectrometer (Agilent Technologies, CA, USA). Samples were separated as previously reported [211]. Source conditions were as follows: gas temperature 200 °C, gas flow 14 L/min, nebulizer 35 psi, and capillary voltage 3000V.

TCA cycle metabolite sample preparation and analysis: Kidney cortex samples were prepared as previously published[238]. Internal standards were added each at final concentrations of 20 µM during sample preparation. Samples were reconstituted in 2:1 ACN: water and 5 µL were injected for analysis. A standard curve of a mixture of authentic samples of all measured metabolites was created and processed in the same manner as the samples for quantification and retention time confirmation purposes. LC-MS analysis was performed on an Agilent system consisting of a 1290 UPLC module coupled with 6495 triple quadrupole mass spectrometer (Agilent Technologies, CA, USA). Metabolites were separated on an InfinityLab Poroshell120 HILIC-Z, 2.7 µm, 2.1 × 150 mm column (Agilent Technologies, CA, USA). Mobile phase A was composed of 90% 10 mM ammonium acetate pH 9.0 with ammonia, 10 % acetonitrile (ACN) with 2.5 uM InfinityLab Deactivator Additive (Agilent Technologies, CA, USA) and mobile phase B was composed of 15% 10 mM ammonium acetate pH 9.0 with ammonia, 85% acetonitrile with 2.5 uM InfinityLab Deactivator Additive. The flow rate was 0.25 mL/min, and the gradient was as follows: 0-2 min at 95 % B, 2-5 min at 95% B, 5-5.5 min at 86%, 5.5-8.5 min at 86% B, 8.5-9 min at 84% B, 9-14 min at 84% B, 14-17 min at 80% B, 17-23 min at 60% B, 23-26 min at 60% B, 26-27 min at 95% B, and 27-35 min at 95% B. Column compartment temperature was kept at 25 °C. Data was acquired in negative mode. Transitions for compounds were as follows: α-ketoglutarate 145 → 101 *m/z*, $^{13}C_5$ α-ketoglutarate 150 → 105 *m/z,* cis-aconitate 173 → 85 *m/z*, citrate/isocitrate 191 →110.9 *m/z*, $^{13}C_6$ citrate 191 → 110.9 *m/z*, fumarate 115 → 119 *m/z*, $^{13}C_4$ fumarate 119 → 74 *m/z*, malate 133 → 71.1 *m/z*, $^{13}C_4$ malate 133 → 71.1, *m/z*, succinate 117 → 72.8 *m/z*, $^{13}C_4$ succinate 121 → 76.1

m/z. Source conditions were as follows: gas temperature 225 °C, gas flow 13 L/min, nebulizer 35 psi, and capillary voltage 3500V.

Western blot: Kidney cortex samples were homogenized in 2% SDS, 10% glycerol, 0.05 mM Tris pH 6.8 with 1X Halt™ Protease Inhibitor Cocktail (Thermofischer). The lysate was sonicated on ice for 30 s and centrifuged at 4 °C for 10 min at 17,000 x g. The supernatant was quantified for protein concentration with the DC protein assay kit (Bio-Rad). 20 µg of protein were separated on 12% SDS-PAGE gel and transferred to PVDF membranes. Membranes were probed with D2HGH and L2HGH antibodies.

Data analysis and statistics: Quality control samples were made by pooling all the samples in the queue and run intermittently to control for machine drift and sample stability. Peak areas were extracted with Agilent Mass Hunter Workstation Software Quantitiative Analysis for QQQ version B.07.01. Peak areas were normalized to internal standard before quantification. All statistics were performed with GraphPad Prism 7. Data was analyzed with student's t-test with FDR correction where indicated or One-way ANOVA with Tukey's post-hoc correction.

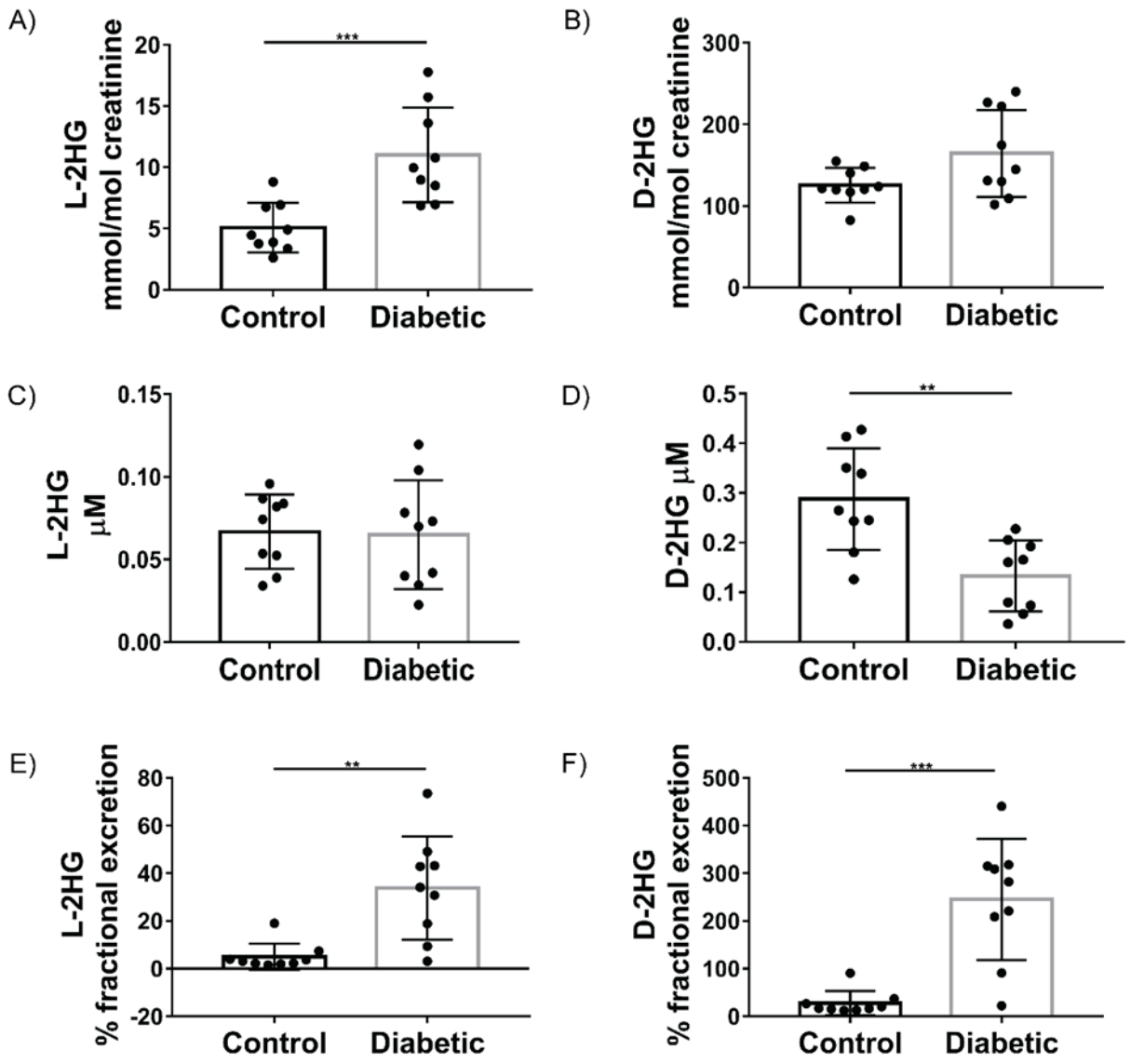

Figure 4-1 Concentration of L and D-2HG (±SD) in plasma and urine and calculated percent fractional excretion of each metabolite from Control (*db*/+) and Diabetic (*db/db*) and mice.

A) Urinary L-2HG and B) Urinary D-2HG levels normalized creatinine, C) plasma L-2HG levels, D) plasma D-2HG levels, E) % fractional excretion of L-2HG, F) % fractional excretion of D-2HG. Student's t-test, *** = p value ≤0.001, **** = p value ≤0.0001.

TCA cycle metabolite	concentration *db/+* (SD)	concentration *db/db* (SD)	p-value	q-value
α-ketoglutaric acid	37.0 (0.41) pmol/mg	88.9 (0.97) pmol/mg	0.011	0.013
fumarate	0.98 (0.31) nmol/mg	1.67 (0.53) nmol/mg	0.008	0.013
malate	1.63 (0.49) nmol/mg	3.27 (1.28) nmol/mg	0.005	0.012
succinate	1.50 (0.63) nmol/mg	2.42 (0.43) nmol/mg	0.006	0.013
cis-aconitate	94.5 (123) pmol/mg	747.5 (475) pmol/mg	0.002	0.012
citrate/isocitrate	0.64 (0.24) nmol/mg	1.26 (0.56) nmol/mg	0.014	0.014

Table 4-1 Concentration of TCA cycle metabolites from *db/+* vs. *db/db* kidney cortex.

Concentration of each metabolite was normalized to tissue protein. Q-value was calculated with Benjamini, Krieger and Yekutieli procedure. *n* = 8-9.

TCA cycle metabolite	concentration *db/+* (SD)	concentration *db/db* (SD)	p-value	q-value
α-ketoglutaric acid	7.15 (5.97) pmol/µL	4.79 (1.82) pmol/µL	0.305	0.6163
fumarate	2.15 (0.64) pmol/µL	3.61 (1.65) pmol/µL	0.053	0.1615
malate	5.81(1.22) pmol/µL	9.94 (5.00) pmol/µL	0.047	0.1615
succinate	2.71 (3.92) pmol/µL	4.52 (7.67) pmol/µL	0.585	0.8861
cis-aconitate	0.68 (0.44) pmol/µL	0.69(0.41) pmol/µL	0.994	1.0000
citrate/isocitrate	44.9 (13.9) pmol/µL	43.5 (9.03) pmol/µL	0.821	0.9954

Table 4-2 TCA cycle metabolites in *db/db* and *db/+* plasma.

Concentration of each metabolite was normalized to plasma volume. Q-value was calculated with Benjamini, Krieger and Yekutieli procedure. *n* = 7-8.

TCA cycle metabolite	concentration *db/+* (SD)	concentration *db/db* (SD)	p-value	q-value
α-ketoglutaric acid	30.8 (15.8) mmol/mol	54.8 (24.9) mmol/mol	0.0472	0.2439
fumarate	0.59 (0.08) mmol/mol	0.77 (0.44) mmol/mol	0.4859	0.4908
malate	4.87 (1.50) mmol/mol	3.31 (5.57) mmol/mol	0.3118	0.4908
succinate	7.68 (3.90) mmol/mol	4.61 (2.26) mmol/mol	0.0805	0.2439
cis-aconitate	6.28 (1.53) mmol/mol	5.56 (2.23) mmol/mol	0.4841	0.4908
citrate/isocitrate	182 (29.2) mmol/mol	203 (73.6) mmol/mol	0.4784	0.4908

Table 4-3 TCA cycle metabolites in *db/db* and *db/+* urine.

Concentration of each metabolite was normalized to plasma volume. Q-value was calculated with Benjamini, Krieger and Yekutieli procedure. *n* = 7 – 8.

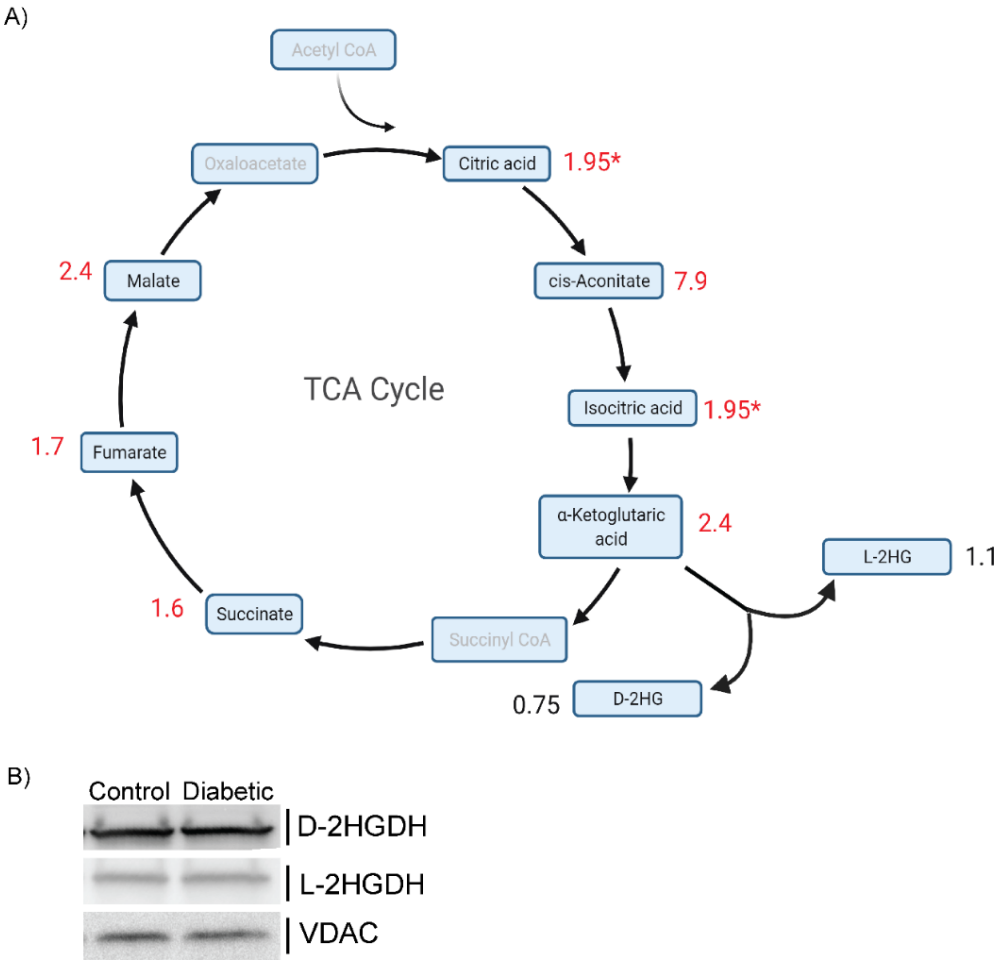

Figure 4-2 Kidney cortex levels of TCA cycle metabolites drive D and L-2HG production.

A) Schematic of TCA cycle with fold change (Control *db/+* vs. diabetic *db/db*) denoted (red if $p < 0.05$ and black if did not meet significance). Metabolites in gray were not measured in the study. *: Citrate and isocitrate were measured as one transition. B) Western blot of db/+ and db/db cortex for D-2HGDH, L-2HGDH, and VDAC ($n = 4$). Fig. 2A created with BioRender.com.

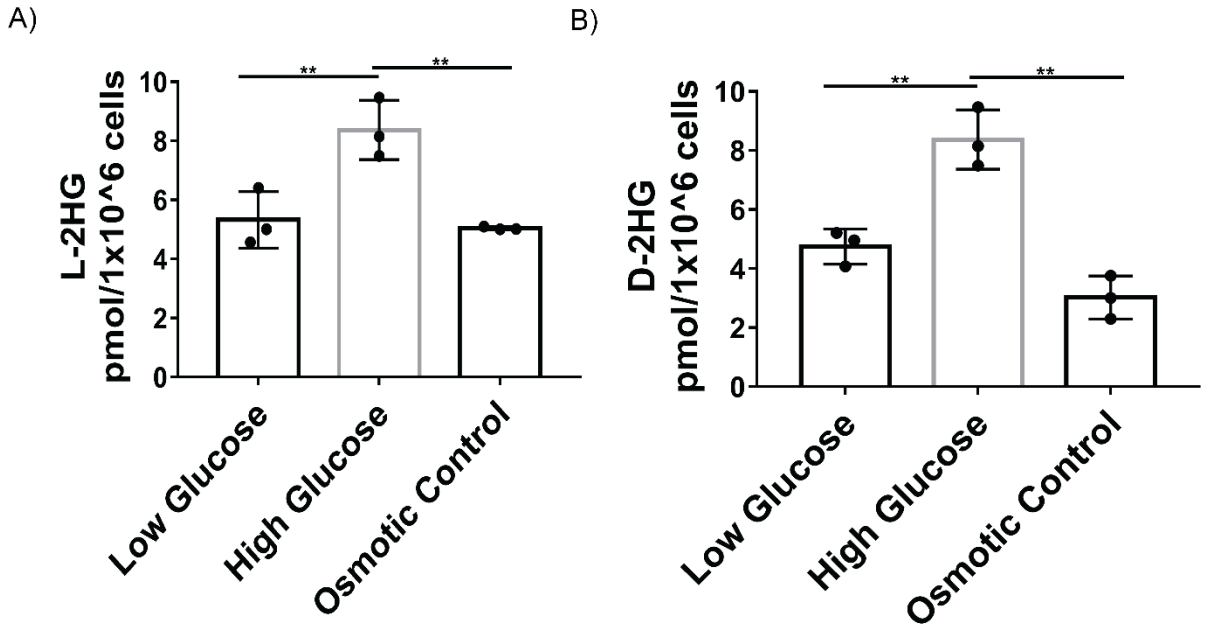

Figure 4-3 HK-2 production of D and L-2HG in high glucose media.

A) L-2HG and B) 2-HG levels from HK-2 cells cultured in 5 mM glucose (low glucose), 25 mM glucose (high glucose), 5mM glucose with 20 mM mannitol (osmotic control). One-way ANOVA with Tukey's post-hoc correction, ** = p value ≤0.01.

TCA cycle metabolite	Low Glucose (SD) pmol/10^5 cells	High Glucose (SD) pmol/10^5 cells	Osmotic Control (SD) pmol/10^5 cells
α-ketoglutaric acid *†§	6.18 (0.37)	7.96 (0.55)	4.31 (0.55)
fumarate *†§	15.4 (1.40)	17.7 (1.34)	10.9 (0.52)
malate *†§	31.7 (1.54)	35.2 (1.37)	24.8 (1.50)
succinate *†§	6.14 (1.09)	13.9 (0.97)	10.3 (0.81)
cis-aconitate *†	0.49 (0.05)	0.79 (0.23)	0.45 (0.09)
citrate/isocitrate *†	12.5 (1.31)	16.3 (1.09)	11.3 (0.40)

Table 4-4 TCA cycle metabolites in HK-2 cells under 5 mM glucose (low glucose), 25 mM glucose (high glucose), and 5 mM glucose and 20 mM mannitol (osmotic control).

Concentration of each metabolite was normalized to the cell count. * : adjusted p-value < 0.05 for low glucose vs high glucose, †: adjusted p-value < 0.05 for osmotic control vs. high glucose, §: adjusted p-value < 0.05 for low glucose vs. osmotic control. One-way ANOVA with Tukey's post-hoc correction. *n* = 4.

Chapter 5

$^{13}C_6$-Glucose Metabolic Flux Analysis Reveals Reduced Mitochondrial Metabolism in T1D Subjects

5.1 Abstract

In diabetes, the kidneys and in particular the proximal tubules are subject to higher levels intracellular glucose and reabsorption load, but exactly how this increased glucose burden affects kidney metabolism is unclear. To investigate the kidney glucose metabolism in normoglycemic and acutely hyperglycemic conditions, we conducted a euglycemic and hyperglycemic clamp study in matched healthy patients, type 1 diabetes (T1D) with no microvascular complications, and T1D patients with diabetic kidney disease (DKD) with $^{13}C_6$-glucose. Liquid chromatography tandem mass spectrometry analysis of patient urine acquired during the study demonstrated reduced labeled TCA metabolites in T1D patients with DKD, suggesting a decrease in mitochondrial metabolism of glucose. Our data suggests that T1D with DKD patients exhibit mitochondrial dysfunction and metabolize glucose differentially from both healthy controls and T1D patients with no DKD.

5.2 Introduction

Significant metabolic reprogramming occurs in DKD. Metabolomic studies of murine models of DKD demonstrate increased glucose metabolism and increased urinary

and tissue lactate production. These changes in metabolism are potentially due to mitochondrial dysfunction, which is a hallmark of DKD; inefficient ATP production due to failing mitochondria may lead to increased fuel utilization to maintain energy production albeit via less efficient methods (e.g., lactate production). Our previous study of *in vivo* glucose metabolism in *db/db* mice kidney cortex demonstrated increased glucose flux into the TCA cycle, contributing to increased tissue accumulation of TCA cycle metabolites. Whether this upregulation in glucose is adaptive or ultimately maladaptive to the kidney is unclear. However, altered levels of TCA cycle metabolites have been found in the urine of DKD patients and have been demonstrated to be valuable biomarker of not only DKD, but C in general.

Stable isotopic labeling metabolomics studies allows for measurement of the relative rate of utilization of specific metabolites of interest. It also allows us to trace the fate of the labeled metabolite. As we previously observed that glucose utilization is upregulated in the *db/db* cortex from metabolic flux analysis conducted with $^{13}C_6$-glucose glucose, we hypothesized that increased glucose utilization by the kidney may also occur in patients with early DKD. We conducted metabolic flux analysis in healthy subjects, T1D patients with no DKD, and T1D with DKD. To understand whether potential differences in glucose utilization between the three groups depending on amount of blood glucose levels, we conducted euglycemic and hyperglycemia clamp studies with $^{13}C_6$-glucose. We assessed the relative labeling percentages of compounds observed in the urine, as a surrogate of measure of kidney metabolism of the $^{13}C_6$-glucose.

5.3 Results

5.3.1 Study Design and Patient Data

Patient study design, patient enrollment, IRB approval and sample collection was overseen and performed by Dr. Rodica Busui and the co-investigators of the clinical trial study: NCT01823406. I performed the sample extraction and analysis portions of the study.

Patients were divided into three groups: normal healthy controls (defined as < HbA1c 6.0), T1D with DKD and other microvascular complications, and T1D with no microvascular complication. The study (**Fig. 5-1**) started with a “pre-clamp” in which patients were infused with $_{12}C^{6}$-glucose glucose to determine glucose and insulin infusion rate in preparation for the following euglycemic clamp portion of the study. During both the pre-clamp and euglycemic clamp portions, blood glucose was maintained at 100 mg/dL ± 20% of target blood. The euglycemic clamp study lasted for 4 hrs, during which plasma and serum were collected at 30 min increments and urine was collected. The hyperglycemic clamp study lasted 4 hrs or until patients could tolerate the hyperglycemia. Plasma, serum and urine were collected similarly to during the euglycemic clamp study.

Table 1 lists the clinical characteristics of the participants of the study. The most notable difference between T1D, no complication and T1D, DKD group are that the DKD patients on average are older, have had a longer duration of T1D, and require significantly higher daily insulin units. Of note, hemoglobin A1C (HbA1C), creatinine and eGFR levels were not significantly different between the T1D, no complications and the T1D, DKD group. Creatinine and eGFR values were significantly different between the T1D, DKD and the healthy control group.

Hyperglycemic clamp study demonstrates increased glucose-derived labeling of urinary metabolites

Urine collected during the hyperglycemic clamp study were pooled for each study subject, processed and analyzed for isotopic labeling of labeled glucose derived metabolites in the urine. **Figure 5-2A** demonstrates an example of urinary malate peak from a patient sample and the extracted ion-chromatograph of the associated malate isotopologues from the malate peak. To compare the relative glucose utilization and labeling of urinary metabolites, we calculated the % isotopologue as shown in **Figure 5-2B**, for isotopologues that correspond to direct catabolism of $^{13}C_6$-glucose. We also assessed the relative level of $^{13}C_6$-glucose excreted into the urine during the hyperglycemic clamp study (**Figure** 5-**2C**); there was no significant difference in $^{13}C_6$-glucose in the urine, suggesting similar levels of kidney glucose uptake and excretion between the three study groups.

Urinary metabolites in the TCA cycle and glycolysis were detected in all three groups. Analysis of the TCA cycle metabolite isotopologues demonstrated significantly increased glucose incorporation into the healthy control urine in comparison to T1D patients with DKD and no DKD for malate, fumarate and α-ketoglutarate. Incorporation into citrate and cis-aconitate were significantly elevated in the healthy control group only in comparison to the T1D DKD patients. Incorporation into glycolytic metabolite lactate was significantly elevated in the healthy control urine, whereas incorporation into pyruvate was not significantly different between any of the groups. Incorporation into secondary glucose metabolite sorbitol was significantly elevated in both the healthy control and T1D with no microvascular complications in comparison to the T1D DKD group.

5.3.2 Euglycemic Clamp Study Demonstrates Minimal Incorporation of Glucose into Urinary Metabolites

TCA cycle metabolites were detected in urine from patients collected during the euglycemic portion of the study, but glycolytic intermediates (lactate, pyruvate, and sorbitol) in addition to $^{13}C_6$-glucose were not detected. In comparison to metabolites from the hyperglycemic clamp study, minimal labeled carbon incorporation was observed into metabolites from the euglycemic clamp study for malate, fumarate, citrate, cis-aconitate, and α-ketoglutarate. Zero abundances were frequently observed for the M+2 isotopologues, and no significant differences were observed between the three groups except for cis-aconitate, which demonstrated significantly elevated incorporation in the healthy control urine in comparison to the T1D DKD group.

5.4 Discussion

Our glucose labeling studies suggest that T1D results in decreased glucose mitochondrial metabolism, compared to healthy subjects under hyperglycemic conditions. This difference was most consistent between healthy controls and T1D with DKD. Under normoglycemic conditions, all three groups demonstrated minimal labeling of TCA cycle metabolites from glucose. Our data suggests that metabolic changes occur in T1D that results in reduced glucose mitochondrial metabolism. Because no significant differences were observed in incorporation between T1D, DKD and T1D, no complication patients, we cannot necessarily assume a DKD specific effect on kidney mitochondria.

Metabolites in the urine are the products of two separate processes: filtration of plasma (systemic metabolism) and secretion by the tubules (kidney metabolism). The current study gives an incomplete picture of glucose metabolism in the three groups. Measurement of plasma metabolites and calculation of fractional excretion of isotopologues of interest will give more information about kidney specific glucose

metabolism. Increased fractional excretion, for example, indicates increased urinary metabolites levels independent of GFR and systematic production of the metabolite, and is likely due to increased tubular excretion, decreased tubular reabsorption or increased kidney production. CKD results in insulin resistance; a hyperinsulinemic-euglycemic clamp study of control and CKD patients found attenuated reduction in plasma amino acids, including glutamine which is processed by the mitochondria, levels by insulin in the CKD patients[239]. It is possible that reduction in urinary TCA cycle metabolite labeling occurs due to insulin resistance in T1D, DKD patients. Although the blood glucose levels were carefully titrated during clamp studies, it is possible that decreased uptake and metabolism of glucose could occur between subjects and measurement of plasma metabolites will demonstrate whether systemic insulin resistance or kidney-specific insulin resistance may underlie the differential labeling we observe between the groups.

The level of urinary TCA cycle metabolites in relation to DKD is associated with the disease severity. In general, higher levels of TCA cycle metabolites are identified in the urine in early DKD and reduced levels of urinary TCA cycle metabolites are found in late DKD[240]. Analysis of the family investigation nephropathy and diabetes cohort found elevated urinary citrate, succinate, fumarate and malate baseline levels from DKD progressors in comparison to the resistors. These patients all displayed normal eGFR levels (>90 mL/min/1.73 m^2)[85]. Studies with DKD patients with significantly reduced eGFR demonstrate lower urinary aconitic acid and citrate in comparison to healthy subjects and diabetic patients with no DKD[228]. Citric and aconitic acid have been found to predict DKD progression in the diabetic CRIC cohort[230] and in another study by Liu *et. al*[227]*.* In our study, the T1D, DKD subjects were still in early phase of disease. We hypothesized that

increased renal glucose metabolism will occur in DKD patients and contribute to increased TCA cycle levels found in early DKD. Since no significant difference in glucose flux is observed between T1D, DKD and T1D, no complication patient, we suspect that altered fuel utilization, such as fatty acids and glutamate, may underlie the increased TCA cycle levels observed in early DKD.

A limitation of our study is that our targeted screen was able to consistently measure only a subset of metabolites in the glycolytic pathway and mitochondrial metabolism. We suspect that urine samples, which are high in inorganic salts and urea, can disrupt our hydrophilic interaction chromatography method, thus making retention and sufficient peak resolution difficult for lower abundant urinary metabolites. A method which allows for deeper coverage of urinary metabolites may uncover more information about glucose utilization in the kidney. On the other hand, the percent labeling of metabolites in the TCA cycle and glycolysis are quantifiable but low and suggests labeling of secondary metabolites outside of the central carbon pathway may not occur at sufficiently high levels for detection.

5.5 Materials and Methods

Urine preparation: Urine samples collected during the study were pooled for each patient and for the euglycemic and hyperglycemic clamp portions of the study. Pooled urine creatinine was measured as previously described. Urine volumes equaling to 40 nmoles of creatinine were transferred to glass vials and taken to dryness under nitrogen. Samples were then reconstituted with 30 µL of 2:1 acetonitrile: water solution, and 1µL of this sample was injected for analysis.

Liquid-chromatography and mass spectrometry (LC-MS) analysis: Samples were separated as previously described. Metabolites were analyzed on the Agilent 6456 QTOF mass spectrometer coupled to Agilent 1290 LC. Data was collected in negative mode, with gas temp at 225 °C, drying gas at 10 L/min, nebulizer at 40 psi, sheath gas temp 300 °C, and sheath gas flow at 12 L/min. Fragmentor voltage was set at 125 V, skimmer at 65 V, and VCap at 3000 V. Authentic standards of all measured metabolites were run separately and spiked into pooled samples for verification of metabolite and retention time.

Data analysis and statistics: Resulting data was analyzed with Agilent MassHunter Profinder 10.0. Batch isotopologue extraction was used with a previously generated metabolite library based on retention times of authentic samples. The isotope purity was set as 99%, and ion qualification settings included match tolerance mass of ±30 ppm, retention times ±0.2 min and coelution threshold of ≥ 0.50. Percent of isotopologues representing initial glucose metabolism (M+6 or M+3 for glycolytic metabolites, M+2 for first cycle of TCA cycle for all metabolites) were analyzed with One-Way ANOVA with Tukey's post-hoc correction with Graph Pad Prism 7.0.

Variables		Healthy controls	T1D, No complications	T1D, DKD
n (M/F)		9 (4/5)	9 (3/6)	18 (11/7)
Age (years) º		40 +/- 5	24 +/- 1	47 +/- 4
Diabetes Duration (years) º*		-	8 +/- 1	28 +/- 3
HbA1c (%) §†		5.5 +/- 0.1	8.0 +/- 0.4	7.9 +/- 0.3
BMI (kg/m2) †		24.3 +/- 1.4	25.1 +/- 0.7	28.2 +/- 1.9
Resting HR (bpm)		73 +/- 2	71 +/- 5	72 +/- 3
SBP (mm Hg)		121 +/- 3	118 +/- 5	132 +/- 4
DBP (mm Hg)		72 +/- 3	65 +/- 2	71 +/- 3
Creatinine †		0.76 +/- 0.03	0.86 +/- 0.05	1.02 +/- 0.06
eGFR (mL/min/1.73 m2) †		111 +/- 7	104 +/- 7	81.7 +/- 7
Triglyceride, mg/dL		97 +/- 12	86 +/- 20	96 +/- 11
HDLc, mg/dl		62 +/- 9	64 +/- 4	66 +/- 4
LDLc, mg/dl		91 +/- 7	83 +/- 7	89 +/- 8
Urine Albumin to Creatinine Ratio (ACR)		-	14 +/- 2	288 +/- 233
Diabetic retinopathy (*n*)	Mild NPDR	-	-	5
	Moderate NPDR			1
	Severe NPDR			2
	PDR			6
	With macular edema			4
Total Daily Dose Insulin (units) º*		-	43.6 +/- 5.2	78 +/- 4.5
Statin use *(n*)	Low intensity	0	0	2
	Moderate intensity	0	0	6
	High intensity	0	0	2
ACEi/ARB use (*n*)		0	0	10
Antihypertensive therapy (*n*)	1 medication	0	0	4
	2 medications	0	0	1
	≥3 medications	0	0	5
History of alcohol use (*n*)		2	4	9
History of tobacco use (*n*)		1	0	8

Table 5-1 Clinical characteristics of study participants.

One-ANOVA with Tukey's post-hoc correction §: $p < 0.05$ healthy controls vs. T1D, no complications, †: $p < 0.05$ healthy control vs. T1D, DKD, º: $p < 0.05$ T1D, no complications vs. T1D, DKD. º*: $p < 0.05$ healthy control vs. T1D, DKD, º: $p < 0.05$ T1D, no complications for student's t-test. Data are means +/- SEM unless otherwise indicated.

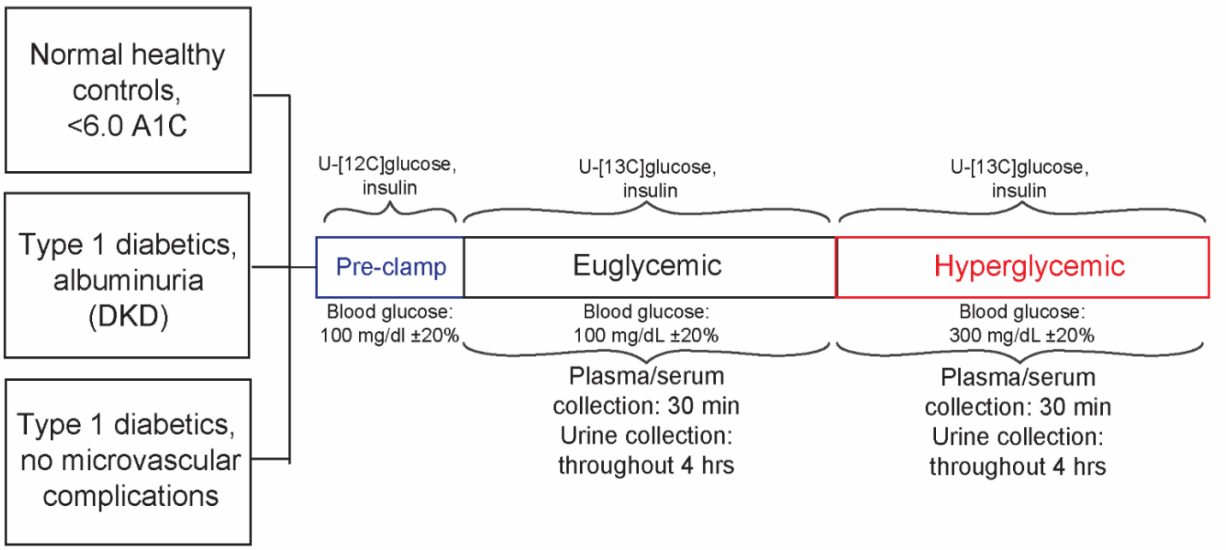

Figure 5-1 Schematic of euglycemic-hyperglycemic study

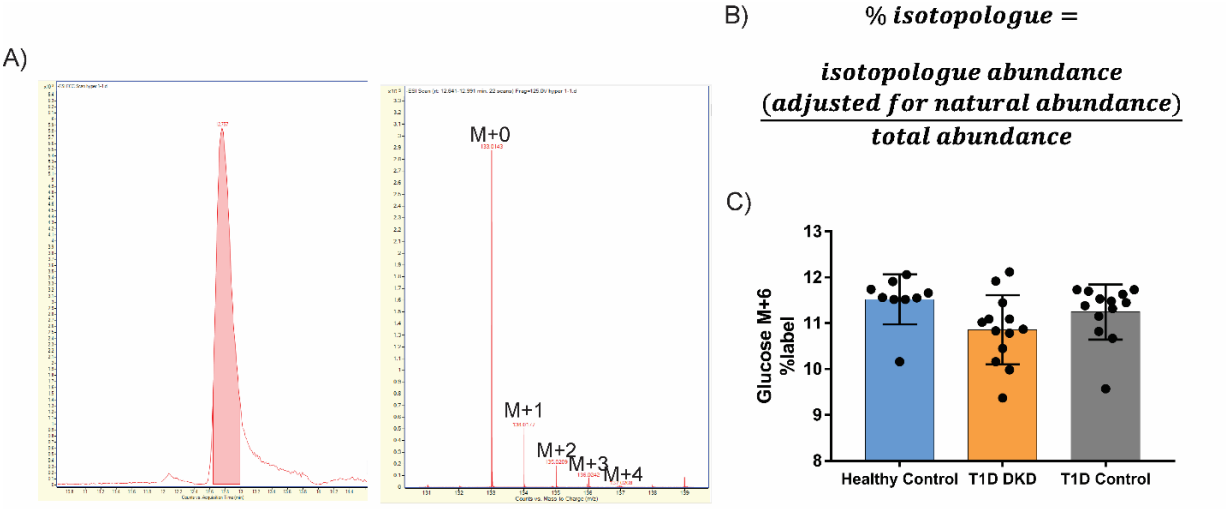

Figure 5-2 Glucose flux study information

A) Urinary malate LC-MS chromatogram from a urine sample and corresponding MS spectra of Fig. A with labeled isotoplogues (M+0, M+1, etc). B) Formula for calculating %label for isotopologue of interest of a metabolite. C) Labeled urinary glucose (M+6) from the hyperglycemic clamp study.

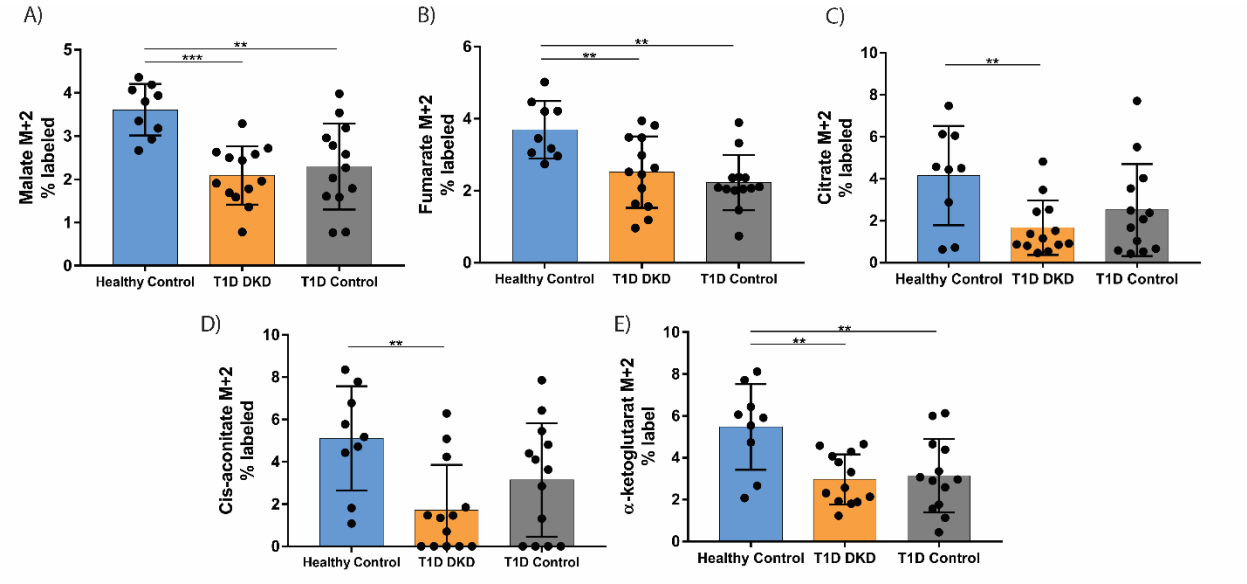

Figure 5-3 Labeled urinary TCA cycle metabolites from hyperglycemic clamp study

A-E: * = p <0.05, ** = p <0.01, *** = p < 0.001, One-way ANOVA with Tukey's post-hoc correction for multiple testing.

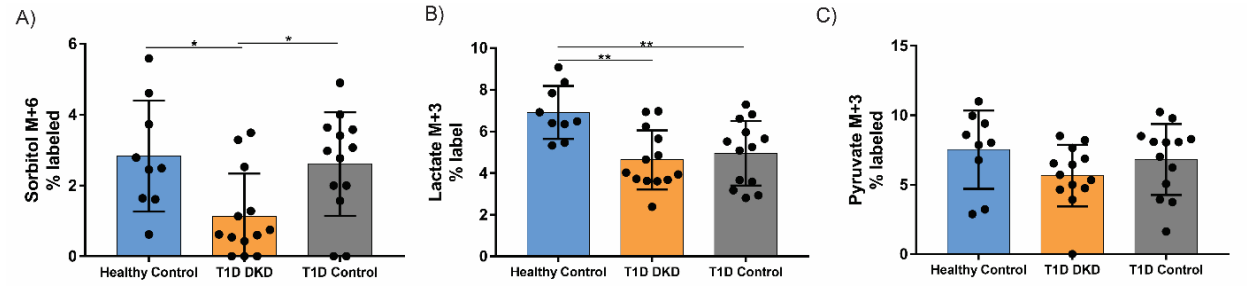

Figure 5-4 Labeled urinary glycolytic metabolites from hyperglycemic clamp study.

A-C: * = p <0.05, ** = <0.01. One-way ANOVA with Tukey's post-hoc correction for multiple testing.

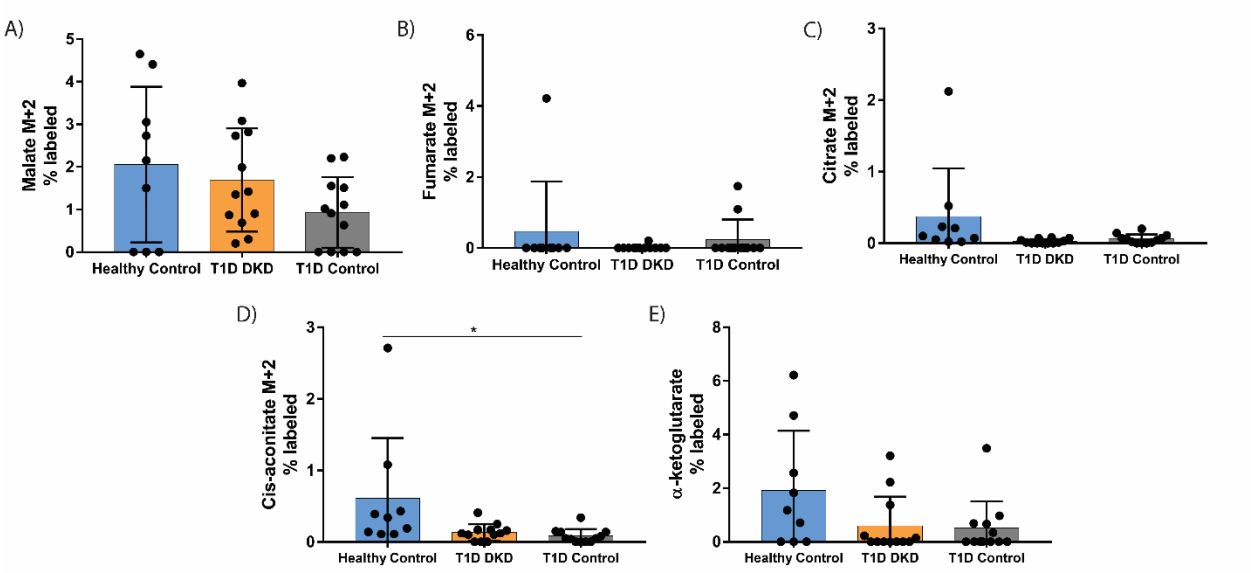

Figure 5-5 Labeled urinary TCA cycle metabolites from euglycemic clamp study.

A-E: * = p <0.05, One-way ANOVA Tukey's post-hoc correction for multiple testing.

Chapter 6

6.1 Discussion

In the first half of this thesis, we explored the role of malonylation and SIRT5 in DKD. We found decreased malonylation in the *db/db* proximal tubules, and that this occurs concurrently with increased glucose flux we observed in our previous studies. The decrease in malonylation is likely due to increased SIRT5 protein levels in the *db/db* mice. As SIRT5 activity and reduction in malonylation has been associated with increased glucose flux in several biological contexts[123,136], we hypothesized that SIRT5 mediates increased glucose utilization in DKD. We postulated that the increase in SIRT5 levels in the *db/db* cortex contributes to disease pathogenesis, as numerous studies with SGLT2 inhibitors have demonstrated that reduction of glucose burden on proximal tubules ameliorates DKD. Contrary to our hypothesis, SIRT5 HFD-STZ mice were relatively protected from DKD, although no metabolic effect of SIRT5 were observed from our metabolomics analysis. While these findings raised the possibility that increase in SIRT5 levels in DKD is adaptive, they were overall difficult to interpret as the background strain of the mice in our studies are relatively resistant to kidney disease and diabetes.

In order to conclusively elucidate the role of SIRT5 in DKD, generating proximal-tubular specific SIRT5 KO or OE mice in a kidney disease susceptible background such as the BKS[217] or DBA/2J[241] backgrounds will likely uncover a more robust DKD phenotype. A more severe DKD phenotype may allow us to uncover the mechanism of

SIRT5 in DKD pathogenesis. For example, in our metabolomics panels, metabolites belonging to the pentose phosphate pathway such as erythrose-4-phosphate was higher in the diabetic SIRT5 WT mice in comparison to the diabetic SIRT5 OE mice, but did not meet significance after multiple testing correction; we suspect that mice models with a more dramatic DKD phenotype may demonstrate larger differences in metabolite levels between the groups. Proximal tubular-specific SIRT5 expression will also confirm that SIRT5 activity in proximal tubules confers its role in DKD. Hershberger *et. al.,* found the global SIRT5 KO mice exhibit increased susceptibility to pressure-overload cardiomyopathy[151], but that this phenotype is not recapitulated in the inducible cardiomyocyte-specific SIRT5 KO mice[242]. Chiba *et. al.,* demonstrated that global SIRT5 mice exhibit resistance to AKI in the ischemia-reperfusion injury model[143]. AKI uniquely affects proximal tubules and therefore somewhat establishes SIRT5 as an important mediator of proximal tubular physiology, but DKD occurs as a result of many different renal cell-type pathologies. Importantly, DKD requires systemic metabolic dysfunction. While we established that many metabolomic parameters were unchanged between SIRT5 WT and OE mice, we cannot conclude that differences in DKD phenotype are not due to differences in systemic metabolism. SIRT5 is a highly context specific pleiotropic regulator; cell-type-specific analysis is essential in elucidating its mechanism in complex diseases.

While our findings in the SIRT5 WT and OE HFD-STZ are confounded by the effect of the background strain, urinary markers of disease and proximal tubular dysfunction were decreased in the SIRT5 OE mice. Although the mechanism of SIRT5 is likely multifold, we found the protective effect of SIRT5 in DKD perplexing; SIRT5 has been

repeatedly demonstrated to upregulate glucose utilization and aerobic glycolysis, and these processes are associated with epithelial-mesenchymal transition, fibroblast activation and unfavorable metabolic rewiring in DKD. We hypothesize that SIRT5 is important in conferring metabolic flexibility. SIRT5 regulates immune cell activation[124,125], and BAT and WAT activation in thermoregulation[126,194], which are cell types in which metabolic reprogramming and fuel switching needs to occur relatively rapidly. Upregulation of SIRT5 in such instances may allow for rapid metabolic rewiring that creates a metabolic milieu favorable for subsequent permanent cellular changes. In proximal tubules in DKD, it is possible that SIRT5 facilitates energy generation through non-mitochondrial pathways in the context of mitochondrial stress without committing the proximal tubules to upregulate mechanisms to rewire metabolism, which may lead to untoward consequences such as dedifferentiation. We posit that SIRT5 is an important metabolic regulator in biological contexts that require rapid metabolic rewiring or display innate metabolic inflexibility; further studies of SIRT5 in such biological contexts will be interesting.

Proteomic analysis of malonylated proteomics in the *db/db* and *db/+* mice found that proteins with significantly decreased malonylation are enriched in glycolysis/gluconeogenesis and peroxisomes (peroxisomal FAO). Gluconeogenesis and peroxisomes of special interest to proximal tubular physiology as proximal tubules are the only cells known to be capable of significant gluconeogenesis, other than hepatocytes, and are especially enriched in peroxisomes in comparison to other cells. Gluconeogenesis by proximal tubules is increasingly becoming recognized as an important regulator of systemic metabolism. Gluconeogenesis by the kidney can

contribute up to 40% of plasma glucose levels in postabsorptive states[243]. In diabetes, kidney gluconeogenesis is aberrantly increased due to upregulation of key gluconeogenic enzymes: phosphoenolpyruvate carboxykinase (PEPCK) and glucose-6-phosphatase[244,245]. Gluconeogenic substrates of proximal tubules include lactate, glutamine, glycerol and alanine, with the first two substrates being the most preferred[243]. In a study of isolated proximal tubules from STZ-treated and control rats, gluconeogenesis was upregulated by 69% with addition of lactate, 56% with glutamine, and 50% with glycerol in the diabetic proximal tubules compared to the controls[246]. Currently, the role of gluconeogenesis in proximal tubular glucose metabolism in DKD is not well understood. Could aberrantly elevated gluconeogenesis in proximal tubules in diabetes contribute to the generation of glycolytic intermediates that accumulate and produce toxic metabolic byproducts that contribute to disease? We hypothesize that SIRT5 demalonylation encourages net glucose consumption through glycolysis, rather than production, and may therefore confer its protective effect in DKD.

Gluconeogenesis by the liver and kidney are both physiologically important, but it would be of interest to study whether reduction in gluconeogenesis in the kidney can reduce DKD pathogenesis. A recent study of liver-specific KO of cytosolic PEPCK found compensatory renal upregulation of gluconeogenesis[247]. In the same vein, if reduction in renal specific gluconeogenesis occurs and compensatory hepatic gluconeogenesis is increased to maintain euglycemia and therefore no systemic ramification occurs, can proximal tubular specific reduction in glucose burden have asalutary impact on DKD? Proximal-tubular specific cytosolic or mitochondrial PEPCK knockout diabetic mice would[248], for example, address the role of renal gluconeogenesis in DKD.

There is conflicting data on the effect of SGLT2 inhibition on renal gluconeogenesis in diabetes. First, SGLT2 inhibition results in increased endogenous glucose production in both normal and diabetic patients, likely as a compensatory mechanism to normalize plasma glucose levels from glycosuria[249]. Whether this increase in glucose production is due to hepatic and/or renal gluconeogenesis is unclear. Akita mice treated with 15 weeks of empagliflozin demonstrated attenuation of the increase in renal PEPCK mRNA levels[61], suggesting that SGLT2is inhibit the aberrant increase in gluconeogenesis in DKD. However, in a study of *ob/ob* and STZ treated C57BL/6J mice, expression of PEPCK mRNA was downregulated in the cortex in the fed state. Treatment of STZ mice with phlorizin, which blocks SGLT1 and SGLT2 activity, resulted in the normalization of PEPCK and F6P mRNA levels in the diabetic cortex[250]. While the current evidence suggests that renal gluconeogenesis is a dynamic process and therefore markers of gluconeogenesis may heavily depend on the model of DKD and the fed/fasted states of the murine models, treatment of mice with SGLT2is result in normalization of gluconeogenesis in DKD.

Peroxisomes contain over >50 enzymes and catalyze numerous processes including oxidative stress defense, FAO, glyoxylate metabolism, and lipid and cholesterol synthesis[251]. While an important organelle, its role in kidney physiology and disease is relatively understudied. Patients with Zellweger syndrome, which occurs when peroxisomal deficiencies due to mutations in the Pex genes, results in renal cysts, amongst other numerous disease manifestations[252]. Pex 11a KO mice demonstrate increased interstitial fibrosis in the context of deoxycorticosterone acetate–salt [DOCA-salt]) hypertensive kidney disease and FFA-bound BSA-overload nephropathy[253]. A

particular peroxisomal protein of interest is EHHADH, which catalyzes the second and third reaction in peroxisomal β-oxidation. A recent study of global EHHADH KO mice demonstrated renal hypertrophy with mild GFR reduction and evidence of proximal tubular injury in male mice, but not female or orchiectomized EHHADH KO male mice. Metabolomic profiling of the EHHADH KO mice demonstrated increased levels of glycosphingolipids, such as glucosylceramides and lactosylceramides[254]. Peroxisomal FAO has been demonstrated in several contexts to compensate for deficiencies in mitochondrial β-oxidation and therefore is likely important in the context of DKD. What is unclear is how peroxisomes contribute to *de novo* lipogenesis of complex lipids such as glucosylceramides whose levels are normally tightly regulated. FAO and lipogenesis are linked. Reduction in FAO can lead shunting of fatty acids to complex lipid synthesis; the increased glucosylceramide levels from EHHADH deficiency is likely due to reduced peroxisomal FAO. However, why EHHADH deficiency results specifically in the elevation of glucosylceramides is unclear. Lipid profiling of proximal tubular specific EHHADH deficient or other members of the peroxisomal β-oxidation pathway in DKD may provide insight into what lipogenic pathways are altered specifically due to reduction in peroxisomal FAO in DKD.

In this thesis, we primarily focused on proximal tubular metabolism and its role in DKD. However, how proximal tubular metabolism affects metabolism and function of other cell types in the kidney has yet to be well elucidated. We posit that as proximal tubules are metabolically active cell types with high innate capacity of both metabolite catabolism and anabolism, it may serve as a remover of toxic metabolic byproducts or supplementer of metabolites important to other renal cells. Single-cell transcriptomics

data of healthy and DKD kidneys may be able to identify metabolic pathways that are limited to proximal tubules and test their important in DKD pathogenesis.

In the second half of this thesis, we characterized the consequences of metabolic reprogramming in DKD. We found elevated urinary levels of L and D-2HG, likely due to the dramatic increase in TCA cycle metabolites in the *db/db* cortex. 2-HG is a metabolite that likely confers its own biological function, in addition to serving as a biomarker of DKD. We then conducted metabolic flux analysis in control a T1D patients with and without DKD with $^{13}C_6$-glucose and found reduction in incorporation of labeled glucose into TCA cycle metabolites in T1D patients. Our results suggested reduced mitochondrial activity in the kidney of diabetic patients, with the caveat that plasma metabolomic analysis is necessary to understand how systemic metabolism contributes to the urinary isotopologue levels.

Metabolic reprogramming in DKD results in aberrant levels of metabolites that occur at the tissue level and eventually the systemic circulation in the context of falling GFR. Although we are aware of numerous bioactive metabolites, such as 2-HG, that are elevated in DKD, feasible therapeutics against specific metabolite or metabolic pathways effective in treating DKD without severe side effects are difficult to find. One therapy we are interested in investigating is eliglustat, an inhibitor of glucosylceramide synthase (GSL) used to treat type 1 Gaucher's Disease[255]. Glycosphingolipids are bioactive lipids that make up cell membranes and lipid rafts for many receptors including insulin and insulin growth factor receptors. Levels of glucosylceramides are elevated in many renal diseases including in DKD[256,257], polycystic kidney disease[258,259] and renal cell carcinoma[260]. Glucosylceramides are known to mediate cellular proliferation and growth,

although the exact mechanisms are not understood. Treatment of mesangial cells in hyperglycemic conditions in culture with GSL reduces hypertrophy and fibrosis[257]. Treatment of mice with PKD1, JCK and PCY mice with eliglustat reduced cyst growth[259], and currently GSL inhibitors are being tested for ADPKD in clinical trials (NCT03523728). We propose that treatment of DKD with GSL inhibitors can reduce kidney hypertrophy that occurs in early DKD and reduce the risk of progression. We propose that it is the imbalance in the ratio of glycosphingolipids such as GM3, which has been associated with insulin resistance[261], and precursors to glycosphingolipid synthesis such as ceramide-1-phosphate, which has been demonstrated to improve insulin sensitivity and reduce DKD pathogenesis in *db/db* mice[262], contributes to aberrant signaling which results in renal growth and hypertrophy.

In conclusion, metabolic reprogramming in DKD contributes to disease. We have examined mechanisms that underlie metabolic reprogramming in DKD and its consequences. We propose that further understanding of how metabolism is altered in DKD will reveal therapeutic strategies.

References

1. Jha, V. *et al.* Chronic kidney disease: global dimension and perspectives. *The Lancet* **382**, 260–272 (2013).
2. *2020 USRDS Annual Data Report: Epidemiology of kidney disease in the United States*. https://adr.usrds.org/2020.
3. Qian, Y., Feldman, E., Pennathur, S., Kretzler, M. & Brosius, F. C. Mechanisms of Glomerulosclerosis in Diabetic Nephropathy. *Diabetes* **57**, 1439–1445 (2008).
4. Dalla, V. M., Saller, A., Mauer, M. & Fioretto, P. Role of mesangial expansion in the pathogenesis of diabetic nephropathy. *J. Nephrol.* **14 Suppl 4**, S51-7 (2001).
5. Mauer, S. M. *et al.* Structural-functional relationships in diabetic nephropathy. *J. Clin. Invest.* **74**, 1143–1155 (1984).
6. Alsaad, K. O. & Herzenberg, A. M. Distinguishing diabetic nephropathy from other causes of glomerulosclerosis: an update. *J. Clin. Pathol.* **60**, 18–26 (2007).
7. Mazzucco, G. *et al.* Different patterns of renal damage in type 2 diabetes mellitus: A multicentric study on 393 biopsies. *Am. J. Kidney Dis.* **39**, 713–720 (2002).
8. Tervaert, T. W. C. *et al.* Pathologic Classification of Diabetic Nephropathy. *J. Am. Soc. Nephrol.* **21**, 556–563 (2010).
9. Afkarian, M. *et al.* Clinical Manifestations of Kidney Disease Among US Adults With Diabetes, 1988-2014. *JAMA* **316**, 602–610 (2016).

10. Krolewski, A. S., Skupien, J., Rossing, P. & Warram, J. H. Fast renal decline to end-stage renal disease: an unrecognized feature of nephropathy in diabetes. *Kidney Int.* **91**, 1300–1311 (2017).
11. Schulz, L. O. *et al.* Effects of Traditional and Western Environments on Prevalence of Type 2 Diabetes in Pima Indians in Mexico and the U.S. *Diabetes Care* **29**, 1866–1871 (2006).
12. Nelson, R. G. *et al.* Development and Progression of Renal Disease in Pima Indians with Non-Insulin-Dependent Diabetes Mellitus. *N. Engl. J. Med.* **335**, 1636–1642 (1996).
13. Pavkov, M. E., Knowler, W. C., Hanson, R. L. & Nelson, R. G. Diabetic Nephropathy in American Indians, with a Special Emphasis on the Pima Indians. *Curr. Diab. Rep.* **8**, 486–493 (2008).
14. Palatini, P. Glomerular hyperfiltration: a marker of early renal damage in pre-diabetes and pre-hypertension. *Nephrol. Dial. Transplant.* **27**, 1708–1714 (2012).
15. Nakagawa, T., Kosugi, T., Haneda, M., Rivard, C. J. & Long, D. A. Abnormal Angiogenesis in Diabetic Nephropathy. *Diabetes* **58**, 1471–1478 (2009).
16. Liu, E. *et al.* Increased Expression of Vascular Endothelial Growth Factor in Kidney Leads to Progressive Impairment of Glomerular Functions. *J. Am. Soc. Nephrol.* **18**, 2094–2104 (2007).
17. Oltean, S. *et al.* Vascular Endothelial Growth Factor-A165b Is Protective and Restores Endothelial Glycocalyx in Diabetic Nephropathy. *J. Am. Soc. Nephrol.* **26**, 1889–1904 (2015).

18. Zhao, H. J. *et al.* Endothelial Nitric Oxide Synthase Deficiency Produces Accelerated Nephropathy in Diabetic Mice. *J. Am. Soc. Nephrol.* **17**, 2664–2669 (2006).
19. Nakagawa, T. *et al.* Diabetic Endothelial Nitric Oxide Synthase Knockout Mice Develop Advanced Diabetic Nephropathy. *J. Am. Soc. Nephrol.* **18**, 539–550 (2007).
20. Herman-Edelstein, M., Scherzer, P., Tobar, A., Levi, M. & Gafter, U. Altered renal lipid metabolism and renal lipid accumulation in human diabetic nephropathy. *J. Lipid Res.* **55**, 561–572 (2014).
21. Baumer, Y. *et al.* Hyperlipidemia-induced cholesterol crystal production by endothelial cells promotes atherogenesis. *Nat. Commun.* **8**, 1129 (2017).
22. Yin, Q. *et al.* Exendin-4 Ameliorates Lipotoxicity-induced Glomerular Endothelial Cell Injury by Improving ABC Transporter A1-mediated Cholesterol Efflux in Diabetic apoE Knockout Mice. *J. Biol. Chem.* **291**, 26487–26501 (2016).
23. Lin, J. S. & Susztak, K. Podocytes: The Weakest Link in Diabetic Kidney Disease? *Curr. Diab. Rep.* **16**, 45 (2016).
24. Gödel, M. *et al.* Role of mTOR in podocyte function and diabetic nephropathy in humans and mice. *J. Clin. Invest.* **121**, 2197–2209 (2011).
25. Inoki, K. *et al.* mTORC1 activation in podocytes is a critical step in the development of diabetic nephropathy in mice. *J. Clin. Invest.* **121**, 2181–2196 (2011).
26. Niranjan, T. *et al.* The Notch pathway in podocytes plays a role in the development of glomerular disease. *Nat. Med.* **14**, 290–298 (2008).
27. Kato, H. *et al.* Wnt/β-Catenin Pathway in Podocytes Integrates Cell Adhesion, Differentiation, and Survival. *J. Biol. Chem.* **286**, 26003–26015 (2011).

28. Wickman, L. *et al.* Urine Podocyte mRNAs, Proteinuria, and Progression in Human Glomerular Diseases. *J. Am. Soc. Nephrol.* **24**, 2081–2095 (2013).
29. Sato, Y. *et al.* Urine Podocyte mRNAs Mark Progression of Renal Disease. *J. Am. Soc. Nephrol.* **20**, 1041–1052 (2009).
30. Clark, J. Z. *et al.* Representation and relative abundance of cell-type selective markers in whole-kidney RNA-Seq data. *Kidney Int.* **95**, 787–796 (2019).
31. Najafian, B., Crosson, J. T., Kim, Y. & Mauer, M. Glomerulotubular Junction Abnormalities Are Associated with Proteinuria in Type 1 Diabetes. *J. Am. Soc. Nephrol.* **17**, S53–S60 (2006).
32. White, K. E., Marshall, S. M. & Bilous, R. W. Prevalence of atubular glomeruli in type 2 diabetic patients with nephropathy. *Nephrol. Dial. Transplant.* **23**, 3539–3545 (2008).
33. Najafian, B., Kim, Y., Crosson, J. T. & Mauer, M. Atubular Glomeruli and Glomerulotubular Junction Abnormalities in Diabetic Nephropathy. *J. Am. Soc. Nephrol.* **14**, 908–917 (2003).
34. Dong, R. *et al.* IGF-1/IGF-1R blockade ameliorates diabetic kidney disease through normalizing Snail1 expression in a mouse model. *Am. J. Physiol.-Endocrinol. Metab.* **317**, E686–E698 (2019).
35. Li, L. *et al.* Absence of renal enlargement in fructose-fed proximal-tubule-select insulin receptor (IR), insulin-like-growth factor receptor (IGF1R) double knockout mice. *Physiol. Rep.* **4**, e13052 (2016).
36. Lee, M.-J. *et al.* A role for AMP-activated protein kinase in diabetes-induced renal hypertrophy. *Am. J. Physiol.-Ren. Physiol.* **292**, F617–F627 (2007).

37. Thomson, S. C. *et al.* Ornithine decarboxylase, kidney size, and the tubular hypothesis of glomerular hyperfiltration in experimental diabetes. *J. Clin. Invest.* **107**, 217–224 (2001).

38. Pedersen, S. B., Flyvbjerg, A. & Richelsen, B. Inhibition of renal ornithine decarboxylase activity prevents kidney hypertrophy in experimental diabetes. *Am. J. Physiol.-Cell Physiol.* **264**, C453–C456 (1993).

39. Zador, I. Z. *et al.* A role for glycosphingolipid accumulation in the renal hypertrophy of streptozotocin-induced diabetes mellitus. *J. Clin. Invest.* **91**, 797–803 (1993).

40. Vallon, V., Blantz, R. C. & Thomson, S. Glomerular Hyperfiltration and the Salt Paradox in Early Type 1 Diabetes Mellitus: A Tubulo-Centric View. *J. Am. Soc. Nephrol.* **14**, 530–537 (2003).

41. Vallon, V., Richter, K., Blantz, R. C., Thomson, S. & Osswald, H. Glomerular Hyperfiltration in Experimental Diabetes Mellitus: Potential Role of Tubular Reabsorption. *J. Am. Soc. Nephrol.* **10**, 2569–2576 (1999).

42. Vallon, V. & Thomson, S. C. The tubular hypothesis of nephron filtration and diabetic kidney disease. *Nat. Rev. Nephrol.* **16**, 317–336 (2020).

43. Tan, S. M. *et al.* Complement C5a Induces Renal Injury in Diabetic Kidney Disease by Disrupting Mitochondrial Metabolic Agility. *Diabetes* **69**, 83–98 (2020).

44. Lai, H. *et al.* Podocyte and endothelial-specific elimination of BAMBI identifies differential transforming growth factor-β pathways contributing to diabetic glomerulopathy. *Kidney Int.* **98**, 601–614 (2020).

45. Hasegawa, K. *et al.* Renal tubular Sirt1 attenuates diabetic albuminuria by epigenetically suppressing Claudin-1 overexpression in podocytes. *Nat. Med.* **19**, 1496–1504 (2013).

46. Muraoka, H. *et al.* Role of Nampt-Sirt6 Axis in Renal Proximal Tubules in Extracellular Matrix Deposition in Diabetic Nephropathy. *Cell Rep.* **27**, 199-212.e5 (2019).

47. Brinkkoetter, P. T. *et al.* Anaerobic Glycolysis Maintains the Glomerular Filtration Barrier Independent of Mitochondrial Metabolism and Dynamics. *Cell Rep.* **27**, 1551-1566.e5 (2019).

48. van Timmeren, M. M. *et al.* Tubular kidney injury molecule-1 in protein-overload nephropathy. *Am. J. Physiol.-Ren. Physiol.* **291**, F456–F464 (2006).

49. Abbate, M., Zoja, C. & Remuzzi, G. How Does Proteinuria Cause Progressive Renal Damage? *J. Am. Soc. Nephrol.* **17**, 2974–2984 (2006).

50. Landgraf, S. S. *et al.* 5-Lypoxygenase Products Are Involved in Renal Tubulointerstitial Injury Induced by Albumin Overload in Proximal Tubules in Mice. *PLOS ONE* **9**, e107549 (2014).

51. Khan, S. *et al.* Kidney Proximal Tubule Lipoapoptosis Is Regulated by Fatty Acid Transporter-2 (FATP2). *J. Am. Soc. Nephrol. JASN* **29**, 81–91 (2018).

52. Baines, R. J. *et al.* CD36 mediates proximal tubular binding and uptake of albumin and is upregulated in proteinuric nephropathies. *Am. J. Physiol.-Ren. Physiol.* **303**, F1006–F1014 (2012).

53. Su, H. *et al.* Podocyte-derived extracellular vesicles mediate renal proximal tubule cells dedifferentiation via microRNA-221 in diabetic nephropathy. *Mol. Cell. Endocrinol.* **518**, 111034 (2020).
54. Huang, Y. *et al.* Extracellular Vesicles From High Glucose-Treated Podocytes Induce Apoptosis of Proximal Tubular Epithelial Cells. *Front. Physiol.* **11**, (2020).
55. Ghezzi, C., Loo, D. D. F. & Wright, E. M. Physiology of renal glucose handling via SGLT1, SGLT2 and GLUT2. *Diabetologia* **61**, 2087–2097 (2018).
56. Santer, R. & Calado, J. Familial Renal Glucosuria and SGLT2: From a Mendelian Trait to a Therapeutic Target. *Clin. J. Am. Soc. Nephrol.* **5**, 133–141 (2010).
57. Wanner, C. *et al.* Empagliflozin and Progression of Kidney Disease in Type 2 Diabetes. *N. Engl. J. Med.* **375**, 323–334 (2016).
58. Neal, B. *et al.* Canagliflozin and Cardiovascular and Renal Events in Type 2 Diabetes. *N. Engl. J. Med.* **377**, 644–657 (2017).
59. Mosenzon, O. *et al.* Effects of dapagliflozin on development and progression of kidney disease in patients with type 2 diabetes: an analysis from the DECLARE–TIMI 58 randomised trial. *Lancet Diabetes Endocrinol.* **7**, 606–617 (2019).
60. Ingelfinger, J. R. & Rosen, C. J. Clinical Credence — SGLT2 Inhibitors, Diabetes, and Chronic Kidney Disease. *N. Engl. J. Med.* **380**, 2371–2373 (2019).
61. Vallon, V. *et al.* SGLT2 inhibitor empagliflozin reduces renal growth and albuminuria in proportion to hyperglycemia and prevents glomerular hyperfiltration in diabetic Akita mice. *Am. J. Physiol. - Ren. Physiol.* **306**, F194–F204 (2014).

62. Gallo, L. A. *et al.* Once daily administration of the SGLT2 inhibitor, empagliflozin, attenuates markers of renal fibrosis without improving albuminuria in diabetic db/db mice. *Sci. Rep.* **6**, 26428 (2016).
63. Kogot-Levin, A. *et al.* Proximal Tubule mTORC1 Is a Central Player in the Pathophysiology of Diabetic Nephropathy and Its Correction by SGLT2 Inhibitors. *Cell Rep.* **32**, 107954 (2020).
64. Tomita, I. *et al.* SGLT2 Inhibition Mediates Protection from Diabetic Kidney Disease by Promoting Ketone Body-Induced mTORC1 Inhibition. *Cell Metab.* **32**, 404-419.e6 (2020).
65. Kim, S. R. *et al.* SGLT2 inhibition modulates NLRP3 inflammasome activity via ketones and insulin in diabetes with cardiovascular disease. *Nat. Commun.* **11**, 2127 (2020).
66. Maejima, Y. SGLT2 Inhibitors Play a Salutary Role in Heart Failure via Modulation of the Mitochondrial Function. *Front. Cardiovasc. Med.* **6**, (2020).
67. Hawley, S. A. *et al.* The Na+/glucose co-transporter inhibitor canagliflozin activates AMP-activated protein kinase by inhibiting mitochondrial function and increasing cellular AMP levels. *Diabetes* **65**, 2784–2794 (2016).
68. Osataphan, S. *et al.* SGLT2 inhibition reprograms systemic metabolism via FGF21-dependent and -independent mechanisms. *JCI Insight* **4**, (2019).
69. Li, X. *et al.* Direct Cardiac Actions of the Sodium Glucose Co-Transporter 2 Inhibitor Empagliflozin Improve Myocardial Oxidative Phosphorylation and Attenuate Pressure-Overload Heart Failure. *J. Am. Heart Assoc.* **10**, e018298 (2021).

70. Maki, T. *et al.* Amelioration of diabetic nephropathy by SGLT2 inhibitors independent of its glucose-lowering effect: A possible role of SGLT2 in mesangial cells. *Sci. Rep.* **9**, 4703 (2019).
71. Cassis, P. *et al.* SGLT2 inhibitor dapagliflozin limits podocyte damage in proteinuric nondiabetic nephropathy. *JCI Insight* **3**, e98720.
72. Cherney, D. Z. I. *et al.* Effects of the SGLT2 inhibitor dapagliflozin on proteinuria in non-diabetic patients with chronic kidney disease (DIAMOND): a randomised, double-blind, crossover trial. *Lancet Diabetes Endocrinol.* **8**, 582–593 (2020).
73. Packer, M. *et al.* Cardiovascular and Renal Outcomes with Empagliflozin in Heart Failure. *N. Engl. J. Med.* **383**, 1413–1424 (2020).
74. Anker, S. D. *et al.* Baseline characteristics of patients with heart failure with preserved ejection fraction in the EMPEROR-Preserved trial. *Eur. J. Heart Fail.* **22**, 2383–2392 (2020).
75. Rieg, J. A. D. & Rieg, T. What Does SGLT1 Inhibition Add: Prospects for Dual Inhibition. *Diabetes Obes. Metab.* **21**, 43–52 (2019).
76. Cefalo, C. M. A. *et al.* Sotagliflozin, the first dual SGLT inhibitor: current outlook and perspectives. *Cardiovasc. Diabetol.* **18**, 20 (2019).
77. Li, S.-Y. *et al.* Increasing the level of peroxisome proliferator-activated receptor **γ** coactivator-1**α** in podocytes results in collapsing glomerulopathy. *JCI Insight* **2**, (2017).
78. Coward, R. J. M. *et al.* The Human Glomerular Podocyte Is a Novel Target for Insulin Action. *Diabetes* **54**, 3095–3102 (2005).

79. Forbes, J. M. & Thorburn, D. R. Mitochondrial dysfunction in diabetic kidney disease. *Nat. Rev. Nephrol.* **14**, 291–312 (2018).

80. Klein, K. L., Wang, M.-S., Torikai, S., Davidson, W. D. & Kurokawa, K. Substrate oxidation by isolated single nephron segments of the rat. *Kidney Int.* **20**, 29–35 (1981).

81. Uchida, S. & Endou, H. Substrate specificity to maintain cellular ATP along the mouse nephron. *Am. J. Physiol.-Ren. Physiol.* **255**, F977–F983 (1988).

82. Kang, H. M. *et al.* Defective fatty acid oxidation in renal tubular epithelial cells has a key role in kidney fibrosis development. *Nat. Med.* **21**, 37–46 (2015).

83. Mandel, L. J. Metabolic Substrates, Cellular Energy Production, and the Regulation of Proximal Tubular Transport. *Annu. Rev. Physiol.* **47**, 85–101 (1985).

84. Brownlee, M. The Pathobiology of Diabetic Complications: A Unifying Mechanism. *Diabetes* **54**, 1615–1625 (2005).

85. Sas, K. M. *et al.* Tissue-specific metabolic reprogramming drives nutrient flux in diabetic complications. *JCI Insight* **1**, (2016).

86. Scheijen, J. L. J. M. *et al.* L(+) and D(-) Lactate Are Increased in Plasma and Urine Samples of Type 2 Diabetes as Measured by a Simultaneous Quantification of L(+) and D(-) Lactate by Reversed-Phase Liquid Chromatography Tandem Mass Spectrometry. *Exp. Diabetes Res.* **2012**, 1–10 (2012).

87. Kim, N. H. *et al.* Metabolic changes in urine and serum during progression of diabetic kidney disease in a mouse model. *Arch. Biochem. Biophys.* **646**, 90–97 (2018).

88. Mora-Ortiz, M., Nuñez Ramos, P., Oregioni, A. & Claus, S. P. NMR metabolomics identifies over 60 biomarkers associated with Type II Diabetes impairment in db/db mice. *Metabolomics* **15**, 89 (2019).

89. Li, M. *et al.* GC/TOFMS analysis of metabolites in serum and urine reveals metabolic perturbation of TCA cycle in db/db mice involved in diabetic nephropathy. *Am. J. Physiol.-Ren. Physiol.* **304**, F1317–F1324 (2013).

90. Zhang, G., Darshi, M. & Sharma, K. The Warburg Effect in Diabetic Kidney Disease. *Semin. Nephrol.* **38**, 111–120 (2018).

91. Qi, W. *et al.* Pyruvate kinase M2 activation may protect against the progression of diabetic glomerular pathology and mitochondrial dysfunction. *Nat. Med.* **23**, 753–762 (2017).

92. Vander Heiden, M. G., Cantley, L. C. & Thompson, C. B. Understanding the Warburg Effect: The Metabolic Requirements of Cell Proliferation. *Science* **324**, 1029–1033 (2009).

93. Li, J. *et al.* Renal protective effects of empagliflozin via inhibition of EMT and aberrant glycolysis in proximal tubules. *JCI Insight* **5**, e129034.

94. Lan, R. *et al.* Mitochondrial Pathology and Glycolytic Shift during Proximal Tubule Atrophy after Ischemic AKI. *J. Am. Soc. Nephrol. JASN* **27**, 3356–3367 (2016).

95. Ding, H. *et al.* Inhibiting aerobic glycolysis suppresses renal interstitial fibroblast activation and renal fibrosis. *Am. J. Physiol.-Ren. Physiol.* **313**, F561–F575 (2017).

96. Kang, H. M. *et al.* Defective fatty acid oxidation in renal tubular epithelial cells plays a key role in kidney fibrosis development. *Nat. Med.* **21**, 37–46 (2015).

97. Zhang, H. *et al.* Rosiglitazone reduces renal and plasma markers of oxidative injury and reverses urinary metabolite abnormalities in the amelioration of diabetic nephropathy. *Am. J. Physiol. - Ren. Physiol.* **295**, F1071–F1081 (2008).
98. Miguel, V. *et al.* Renal tubule Cpt1a overexpression protects from kidney fibrosis by restoring mitochondrial homeostasis. *J. Clin. Invest.* (2021) doi:10.1172/JCI140695.
99. Koves, T. R. *et al.* Mitochondrial Overload and Incomplete Fatty Acid Oxidation Contribute to Skeletal Muscle Insulin Resistance. *Cell Metab.* **7**, 45–56 (2008).
100. Ibarra-González, I. *et al.* Optimization of kidney dysfunction prediction in diabetic kidney disease using targeted metabolomics. *Acta Diabetol.* **55**, 1151–1161 (2018).
101. Looker, H. C. *et al.* Biomarkers of rapid chronic kidney disease progression in type 2 diabetes. *Kidney Int.* **88**, 888–896 (2015).
102. Liu, J.-J. *et al.* Profiling of Plasma Metabolites Suggests Altered Mitochondrial Fuel Usage and Remodeling of Sphingolipid Metabolism in Individuals With Type 2 Diabetes and Kidney Disease. *Kidney Int. Rep.* **2**, 470–480 (2016).
103. Niewczas, M. A. *et al.* Uremic solutes and risk of end stage renal disease in type 2 diabetes. *Kidney Int.* **85**, 1214–1224 (2014).
104. van der Kloet, F. M. *et al.* Discovery of early-stage biomarkers for diabetic kidney disease using ms-based metabolomics (FinnDiane study). *Metabolomics* **8**, 109–119 (2012).
105. Afshinnia, F. *et al.* Lipidomics and Biomarker Discovery in Kidney Disease. *Semin. Nephrol.* **38**, 127–141 (2018).

106. Afshinnia, F. *et al.* Increased lipogenesis and impaired β-oxidation predict type 2 diabetic kidney disease progression in American Indians. *JCI Insight* (2019) doi:10.1172/jci.insight.130317.

107. Muoio, D. M. *et al.* Muscle-specific Deletion of Carnitine Acetyltransferase Compromises Glucose Tolerance and Metabolic Flexibility. *Cell Metab.* **15**, 764–777 (2012).

108. Kruger, C. *et al.* Proximal Tubular Cell–Specific Ablation of Carnitine Acetyltransferase Causes Tubular Disease and Secondary Glomerulosclerosis. *Diabetes* **68**, 819 (2019).

109. Zager, R. A., Johnson, A. C. M. & Hanson, S. Y. Renal tubular triglyercide accumulation following endotoxic, toxic, and ischemic injury. *Kidney Int.* **67**, 111–121 (2005).

110. Johnson, A. L. I. C. M., Stahl, A. & Zager, R. A. Triglyceride accumulation in injured renal tubular cells: Alterations in both synthetic and catabolic pathways. *Kidney Int.* **67**, 2196–2209 (2005).

111. Li, S. *et al.* Reduced kidney lipoprotein lipase and renal tubule triglyceride accumulation in cisplatin-mediated acute kidney injury. *Am. J. Physiol.-Ren. Physiol.* **303**, F437–F448 (2012).

112. Herman-Edelstein, M., Scherzer, P., Tobar, A., Levi, M. & Gafter, U. Altered renal lipid metabolism and renal lipid accumulation in human diabetic nephropathy. *J. Lipid Res.* **55**, 561–572 (2014).

113. Weinberg, J. M. Lipotoxicity. *Kidney Int.* **70**, 1560–1566 (2006).

114. Wang, Z. *et al.* Regulation of Renal Lipid Metabolism, Lipid Accumulation, and Glomerulosclerosis in FVBdb/db Mice With Type 2 Diabetes. *Diabetes* **54**, 2328–2335 (2005).

115. Jiang, T. *et al.* Diet-induced Obesity in C57BL/6J Mice Causes Increased Renal Lipid Accumulation and Glomerulosclerosis via a Sterol Regulatory Element-binding Protein-1c-dependent Pathway. *J. Biol. Chem.* **280**, 32317–32325 (2005).

116. Lin, Y.-C. *et al.* Nifedipine Exacerbates Lipogenesis in the Kidney via KIM-1, CD36, and SREBP Upregulation: Implications from an Animal Model for Human Study. *Int. J. Mol. Sci.* **21**, (2020).

117. Carrico, C., Meyer, J. G., He, W., Gibson, B. W. & Verdin, E. The Mitochondrial Acylome Emerges: Proteomics, Regulation by Sirtuins, and Metabolic and Disease Implications. *Cell Metab.* **27**, 497–512 (2018).

118. Wagner, G. R. & Payne, R. M. Widespread and Enzyme-independent Nϵ-Acetylation and Nϵ-Succinylation of Proteins in the Chemical Conditions of the Mitochondrial Matrix. *J. Biol. Chem.* **288**, 29036–29045 (2013).

119. Rardin, M. J. *et al.* SIRT5 Regulates the Mitochondrial Lysine Succinylome and Metabolic Networks. *Cell Metab.* **18**, 920–933 (2013).

120. Sadhukhan, S. *et al.* Metabolomics-assisted proteomics identifies succinylation and SIRT5 as important regulators of cardiac function. *Proc. Natl. Acad. Sci.* 201519858 (2016) doi:10.1073/pnas.1519858113.

121. Bowman, C. E. *et al.* The Mammalian Malonyl-CoA Synthetase ACSF3 Is Required for Mitochondrial Protein Malonylation and Metabolic Efficiency. *Cell Chem. Biol.* **24**, 673-684.e4 (2017).

122. Park, J. *et al.* SIRT5-Mediated Lysine Desuccinylation Impacts Diverse Metabolic Pathways. *Mol. Cell* **50**, 919–930 (2013).
123. Nishida, Y. *et al.* SIRT5 Regulates both Cytosolic and Mitochondrial Protein Malonylation with Glycolysis as a Major Target. *Mol. Cell* **59**, 321–332 (2015).
124. Wang, F. *et al.* SIRT5 Desuccinylates and Activates Pyruvate Kinase M2 to Block Macrophage IL-1β Production and to Prevent DSS-Induced Colitis in Mice. *Cell Rep.* **19**, 2331–2344 (2017).
125. Galván-Peña, S. *et al.* Malonylation of GAPDH is an inflammatory signal in macrophages. *Nat. Commun.* **10**, 338 (2019).
126. Wang, G. *et al.* Regulation of UCP1 and Mitochondrial Metabolism in Brown Adipose Tissue by Reversible Succinylation. *Mol. Cell* **74**, 844-857.e7 (2019).
127. Peng, C. *et al.* The First Identification of Lysine Malonylation Substrates and Its Regulatory Enzyme. *Mol. Cell. Proteomics MCP* **10**, (2011).
128. Du, J. *et al.* Sirt5 Is a NAD-Dependent Protein Lysine Demalonylase and Desuccinylase. *Science* **334**, 806–809 (2011).
129. Tan, M. *et al.* Lysine Glutarylation Is a Protein Posttranslational Modification Regulated by SIRT5. *Cell Metab.* **19**, 605–617 (2014).
130. Chen, X. *et al.* SIRT5 inhibits peroxisomal ACOX1 to prevent oxidative damage and is downregulated in liver cancer. *EMBO Rep.* **19**, (2018).
131. Imai, S. & Guarente, L. It takes two to tango: NAD+ and sirtuins in aging/longevity control. *Npj Aging Mech. Dis.* **2**, 1–6 (2016).

132. Buler, M., Aatsinki, S.-M., Izzi, V., Uusimaa, J. & Hakkola, J. SIRT5 is under the control of PGC-1α and AMPK and is involved in regulation of mitochondrial energy metabolism. *FASEB J.* **28**, 3225–3237 (2014).

133. Bentley, N. L. *et al.* Protein hypoacylation induced by Sirt5 overexpression has minimal metabolic effect in mice. *Biochem. Biophys. Res. Commun.* **503**, 1349–1355 (2018).

134. Kulkarni, R. A. *et al.* Discovering Targets of Non-Enzymatic Acylation by Thioester Reactivity Profiling. *Cell Chem. Biol.* **24**, 231–242 (2017).

135. Hirschey, M. D. & Zhao, Y. Metabolic Regulation by Lysine Malonylation, Succinylation, and Glutarylation. *Mol. Cell. Proteomics* **14**, 2308–2315 (2015).

136. Barbi de Moura, M., Uppala, R., Zhang, Y., Van Houten, B. & Goetzman, E. S. Overexpression of Mitochondrial Sirtuins Alters Glycolysis and Mitochondrial Function in HEK293 Cells. *PLoS ONE* **9**, e106028 (2014).

137. Zhou, L. *et al.* SIRT5 promotes IDH2 desuccinylation and G6PD deglutarylation to enhance cellular antioxidant defense. *EMBO Rep.* **17**, 811–822 (2016).

138. Gao, W. *et al.* Targeting oxidative pentose phosphate pathway prevents recurrence in mutant Kras colorectal carcinomas. *PLOS Biol.* **17**, e3000425 (2019).

139. Colak, G. *et al.* Proteomic and Biochemical Studies of Lysine Malonylation Suggest Its Malonic Aciduria-associated Regulatory Role in Mitochondrial Function and Fatty Acid Oxidation. *Mol. Amp Cell. Proteomics* **14**, 3056 (2015).

140. Gut, P. *et al.* SUCLA2 mutations cause global protein succinylation contributing to the pathomechanism of a hereditary mitochondrial disease. *Nat. Commun.* **11**, 5927 (2020).

141. Zhang, Y. *et al.* SIRT3 and SIRT5 Regulate the Enzyme Activity and Cardiolipin Binding of Very Long-Chain Acyl-CoA Dehydrogenase. *PLoS ONE* **10**, e0122297 (2015).
142. Goetzman, E. S. *et al.* Impaired mitochondrial medium-chain fatty acid oxidation drives periportal macrovesicular steatosis in sirtuin-5 knockout mice. *Sci. Rep.* **10**, 18367 (2020).
143. Chiba, T. *et al.* Sirtuin 5 Regulates Proximal Tubule Fatty Acid Oxidation to Protect against AKI. *J. Am. Soc. Nephrol.* **30**, 2384–2398 (2019).
144. Meyer, J. G. *et al.* Quantification of Lysine Acetylation and Succinylation Stoichiometry in Proteins Using Mass Spectrometric Data-Independent Acquisitions (SWATH). *J. Am. Soc. Mass Spectrom.* **27**, 1758–1771 (2016).
145. Analysis of acetylation stoichiometry suggests that SIRT3 repairs nonenzymatic acetylation lesions. *EMBO J.* **34**, 2620–2632 (2015).
146. Hansen, B. K. *et al.* Analysis of human acetylation stoichiometry defines mechanistic constraints on protein regulation. *Nat. Commun.* **10**, 1055 (2019).
147. Bruning, U. *et al.* Impairment of Angiogenesis by Fatty Acid Synthase Inhibition Involves mTOR Malonylation. *Cell Metab.* (2018) doi:10.1016/j.cmet.2018.07.019.
148. James, A. M. *et al.* The Causes and Consequences of Nonenzymatic Protein Acylation. *Trends Biochem. Sci.* **43**, 921–932 (2018).
149. Yu, J. *et al.* Metabolic Characterization of a Sirt5 deficient mouse model. *Sci. Rep.* **3**, (2013).

150. Fisher-Wellman, K. H. *et al.* Respiratory Phenomics across Multiple Models of Protein Hyperacylation in Cardiac Mitochondria Reveals a Marginal Impact on Bioenergetics. *Cell Rep.* **26**, 1557-1572.e8 (2019).
151. Hershberger, K. A. *et al.* Sirtuin 5 is required for mouse survival in response to cardiac pressure overload. *J. Biol. Chem.* **292**, 19767–19781 (2017).
152. Zhang, M. *et al.* SIRT5 deficiency suppresses mitochondrial ATP production and promotes AMPK activation in response to energy stress. *PLOS ONE* **14**, e0211796 (2019).
153. Du, Y. *et al.* Lysine Malonylation Is Elevated in Type 2 Diabetic Mouse Models and Enriched in Metabolic Associated Proteins. *Mol. Cell. Proteomics* **14**, 227–236 (2015).
154. Zhu, S. *et al.* Sirt5 Deficiency Causes Posttranslational Protein Malonylation and Dysregulated Cellular Metabolism in Chondrocytes Under Obesity Conditions. *CARTILAGE* 1947603521993209 (2021) doi:10.1177/1947603521993209.
155. Liu, H. *et al.* Cellular carbon stress is a mediator of obesity-associated osteoarthritis development. *Osteoarthritis Cartilage* (2021) doi:10.1016/j.joca.2021.04.016.
156. Du, Y. *et al.* SIRT5 deacylates metabolism-related proteins and attenuates hepatic steatosis in ob/ob mice. *EBioMedicine* **36**, 347–357 (2018).
157. Guan, Y. & Hao, C.-M. SIRT1 and Kidney Function. *Kidney Dis.* **1**, 258–265 (2016).
158. Huang, W. *et al.* Sirt6 deficiency results in progression of glomerular injury in the kidney. *Aging* **9**, 1069–1081 (2017).
159. Haschler, T. N. *et al.* Sirtuin 5 depletion impairs mitochondrial function in human proximal tubular epithelial cells. *Sci. Rep.* **11**, 15510 (2021).

160. Hocher, B. & Adamski, J. Metabolomics for clinical use and research in chronic kidney disease. *Nat. Rev. Nephrol.* **13**, 269–284 (2017).

161. Emwas, A.-H. *et al.* NMR Spectroscopy for Metabolomics Research. *Metabolites* **9**, (2019).

162. Ren, J.-L., Zhang, A.-H., Kong, L. & Wang, X.-J. Advances in mass spectrometry-based metabolomics for investigation of metabolites. *RSC Adv.* **8**, 22335–22350 (2018).

163. Grove, K. J. *et al.* Diabetic nephropathy induces alterations in the glomerular and tubule lipid profiles. *J. Lipid Res.* **55**, 1375–1385 (2014).

164. Miyamoto, S. *et al.* Mass Spectrometry Imaging Reveals Elevated Glomerular ATP/AMP in Diabetes/obesity and Identifies Sphingomyelin as a Possible Mediator. *EBioMedicine* **7**, 121–134 (2016).

165. Zhou, W., Yang, S. & Wang, P. G. Matrix effects and application of matrix effect factor. *Bioanalysis* **9**, 1839–1844 (2017).

166. Abbas, I. *et al.* Kidney Lipidomics by Mass Spectrometry Imaging: A Focus on the Glomerulus. *Int. J. Mol. Sci.* **20**, 1623 (2019).

167. Wernisch, S. & Pennathur, S. Application of differential mobility-mass spectrometry for untargeted human plasma metabolomic analysis. *Anal. Bioanal. Chem.* **411**, 6297–6308 (2019).

168. Wernisch, S., Afshinnia, F., Rajendiran, T. & Pennathur, S. Probing the application range and selectivity of a differential mobility spectrometry – mass spectrometry platform for metabolomics. *Anal. Bioanal. Chem.* **410**, 2865–2877 (2018).

169. Spalding, J. L., Naser, F. J., Mahieu, N. G., Johnson, S. L. & Patti, G. J. Trace phosphate improves ZIC-pHILIC peak shape, sensitivity, and coverage for untargeted metabolomics. *J. Proteome Res.* **17**, 3537–3546 (2018).
170. Hsiao, J. J., Potter, O. G., Chu, T.-W. & Yin, H. Improved LC/MS Methods for the Analysis of Metal-Sensitive Analytes Using Medronic Acid as a Mobile Phase Additive. *Anal. Chem.* **90**, 9457–9464 (2018).
171. Lu, W. *et al.* Metabolite Measurement: Pitfalls to Avoid and Practices to Follow. *Annu. Rev. Biochem.* **86**, 277–304 (2017).
172. Solati, Z., Edel, A. L., Shang, Y., O, K. & Ravandi, A. Oxidized phosphatidylcholines are produced in renal ischemia reperfusion injury. *PLOS ONE* **13**, e0195172 (2018).
173. Perkovic, V. *et al.* Canagliflozin and Renal Outcomes in Type 2 Diabetes and Nephropathy. *N. Engl. J. Med.* **380**, 2295–2306 (2019).
174. Packer, M. *et al.* Cardiovascular and Renal Outcomes with Empagliflozin in Heart Failure. *N. Engl. J. Med.* **383**, 1413–1424 (2020).
175. Forbes, J. M. & Thorburn, D. R. Mitochondrial dysfunction in diabetic kidney disease. *Nat. Rev. Nephrol.* **14**, 291–312 (2018).
176. Aperia, A., Larsson, L. & Zetterstrom, R. Hormonal induction of Na-K-ATPase in developing proximal tubular cells. *Am. J. Physiol.-Ren. Physiol.* **241**, F356–F360 (1981).
177. Hue, L. & Taegtmeyer, H. The Randle cycle revisited: a new head for an old hat. *Am. J. Physiol. - Endocrinol. Metab.* **297**, E578–E591 (2009).
178. Wagner, G. R. & Hirschey, M. D. Non-enzymatic protein acylation as a carbon stress regulated by sirtuin deacylases. *Mol. Cell* **54**, 5–16 (2014).

179. Schilling, B. *et al.* Platform-independent and Label-free Quantitation of Proteomic Data Using MS1 Extracted Ion Chromatograms in Skyline: APPLICATION TO PROTEIN ACETYLATION AND PHOSPHORYLATION. *Mol. Cell. Proteomics* **11**, 202–214 (2012).

180. Lin, J. B., Lin, J. B., Chen, H. C., Chen, T. & Apte, R. S. Combined SIRT3 and SIRT5 deletion is associated with inner retinal dysfunction in a mouse model of type 1 diabetes. *Sci. Rep.* **9**, 3799 (2019).

181. Baek, J. & Pennathur, S. Urinary 2-Hydroxyglutarate Enantiomers Are Markedly Elevated in a Murine Model of Type 2 Diabetic Kidney Disease. *Metabolites* **11**, 469 (2021).

182. Zhao, S. *et al.* Regulation of Cellular Metabolism by Protein Lysine Acetylation. *Science* **327**, 1000–1004 (2010).

183. Onorato, J. M. *et al.* Liquid-liquid extraction coupled with LC/MS/MS for monitoring of malonyl-CoA in rat brain tissue. *Anal. Bioanal. Chem.* **397**, 3137–3142 (2010).

184. Bandyopadhyay, G. K., Yu, J. G., Ofrecio, J. & Olefsky, J. M. Increased Malonyl-CoA Levels in Muscle From Obese and Type 2 Diabetic Subjects Lead to Decreased Fatty Acid Oxidation and Increased Lipogenesis; Thiazolidinedione Treatment Reverses These Defects. *Diabetes* **55**, 2277–2285 (2006).

185. Sharma, K., McCue, P. & Dunn, S. R. Diabetic kidney disease in the db/dbmouse. *Am. J. Physiol.-Ren. Physiol.* **284**, F1138–F1144 (2003).

186. Gilbert, E. R., Fu, Z. & Liu, D. Development of a Nongenetic Mouse Model of Type 2 Diabetes. *Journal of Diabetes Research*

https://www.hindawi.com/journals/jdr/2011/416254/ (2011) doi:10.1155/2011/416254.

187. Skovsø, S. Modeling type 2 diabetes in rats using high fat diet and streptozotocin. *J. Diabetes Investig.* **5**, 349–358 (2014).

188. Chou, Y.-J. *et al.* Renal Protective Effects of Low Molecular Weight of Inonotus obliquus Polysaccharide (LIOP) on HFD/STZ-Induced Nephropathy in Mice. *Int. J. Mol. Sci.* **17**, (2016).

189. Carvalho, A. L. *et al.* High fat diet attenuates hyperglycemia, body composition changes, and bone loss in male streptozotocin-induced type 1 diabetic mice. *J. Cell. Physiol.* **233**, 1585–1600.

190. O'Brien, P. D. *et al.* Juvenile murine models of prediabetes and type 2 diabetes develop neuropathy. *Dis. Model. Mech.* dmm.037374 (2018) doi:10.1242/dmm.037374.

191. Hull, R. L. *et al.* Dietary-fat-induced obesity in mice results in beta cell hyperplasia but not increased insulin release: evidence for specificity of impaired beta cell adaptation. *Diabetologia* **48**, 1350–1358 (2005).

192. Mosser, R. E. *et al.* High-fat diet-induced β-cell proliferation occurs prior to insulin resistance in C57Bl/6J male mice. *Am. J. Physiol.-Endocrinol. Metab.* **308**, E573–E582 (2015).

193. Naggert, J. K., Mu, J.-L., Frankel, W., Bailey, D. W. & Paigen, B. Genomic analysis of the C57BL/Ks mouse strain. *Mamm. Genome* **6**, 131–133 (1995).

194. Shuai, L. *et al.* SIRT5 Regulates Brown Adipocyte Differentiation and Browning of Subcutaneous White Adipose Tissue. *Diabetes* **68**, 1449–1461 (2019).

195. Lin, Z.-F. *et al.* SIRT5 desuccinylates and activates SOD1 to eliminate ROS. *Biochem. Biophys. Res. Commun.* **441**, 191–195 (2013).

196. Banks, C. J. & Andersen, J. L. Mechanisms of SOD1 regulation by post-translational modifications. *Redox Biol.* **26**, 101270 (2019).

197. Fujita, H. *et al.* SOD1, but not SOD3, deficiency accelerates diabetic renal injury in C57BL/6-Ins2Akita diabetic mice. *Metabolism* **61**, 1714–1724 (2012).

198. Hwang, I. *et al.* Catalase Deficiency Accelerates Diabetic Renal Injury Through Peroxisomal Dysfunction. *Diabetes* **61**, 728–738 (2012).

199. Schlicker, C. *et al.* Substrates and Regulation Mechanisms for the Human Mitochondrial Sirtuins Sirt3 and Sirt5. *J. Mol. Biol.* **382**, 790–801 (2008).

200. Zhang, R. *et al.* SIRT5 Promotes Hepatocellular Carcinoma Progression by Regulating Mitochondrial Apoptosis. *J. Cancer* **10**, 3871–3882 (2019).

201. Hesp, A. C. *et al.* The role of renal hypoxia in the pathogenesis of diabetic kidney disease: a promising target for newer renoprotective agents including SGLT2 inhibitors? *Kidney Int.* **98**, 579–589 (2020).

202. Shayman, J. A. Targeting Glucosylceramide Synthesis in the Treatment of Rare and Common Renal Disease. *Semin. Nephrol.* **38**, 183–192 (2018).

203. Sas, K. M. *et al.* Shared and distinct lipid-lipid interactions in plasma and affected tissues in a diabetic mouse model. *J. Lipid Res.* **59**, 173–183 (2018).

204. Russo, L. M. *et al.* Impaired Tubular Uptake Explains Albuminuria in Early Diabetic Nephropathy. *J. Am. Soc. Nephrol.* **20**, 489 (2009).

205. Peruchetti, D. de B., Silva-Aguiar, R. P., Siqueira, G. M., Dias, W. B. & Caruso-Neves, C. High glucose reduces megalin-mediated albumin endocytosis in renal

proximal tubule cells through protein kinase B O-GlcNAcylation. *J. Biol. Chem.* **293**, 11388–11400 (2018).

206. Van Schaftingen, E., Rzem, R. & Veiga-da-Cunha, M. l-2-Hydroxyglutaric aciduria, a disorder of metabolite repair. *J. Inherit. Metab. Dis.* **32**, 135–142 (2009).
207. Ward, P. S. *et al.* The common feature of leukemia-associated IDH1 and IDH2 mutations is a neomorphic enzymatic activity that converts α-ketoglutarate to 2-hydroxyglutarate. *Cancer Cell* **17**, 225–234 (2010).
208. Dang, L. *et al.* Cancer-associated IDH1 mutations produce 2-hydroxyglutarate. *Nature* **462**, 739 (2009).
209. Fan, J. *et al.* Human Phosphoglycerate Dehydrogenase Produces the Oncometabolite d-2-Hydroxyglutarate. *ACS Chem. Biol.* **10**, 510–516 (2015).
210. Intlekofer, A. M. *et al.* Hypoxia Induces Production of L-2-Hydroxyglutarate. *Cell Metab.* **22**, 304–311 (2015).
211. Intlekofer, A. M. *et al.* L-2-Hydroxyglutarate production arises from noncanonical enzyme function at acidic pH. *Nat. Chem. Biol.* **13**, 494–500 (2017).
212. Nadtochiy, S. M. *et al.* Acidic pH Is a Metabolic Switch for 2-Hydroxyglutarate Generation and Signaling. *J. Biol. Chem.* **291**, 20188–20197 (2016).
213. Xu, W. *et al.* Oncometabolite 2-Hydroxyglutarate Is a Competitive Inhibitor of α-Ketoglutarate-Dependent Dioxygenases. *Cancer Cell* **19**, 17–30 (2011).
214. Xu, T. *et al.* Metabolic control of T H 17 and induced T reg cell balance by an epigenetic mechanism. *Nature* **548**, 228–233 (2017).
215. Tyrakis, P. A. *et al.* The immunometabolite S-2-hydroxyglutarate regulates CD8+ T-lymphocyte fate. *Nature* **540**, 236–241 (2016).

216. Fitzpatrick, S. F. *et al.* 2-Hydroxyglutarate Metabolism Is Altered in an in vivo Model of LPS Induced Endotoxemia. *Front. Physiol.* **11**, (2020).

217. Brosius, F. C. *et al.* Mouse Models of Diabetic Nephropathy. *J. Am. Soc. Nephrol.* **20**, 2503–2512 (2009).

218. Levey, A. S. *et al.* Definition and classification of chronic kidney disease: A position statement from Kidney Disease: Improving Global Outcomes (KDIGO). *Kidney Int.* **67**, 2089–2100 (2005).

219. Bivona, B. J., Park, S. & Harrison-Bernard, L. M. Glomerular filtration rate determinations in conscious type II diabetic mice. *Am. J. Physiol. - Ren. Physiol.* **300**, F618–F625 (2011).

220. Wei, P. Z. *et al.* Metabolomic Changes of Human Proximal Tubular Cell Line in High Glucose Environment. *Sci. Rep.* **9**, (2019).

221. Hyeon, J. S., Jung, Y., Lee, G., Ha, H. & Hwang, G.-S. Urinary Metabolomic Profiling in Streptozotocin-Induced Diabetic Mice after Treatment with Losartan. *Int. J. Mol. Sci.* **21**, (2020).

222. Cheng, Q.-Y. *et al.* Sensitive Determination of Onco-metabolites of D- and L-2-hydroxyglutarate Enantiomers by Chiral Derivatization Combined with Liquid Chromatography/Mass Spectrometry Analysis. *Sci. Rep.* **5**, 15217 (2015).

223. Fu, X. *et al.* 2-Hydroxyglutarate Inhibits ATP Synthase and mTOR Signaling. *Cell Metab.* **22**, 508–515 (2015).

224. Karlstaedt, A. *et al.* Oncometabolite d-2-hydroxyglutarate impairs α-ketoglutarate dehydrogenase and contractile function in rodent heart. *Proc. Natl. Acad. Sci. U. S. A.* **113**, 10436–10441 (2016).

225. Brinkley, G. *et al.* Teleological role of L-2-hydroxyglutarate dehydrogenase in the kidney. *Dis. Model. Mech.* **13**, (2020).

226. MCLAIN, A. L., SZWEDA, P. A. & SZWEDA, L. I. α-Ketoglutarate dehydrogenase: A mitochondrial redox sensor. *Free Radic. Res.* **45**, 29–36 (2011).

227. Liu, J.-J. *et al.* Urine Tricarboxylic Acid Cycle Metabolites Predict Progressive Chronic Kidney Disease in Type 2 Diabetes. *J. Clin. Endocrinol. Metab.* **103**, 4357–4364 (2018).

228. Sharma, K. *et al.* Metabolomics Reveals Signature of Mitochondrial Dysfunction in Diabetic Kidney Disease. *J. Am. Soc. Nephrol. JASN* **24**, 1901–1912 (2013).

229. Li, L. *et al.* Metabolomics reveal mitochondrial and fatty acid metabolism disorders that contribute to the development of DKD in T2DM patients. *Mol. Biosyst.* **13**, 2392–2400 (2017).

230. Kwan, B. *et al.* Metabolomic Markers of Kidney Function Decline in Patients With Diabetes: Evidence From the Chronic Renal Insufficiency Cohort (CRIC) Study. *Am. J. Kidney Dis.* **76**, 511–520 (2020).

231. Zhang, G. *et al.* DESI-MSI and METASPACE indicates lipid abnormalities and altered mitochondrial membrane components in diabetic renal proximal tubules. *Metabolomics Off. J. Metabolomic Soc.* **16**, 11 (2020).

232. Grove, K. J. *et al.* Diabetic nephropathy induces alterations in the glomerular and tubule lipid profiles1. *J. Lipid Res.* **55**, 1375–1385 (2014).

233. Miyamoto, S. *et al.* Mass Spectrometry Imaging Reveals Elevated Glomerular ATP/AMP in Diabetes/obesity and Identifies Sphingomyelin as a Possible Mediator. *EBioMedicine* **7**, 121–134 (2016).

234. Longuespée, R. *et al.* Rapid detection of 2-hydroxyglutarate in frozen sections of IDH mutant tumors by MALDI-TOF mass spectrometry. *Acta Neuropathol. Commun.* **6**, 21 (2018).

235. Qiu, C. *et al.* Cytosine methylation predicts renal function decline in American Indians. *Kidney Int.* **93**, 1417–1431 (2018).

236. Chen, Z. *et al.* Epigenomic profiling reveals an association between persistence of DNA methylation and metabolic memory in the DCCT/EDIC type 1 diabetes cohort. *Proc. Natl. Acad. Sci.* **113**, E3002–E3011 (2016).

237. Zhang, H. *et al.* Rosiglitazone reduces renal and plasma markers of oxidative injury and reverses urinary metabolite abnormalities in the amelioration of diabetic nephropathy. *Am. J. Physiol. - Ren. Physiol.* **295**, F1071–F1081 (2008).

238. Nakayasu, E. S. *et al.* MPLEx: a Robust and Universal Protocol for Single-Sample Integrative Proteomic, Metabolomic, and Lipidomic Analyses. *mSystems* **1**, (2016).

239. Roshanravan, B. *et al.* Chronic kidney disease attenuates the plasma metabolome response to insulin. *JCI Insight* **3**, (2018).

240. Hasegawa, S. & Inagi, R. Harnessing Metabolomics to Describe the Pathophysiology Underlying Progression in Diabetic Kidney Disease. *Curr. Diab. Rep.* **21**, 21 (2021).

241. Gurley, S. B. *et al.* Influence of genetic background on albuminuria and kidney injury in Ins2+/C96Y (Akita) mice. *Am. J. Physiol. - Ren. Physiol.* **298**, F788–F795 (2010).

242. Hershberger, K. A. *et al.* Ablation of *Sirtuin5* in the postnatal mouse heart results in protein succinylation and normal survival in response to chronic pressure overload. *J. Biol. Chem.* **293**, 10630–10645 (2018).

243. Gerich, J. E., Meyer, C., Woerle, H. J. & Stumvoll, M. Renal Gluconeogenesis: Its importance in human glucose homeostasis. *Diabetes Care* **24**, 382–391 (2001).
244. Eid, A. *et al.* Intrinsic Gluconeogenesis Is Enhanced in Renal Proximal Tubules of Zucker Diabetic Fatty Rats. *J. Am. Soc. Nephrol.* **17**, 398–405 (2006).
245. Liu, Q. *et al.* Inhibition of NF-κB Reduces Renal Inflammation and Expression of PEPCK in Type 2 Diabetic Mice. *Inflammation* **41**, 2018–2029 (2018).
246. Eid, A. *et al.* Intrinsic Gluconeogenesis Is Enhanced in Renal Proximal Tubules of Zucker Diabetic Fatty Rats. *J. Am. Soc. Nephrol.* **17**, 398–405 (2006).
247. Rahim, M. *et al.* Multitissue $^{2}H/^{13}C$ flux analysis reveals reciprocal upregulation of renal gluconeogenesis in hepatic PEPCK-C–knockout mice. *JCI Insight* **6**, (2021).
248. Stark, R. *et al.* A Role for Mitochondrial Phosphoenolpyruvate Carboxykinase (PEPCK-M) in the Regulation of Hepatic Gluconeogenesis. *J. Biol. Chem.* **289**, 7257–7263 (2014).
249. Wolf, P. *et al.* Gluconeogenesis, But Not Glycogenolysis, Contributes to the Increase in Endogenous Glucose Production by SGLT-2 Inhibition. *Diabetes Care* **44**, 541–548 (2021).
250. Sasaki, M. *et al.* Dual Regulation of Gluconeogenesis by Insulin and Glucose in the Proximal Tubules of the Kidney. *Diabetes* **66**, 2339 (2017).
251. Wiese, S. *et al.* Proteomics Characterization of Mouse Kidney Peroxisomes by Tandem Mass Spectrometry and Protein Correlation Profiling*. *Mol. Cell. Proteomics* **6**, 2045–2057 (2007).
252. Fujiki, Y. *et al.* Recent insights into peroxisome biogenesis and associated diseases. *J. Cell Sci.* **133**, (2020).

253. Weng, H., Ji, X., Endo, K. & Iwai, N. Pex11a Deficiency Is Associated With a Reduced Abundance of Functional Peroxisomes and Aggravated Renal Interstitial Lesions. *Hypertension* **64**, 1054–1060 (2014).

254. Ranea-Robles, P. *et al.* Peroxisomal L-bifunctional protein (EHHADH) deficiency causes male-specific kidney hypertrophy and proximal tubular injury in mice. *Kidney360* 10.34067/KID.0003772021 (2021) doi:10.34067/KID.0003772021.

255. Shayman, J. A. Targeting Glycosphingolipid Metabolism to Treat Kidney Disease. *Nephron* **134**, 37–42 (2016).

256. Zador, I. Z. *et al.* A role for glycosphingolipid accumulation in the renal hypertrophy of streptozotocin-induced diabetes mellitus. *J. Clin. Invest.* **91**, 797–803 (1993).

257. Subathra, M. *et al.* Kidney glycosphingolipids are elevated early in diabetic nephropathy and mediate hypertrophy of mesangial cells. *Am. J. Physiol.-Ren. Physiol.* **309**, F204–F215 (2015).

258. Deshmukh, G. D., Radin, N. S., Gattone, V. H. & Shayman, J. A. Abnormalities of glycosphingolipid, sulfatide, and ceramide in the polycystic (cpk/cpk) mouse. *J. Lipid Res.* **35**, 1611–1618 (1994).

259. Natoli, T. A. *et al.* Inhibition of glucosylceramide accumulation results in effective blockade of polycystic kidney disease in mouse models. *Nat. Med.* **16**, 788–792 (2010).

260. Chatterjee, S. *et al.* Use of a Glycolipid Inhibitor to Ameliorate Renal Cancer in a Mouse Model. *PLOS ONE* **8**, e63726 (2013).

261. Yamashita, T. *et al.* Enhanced insulin sensitivity in mice lacking ganglioside GM3. *Proc. Natl. Acad. Sci.* **100**, 3445–3449 (2003).

262. Mitrofanova, A. *et al.* SMPDL3b modulates insulin receptor signaling in diabetic kidney disease. *Nat. Commun.* **10**, 2692 (2019).